Examining the effect of salinity on dolphin mortality using Lagrangian particle tracking in a hydrodynamic model

by

Mehrzad Shahidzadehasadi

A dissertation submitted to the Graduate Faculty of
Auburn University
in partial fulfillment of the
requirements for the Degree of
Master of Science

Auburn, Alabama
December 9, 2023

Keywords: Lagrangian particle tracking, Mississippi Sound, EFDC, Bonnet Carré spillway, Dolphin, Back-tracking, Drifter data, Sensitivity analysis, Calibration

Approved by

Dr. Anna Linhoss, Ph.D., Chair, Associate Professor of Biosystems Engineering
Dr. Xing Fang, Ph.D., Professor of Civil Engineering
Dr. Jasmeet Lamba, Ph.D., Associate Professor of Biosystems Engineering

Abstract

Every year, many dolphins are found dead on the beaches and waterways of the Gulf of Mexico and Mississippi Sound. In 2019, an unusual mortality event (UME) happened, where 337 bottlenose dolphins were stranded between Louisiana, Mississippi, Alabama, and Florida. The National Oceanic and Atmospheric Administration (NOAA) determined that the cause of this UME was protracted exposure to low salinity waters, based on observations of skin lesions and the environmental conditions during that period of time. It is often unclear where dolphins initially died, as their carcasses are found stranded on beaches days after they die. To investigate this further, we used a hydrodynamic model (EFDC+) of the Mississippi Sound. Our goal was to track dolphin carcass movement and simulate salinity at the time and location of each predicted dolphin's death. I represented the movement of 19 dolphin carcasses using particles within the lagrangian particle tracking (LPT) module. The results enabled us to predict the original location of death for each dolphin. The average simulated salinity of all the dolphins' most probable original place of death was below five, except for two cases. I compared these results to the salinity of the Mississippi Sound during Bonnet Carré spillway opening and non-opening dates. Our findings highlight the significant impact of the spillway's opening on the reduction of salinity and its association with dolphin mortality. Furthermore, I calibrated our model simulating the movement of dead dolphins using data from GPS-tagged turtle carcasses and wooden effigies in April 2017 collected by NOAA in the same area as our study domain. Firstly, this data was used to conduct a sensitivity analysis on the previously configured LPT model, which involved altering certain parameters. The results from sensitivity analysis were then used to perform a calibration by adjusting the most sensitive parameters to get the best match between the modeled and observed trajectories. The analysis found that adding wind drag to the LPT model significantly improved its predictive capabilities. The study also investigated the effect of transitioning from a two-dimensional (2D) to a three-dimensional (3D) model. The results revealed that in our study domain with smooth bathymetry a 2D model is good enough and more efficient for modeling purposes.

Acknowledgments

I want to thank my parents, Mahdieh and Reza, for always being there to support me and my decisions. Their love and encouragement have meant the world to me, and I'm truly grateful for their unwavering support in everything I do. Thanks, Mom and Dad!

I would also like to thank my supervisor, Dr. Anna Linhoss for believing in me and guiding me through my Master's journey. I entered this field of study having no specific knowledge about it, and Dr. Linhoss taught me so much.

Table of Contents

List of Figures

List of Tables

List of abbreviations

AE	Absolute Error
AL	Alabama
BC	Bonnet Carré
EFDC	Environmental Fluid Dynamic Code
KDE	Kernel Density estimation
LA	Louisiana
LPT	Lagrangian Particle Tracking
MSS	Mississippi Sound
NOAA	National Oceanic and Atmospheric Administration
RMSE	Root Mean Square Error
SA	Sensitivity Analysis
SS	Skill Score
UME	Unusual Mortality Event
USGS	United States Geological Survey

Chapter 1

1. Examining the Effect of Salinity on Dolphin Mortality Using Lagrangian Particle Tracking in a Hydrodynamic Model

This chapter is a version of an article of the same title by Mehrzad Shahidzadehasadi, Anna Linhoss, Debra Moore, Stephen Reichley, Paul Mickle, and Mark Lawrence that has been submitted to the Estuarine, coastal, and shelf sciences journal. Shahidzadehasadi et, al. (2023) "Comparison of Two Dielectric Sensors in Coarse-Grained Soils of Increasing Salinity." Estuarine, coastal, and shelf sciences journal [Manuscript in progress] The information contained in this chapter is exactly the same as the submitted manuscript.

1.1 Abstract

Numerous dolphins are found dead on beaches and waterways of the Gulf of Mexico and Mississippi Sound every year. In 2019 an unusual mortality event (UME) occurred when 337 deceased bottlenose dolphins were stranded between Louisiana, Mississippi, Alabama, and Florida. According to NOAA (NOAA Fisheries, 2022), based on observations of skin lesions or distinct ulcerative dermatitis and other internal pathologic findings and the environmental conditions during that period of time, the identified cause of this UME was determined as protracted exposure to low salinity waters. Dolphin carcasses are often found stranded on beaches days after they die. Consequently, their initial place of death is unknown. In this study, we used an existing 2D hydrodynamic model (EFDC+ 11.2) of the Mississippi Sound simulated by Armandei

et al., (2021) to track dolphin carcass movement and to simulate salinity at the time and location of each predicted dolphin's death. Particles within the Lagrangian particle tracking module were used to represent the movement of 19 dolphin carcasses. A large number of particles (virtual dolphin carcasses) were seeded throughout the model domain and tracked for five days. These results were used to hindcast each dolphin's original location of death. The results indicate that the most likely place of death for 12 dolphins stranded on the beaches of Mississippi, along with the two found on Ship and Horn Islands, was west of their stranding location. For both of the dolphins stranded on Dauphin Island, the most likely place of death was in the Mobile Bay area north of where they were found. The remaining three dolphins found dead on barrier islands, most likely originally died in close proximity to their stranding locations. The average simulated salinity of all the dolphins' most probable original place of death was below five except for two cases. These results are compared to the salinity of the Mississippi Sound during Bonnet Carré spillway opening and non-opening dates. They highlight the significant impact of the spillway's opening on the reduction of salinity and its association with dolphin mortality.

Keywords: Lagrangian particle tracking, Mississippi Sound, EFDC, Bonnet Carré spillway, Dolphin, Back-Tracking

1.2 Introduction

Common bottlenose dolphins are found in many bays, sounds, and estuarine environments, which are characterized by shallow, brackish waters with variable salinity (Hayes et al., 2018). In the north-central region of the Gulf of Mexico, the Mobile Bay/Mississippi Sound (MSS) system is a large freshwater-dominated environment in which dolphin populations vary over spatial and temporal scales (Pitchford et al., 2016). The seasonal abundance and distribution of dolphins in the Mississippi Sound is complicated and might be related to changes in environmental conditions such as salinity (Pitchford et al., 2016).

Low salinity is known to adversely affect dolphin health and cause immune deficiencies (Toms et al., 2021; Booth & Thomas, 2021; McClain et al., 2020; Takeshita et al., 2021). Freshwater causes health issues including skin lesions, electrolyte abnormalities, corneal edema, and hepatobiliary abnormalities (Deming et al., 2020; Toms et al., 2021). Also, testing the blood of dolphins exposed to low salinity waters for long periods of time showed significant increases in blood urea nitrogen and aldosterone and significant decreases in serum sodium, chloride, and calculated serum osmolality (McClain et al., 2020; Takeshita et al., 2021).

Although common bottlenose dolphins can be found in low-salinity waters (<15), they cannot tolerate such conditions for long periods (Hornsby et al. 2017). Hornsby et al. (2017) matched dolphin telemetry data in Barataria Bay, Louisiana (USA), with contemporaneous salinity estimates to establish a salinity threshold and identify preferred dolphin habitats. Dolphins were found more frequently in areas where salinity higher than ~11 was recorded, though sometimes they were found in regions with predicted salinity of ~8 for short periods of time. They were found less frequently in areas with salinities below ~5 (Hornsby et al., 2017). Researchers predicted that

bottlenose dolphins exposed to low salinity waters (<5) for at least two days or areas with less than ten salinity for prolonged periods were more likely to have freshwater-like skin lesions and hepatobiliary abnormalities (Deming et al., 2020; Takeshita et al., 2021). The skin is frequently centrally eroded or ulcerated and has necrosis often with a target-like appearance. It sometimes has velvety matting that is thickened and rough, often green, yellow, or orange (Duignan et al., 2020).

Individual dolphins have different movement patterns, but those movements are not necessarily because of salinity changes or extreme events including Hurricane, algae bloom (Boehning et al., 2023), or flooding (McBride-Kebert & Toms, 2021) in their habitat. Research conducted on the relationship between dolphin movements and the salinity of their habitat revealed the common bottlenose dolphins' tendency to return to their previous habitat regardless of low salinity exposure by monitoring satellite-telemetry tagged dolphins (Takeshita et al., 2021). Furthermore, Hubard et al. (2005) found evidence of site fidelity among dolphins in the Mississippi Sound. These findings collectively indicate that bottlenose dolphins exhibit high levels of site fidelity in their habitat.

The MSS had unusually low salinities in 2019 in association with riverine flooding and two Bonnet Carré (BC) Spillway openings. The BC Spillway is a flood diversion construction built for the purpose of transferring the Mississippi River's freshwater into the Gulf of Mexico, whenever the River's water level gets too high, in order to prevent flooding in New Orleans. The other major freshwater source in the MSS is the Pearl River (watershed drainage area of 22000 km^2), whose flow rates fluctuate between 86 and 2629 m^3/s. According to NOAA, 337 bottlenose dolphins were found dead on the northern Gulf of Mexico beaches in 2019 (between Louisiana and the Florida Panhandle, ~1,400 km of coastline) (NOAA Fisheries, 2022). This event was

classified as an Unusual Mortality Event (NOAA Fisheries, 2022). ‘Under the Marine Mammal Protection Act, an unusual mortality event occurs when an unexpected stranding event happens involving a significant die-off of any marine mammal population and demands immediate response’ (NOAA Fisheries, 2023).

Of the 337 carcasses recovered, 156 (46% of the total UME) were found in the MSS and Mobile Bay region (~200 km of coastline). It is notable that almost half of the dolphins associated with this UME were found in just 15% of the total area included for the UME. Furthermore, the number of deaths that occurred at this time was approximately three times the yearly average number of dolphins stranded on the beaches in the MSS. The UME began in February and continued through November 2019, which coincided with two BC spillway openings. Forty-seven percent of the dolphins stranded on the beaches of Mississippi and 10% of those stranded on the shores of Alabama were identified with freshwater-like skin lesions (NOAA Fisheries, 2022). Since dolphin carcasses were mostly found on beaches, their initial place of death is unknown. This can be estimated using water currents which transport dolphin carcasses to the beach.

The currents that move dolphin bodies after they die can be simulated using hydrodynamic models. Hydrodynamic models are tools for simulating fluid flow and may be equipped with a Lagrangian particle tracking module (LPT). Lagrangian particle tracking is a method of estimating the trajectory of individual solid particles utilizing a velocity field and can represent any number of objects. This method requires a decent representation of the velocity field. The only way to obtain such a velocity field is to use a high-resolution hydrodynamic model (Peltier et al., 2012; Quinlan, 1999).

Lagrangian Drift models are widely used in the literature, simulating stranding events in different locations for a variety of large, floating aquatic species. The animals that have been

studied using LPT include sea turtles (Nero et al., 2013; Santos et al., 2018), Portuguese man of war (Headlam et al., 2020), and stranded carcasses of cetaceans including pygmy sperm whales (Harlan, 2014), fin whales (Díaz-Gamboa et al., 2022), humpback and bryde whales (Junior et al., 2019), harbour porpoise (Haelters et al., 2006; Peltier et al., 2012), cuvier's beaked whale (Carlucci et al., 2020), Short-beaked common dolphins (Gilbert et al., 2021; Peltier et al., 2012), and bottlenose dolphins (Wirasaet et al., 2015). In this study bottlenose dolphins are going to be simulated.

A large variety of software and modeling programs have been used in drift simulations; most of which are well-known hydrodynamic models. Some of these models have a back-tracking module, while others do not. If a back-tracking module is available, the software can track back an object for a specified time period. This allows the tracked object to be identified at the beginning of the time period which makes carcass back-tracking a simple task. On the other hand, models that only do forward tracking need to guess the location of an object at the beginning of the time period by planting numerous particles in the model domain and track them forward to identify the ones that eventually locate at the aforementioned object's location at the end of the time period. Nero et al., (2013) used the American SEAS (AMSEAS) implementation of the Navy Coastal Ocean Model (NCOM) to simulate sea turtle carcass backtrack drifts in the north-central Gulf of Mexico. Díaz-Gamboa et al., (2022); Headlam et al., (2020); and Santos et al., (2018) utilized the ICHTHYOP modeling tool within the Global HYCOM and Regional Ocean Modelling System (ROMS) hydrodynamics models to identify the geographical location of death for a fin whale, Portuguese men of war, and sea turtles. Harlan, (2014) applied the General NOAA Operational Modeling Environment (GNOME) software, which is equipped with both forward-tracking and backtracking modules to estimate the original location of death for sperm whales. Junior et al.,

(2019) used MOHID to simulate the trajectory of humpback and bryde whales. Haelters et al., (2006) simulated drifters of harbor porpoises with the Management Unit of Mathematical Models (MUMM) modeling program. Carlucci et al., (2020) simulate the drifts of Cuvier's beaked whale bodies using the Danish Hydraulic Institute's model, MIKE 3 FM. Wirasaet et al., (2015) used the Advanced Circulation (ADCIRC) program to hindcast dolphin carcasses. Peltier et al., (2012) simulated the trajectories of stranded dolphins and harbor porpoises using MOTHY (Modèle Océanique de Transport d'Hydrocarbures). However, EFDC+ software was never used to track any species as performed in this study.

The objective of this research was to track the origins of dolphin carcasses using a revised version of an existing hydrodynamic model simulated by Armandei et al., (2021) that has been expanded to include Lake Pontchartrain and Mobile Bay and then identify the ranges of salinity in the area at the time of death. This project specifically investigates bottlenose dolphins stranded in the Mississippi Sound and Mobile Bay during the unusual mortality event of 2019.

1.3 Study Area and Data

1.3.1 Study Area

The study area consists of the MSS and Mobile Bay. The Mississippi Sound is a large, shallow, and semi-open sound located in the north-central Gulf of Mexico with a surface area of 2,129 km^2, an average depth of 2.98 m at mean low water, and a salinity range of 0-35 according to USGS water data for several stations in the MSS from 2011 to 2020. From east to west, the MSS extends from Cedar Point, AL, to Half Moon Island, LA, and is bordered to the north by Mississippi and Alabama and to the south by Bay Boudreau, LA, and six barrier islands: Dauphin,

Petit Bois, Horn, East Ship, West Ship, and Cat. It connects with the Gulf through passes between a series of five barrier islands. Mobile Bay is a shallow estuary in the northern Gulf of Mexico, extending 48 km long and ranging from 14–34 km wide. The relatively shallow uniform bathymetry averages 3 m except for the shipping channel which is 12m deep. Mobile Bay is connected to the MSS through Pass Aux Herons outlet in the southwest.

The BC Spillway is a flood diversion structure located on the Mississippi River approximately 52 km upriver from New Orleans. Its purpose is to prevent the Mississippi River from flooding southern Louisiana and New Orleans (Parra et al., 2020). It has been opened 15 times between its construction date in 1931 and 2020, with openings usually occurring in the spring months. The discharge volumes for each opening have been between 2.1 and 30.1 $km^{3,}$ with openings lasting between 13 (in 1975) and 79 days (second opening in 2019); (US Army Corps of Engineers, 2016, 2020). The BC Spillway opening dates, duration, and estimated discharge from U.S. Army Corps of Engineers (USACE) Flood and Post-Flood reports in New Orleans District are presented in Table 1.1.

Year of Opening	**Opening and Closing dates and Duration (days)**	**Estimated total Discharge (km^3)**
1937	Jan 28 – Mar 16 (48)	15.2
1945	Mar 23 – May 18 (57)	30.1
1950	Feb 10 – Mar 19 (38)	13.4
1973	Apr 8 – Jun 21 (75)	23.5
1975	Apr 14 – Apr 26 (13)	2.11
1979	Apr 17 – May 31 (45)	13.9
1983	May 20 – Jun 23 (35)	15.2
1997	Mar 17 – Apr 17 (32)	11.7
2008	Apr 11 – May 8 (28)	7.5
2011	May 9 – Jun 20 (43)	21.9
2016	Jan 10 – Feb 1 (23)	6.9
2018	Mar 8 – Mar 30 (23)	5.8
2019	Feb 27 – Apr 11 (44)	15.1
2019	May 10 – Jul 27 (79)	23.0
2020	Apr 3 – May 1 (29)	4.0

Table 1.1- History of the Bonnet Carré Opening dates, Duration, and estimated total discharge according to USACE (US Army Corps of Engineers, 2016, 2020).

1.3.2 Dolphin Data

The stranded dolphin data comes from the NOAA National Stranding Database Public Access database (NOAA, 2021). The data includes information on every stranded marine mammal in the United States according to the reports from members of the National Stranding Network. The dataset includes carcasses of about 7,000 stranded dolphins, the time and coordinates that they were found, and their decomposition code. For this project, 19 dolphin carcasses found in the model area (Mississippi Sound and Mobile Bay) in 2019 with decomposition codes of two, were simulated (Table 1.2 and Figure 1.1). More information regarding the decomposition codes can be found in Table 1.3. This year was selected because of the documented unusual mortality event and two BC spillway openings.

Observation Date	Latitude	Longitude
13/06/2019	30.253889	-88.193889
05/06/2019	30.318083	-89.319077
05/08/2019	30.35369	-89.12609
18/07/2019	30.34367	-88.73274
29/03/2019	30.393873	-88.914371
27/05/2019	30.324009	-89.215909
30/03/2019	30.38358	-89.01844
28/03/2019	30.392549	-88.934972
10/04/2019	30.22612	-88.58923
03/11/2019	30.251175	-88.079107
23/03/2019	30.25267	-88.88783
29/05/2019	30.32752	-89.20377
02/06/2019	30.24898	-89.06699
02/02/2019	30.37343	-89.06442
11/04/2019	30.30342	-89.2896
23/03/2019	30.31175	-89.25088
30/08/2019	30.288757	-88.049014
04/02/2019	30.245	-88.958333
12/04/2019	30.349377	-88.393576

Table 1.2- Stranded dolphin data location and mortality data (NOAA, 2021)

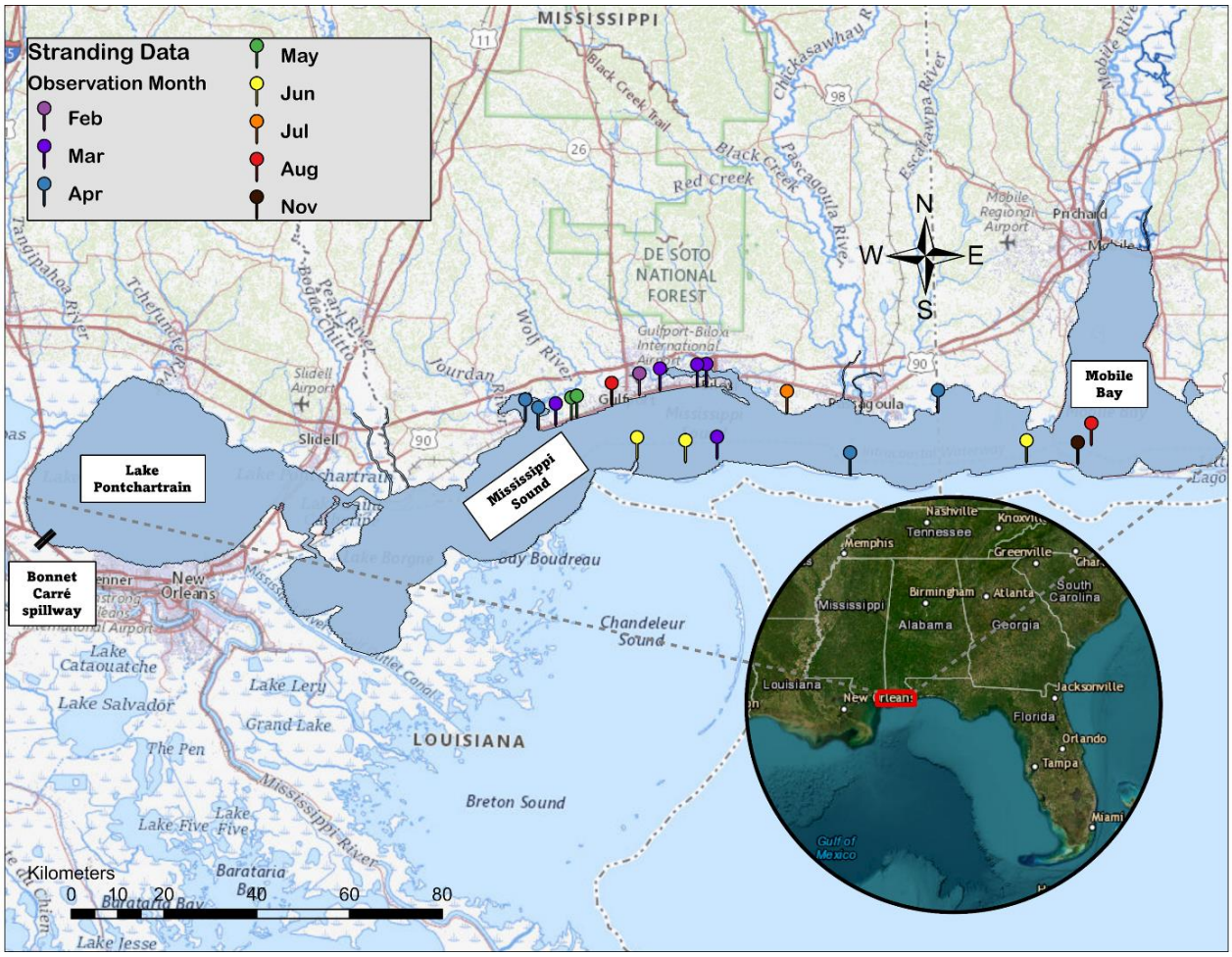

Figure 1.1 - Study Area and Dolphin data in 2019 with decomposition codes 1 and 2 in Mississippi sound distinguished by month of observation.

1.4 Methods

1.4.1 Assumptions

1.4.1.1 Floating after Death

After a dolphin dies it either sinks or drifts as it decomposes, is scavenged, or strands on a shoreline. When it sinks to the bottom of the water column, it often resuspends (Peltier et al., 2012). Whether a carcass sinks or floats depends on the animal's buoyancy. Buoyancy is a function of the animal's body condition and content, including bone, blubber, and lung inflation (Moore et al., 2020). The buoyancy of air-breathing cetaceans is also influenced by gas bubbles created either during decompression when they were alive (Moore et al., 2009) or due to decomposition after death (Quirós et al., 2018). In a study by Woodcock & McBride (1961), the weight of a dolphin was measured after death, and the results indicated that the dolphin would float if it was approximately 5.4 kg and sink if it was slightly greater than 4.1 kg depending on the lung fullness. In an experiment by Peltier et al., (2012) a dolphin carcass and a harbor porpoise carcass were released into the water to test the immersion rate. It showed that both specimen carcasses remained at the sea surface in the first ten days after death and partially submerged after 20 days. In general, studies on whether marine mammals float or sink after death are very few. In this study, the dolphin data are from fresh dead dolphins, which have been dead for a maximum of five days, so it is assumed that all dolphins floated immediately after death.

1.4.1.2 Time since Death

In order to simulate the path of a stranded aquatic species, the time of death must be established. There is not a precise way to estimate the time since death for a stranded carcass. All the methods to address this issue provide a range of days according to the carcass's condition. Some of the projects that have used Lagrangian particle tracking to backtrack the location of a carcass to the location of death assumed that a certain fixed time has passed since the animal's

death (Díaz-Gamboa et al., 2022; Harlan, 2014; Junior et al., 2019; Wirasaet et al., 2015). But others considered the uncertainty in the time since death for their simulations (Carlucci et al., 2020; Haelters et al., 2006; Headlam et al., 2020; Nero et al., 2013; Peltier et al., 2012; Santos et al., 2018).

To overcome this challenge and identify the location of death from stranded carcasses, the number of days before each stranding dolphin died should be determined. The measured parameter that estimates this period of time is the decomposition code. The decomposition code is a condition system that classifies dolphin carcasses into five levels of decomposition. Code one is a live animal and code five is an animal that is mummified or has only skeletal remains. Table 1.3 shows the decomposition codes and death-to-stranding time using visual criteria describing skin erosion (Peltier et al., 2012, 2020). For this study only dolphin carcasses found in 2019 with decomposition code two (freshly dead) were used. These dolphins were chosen because they have been dead and drifting for a relatively short period of time, which reduces the uncertainty of the simulation results.

DECOMPOSITION CODE	CONDITION	TIME PASSED SINCE DEATH
CODE 1: ALIVE ANIMAL	• Blood cells intact • Eyes are clear • No protrusion	< 2 days
CODE 2: FRESH DEAD	• Minimal drying or wrinkling of skin, eyes, and mucus membranes • Tongue and penis not protruding • Eyes are clear • Carcass is not bloated	2 to 5 days
CODE 3: MODERATE	• Bloated, usually intact carcass • Protruding Tongue & Penis • Skin may be cracked and sloughing • Dry Mucus Membranes • Eyes sunken or missing	5 to 15 days
CODE 4: ADVANCED	• Carcass is often damaged by scavengers • Carcass may be intact • Body is collapsed • Skin sloughing or missing • Strong Odor	15 to 30 days

CODE 5: SKELETON/ MUMMIFIED	• No “wet” internal tissues • Skeleton remains	> 30 days

Table 1.3- Dolphin decomposition codes taken directly from (Peltier et al., 2012, 2020).

1.4.2 Hydrodynamic Model

An existing 2D hydrodynamic and water quality model of the MSS simulated in Environmental Fluid Dynamic Code Plus (EFDC+) version 11.2 was used for this study. The Environmental Fluid Dynamics Code (EFDC+ 11.2) software is a multifunctional surface water modeling engine designed to simulate aquatic systems in one, two, and three dimensions. (DSI LLC., 2023; EFDC+ Source Code, 2022).

This model is based on Armandei et al.'s (2021) model of the western Mississippi Sound. The grid has since been expanded to include Lake Pontchartrain and Mobile Bay. The model is composed of a computational curvilinear grid consisting of 70,964 cells (245 rows and 962 columns) with the average grid cell dimensions of 238.52 m in x-direction and 331.88 in Y-direction which covers an area of 5,678.8 km^2 extending from Lake Pontchartrain (LA) in the west to Mobile Bay (AL) in the east (Figure 2B). The unit system is metric, the projection or horizontal datum is WGS 1984, and the vertical datum is NAVD88. The model’s data (boundary conditions, initial conditions, and validation data) were provided from USGS measurement gauge stations available within and near the computational grid (U.S. Geological Survey, 2023). The bathymetric variation of the models’ domain is relatively smooth, and the bathymetry data was provided from NOAA (NOAA Data access viewer, 2023) presented in Figure 1.2A. The model simulates temperature, salinity, currents, and water elevation from 2009 to 2020. There are 18 freshwater inflows and two open boundaries (Tables 1.4 and 1.5 and Figure 1.2B). These average flows are

based on 30 minutes data. The tides are not considered at the open boundaries. Where gauge data was not directly available to input freshwater flows, an area weighted approach was used. Five wind speed and direction time series data from NOAA were used in the model (NOAA National Centers for Environmental Information). The wind stations used are specified in Figure 1.3. Additional details about the model can be found in Armandei et al., (2021).

Flow Boundary	Average Flow 2009-2020 (m3/s)
Amite River	61.38
East Pascagoula River	139.71
East Pearl River	308.54
Jourdan River	22.916
Mobile River	317.49
Tagniphoa River	170.23
Tchnefunte River	35.30
West Pascagoula River	326.13
West Pearl River	185.12
Wolf River	20.54
Fowl River	6.06
Fish River	3.34
Magnolia River	3.12
Old Fort Bayou River	5.72
Bernard Bayou River	5.72
Biloxi Tuxachanie & Tchoutacbouffa River	29.11
Bonnet Carré Spillway	3404.14

Table 1.4- Flow boundary conditions used in the hydrodynamic model.

Open Boundary	Average Water Level (m)	Salinity Time Series	Average Salinity	Temperature Time Series	Average Temperature (°C)
Near Grand Pass	0.3085	Near Grand Pass	18.35	Near Grand Pass	22.22
East Ship	0.3088	East Ship	24.61	East Ship	22.36

Table 1.5- Open boundary conditions used in the hydrodynamic model.

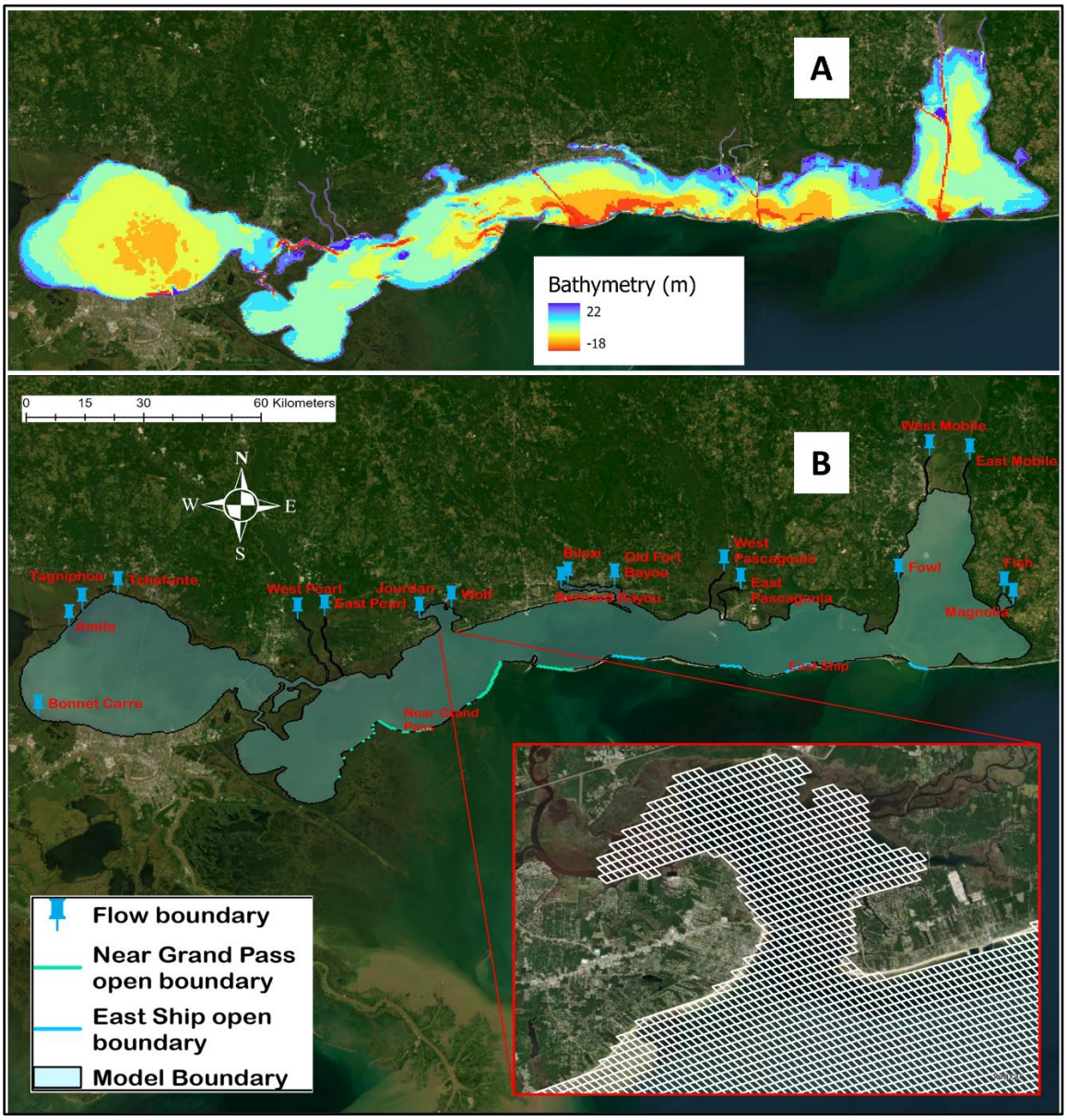

Figure 1.2- A) Bathymetry of the Mississippi Sound. B) Model grid along with the freshwater flow boundary conditions and open boundaries.

A validation showing modeled and measured water surface elevation and salinity results is presented for 2019. The measured salinity and temperature time series data are 15-minute data. The model water surface elevation and salinity validation statistics, including root mean square error (RMSE) and coefficient of determination (R^2) are calculated (Table 1.6). Validation plots for water surface elevation and salinity from three different USGS stations (Figure 1.3) are provided in Figures 1.4 and 1.5. At St. Joseph and Gulfport light stations, there was a vertical offset observed between the measured and simulated data. This offset can be attributed to the infrequent updates of the vertical datums. To address this issue, the measured data at these two stations were adjusted by removing the offset and aligning them with the NAVD88 vertical datum. This correction was applied to ensure comparability and consistency in the vertical reference for the data. To assess the quality of the hydrodynamic simulation and determine if it accurately represents the circulation patterns, a comparison is made between the salinity results of our model and a similar model simulated by Armstrong et al. (2021) and Hendon et al., (2020). While the statistics are not explicitly mentioned in Armstrong et al. (2021) and Hendon et al., (2020), a graphical comparison between their results and ours indicates that our model performs well and provides a realistic representation of the circulation patterns. The under-prediction of salinity in hydrodynamic models can occur due to various reasons, such as limitations in input data, parameterization choices, simplifications and assumptions in the model, inadequate calibration and validation, and uncertainties in physical processes. The hydrodynamic model used in this study is based on an existing model simulated by Armandei et al., (2021) and further elaboration and more detailed insights can be accessed in the Armandei et al., (2021)."

The hydrodynamic model showed poor performance in terms of water surface elevation and salinity during the month of January due to a missing dataset of salinity and water level in the

Near Grand Pass open boundary from January 1st to February 1st. This gap in data is reflected in Figures 1.4 and 1.5. To mitigate the impact of this missing data, the statistical analysis was conducted again, this time excluding the January results. As presented in Table 1.6, this approach led to an improvement in the results.

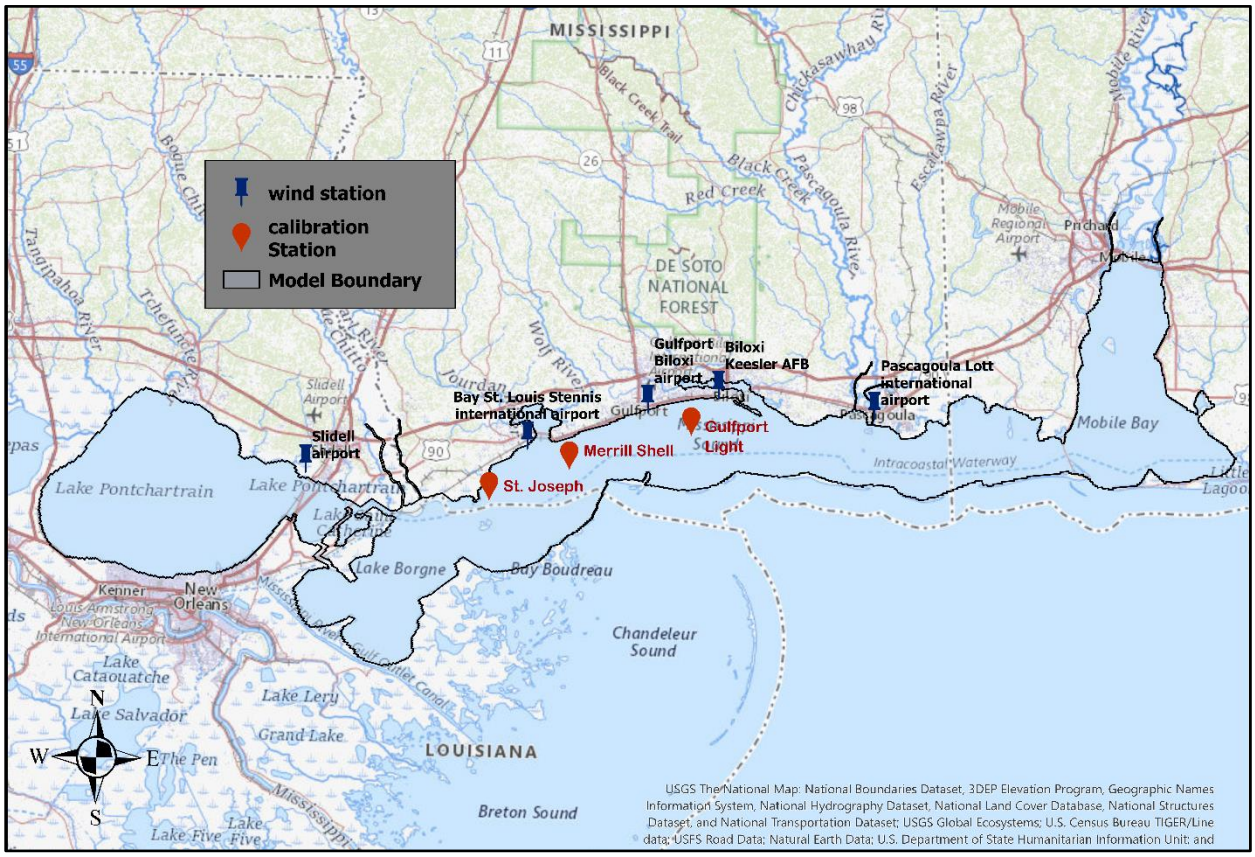

Figure 1.3- Wind stations used as external forcing data in the Hydrodynamic model and the USGS stations used for model validation.

	Water Surface Elevation			Salinity		
Station name	**RMSE (m)***	**R^2***	**R^2****	**RMSE (ppt)***	**R^2***	**R^2****
St. Joseph	0.212	0.446	0.682	5.073	0.377	0.518
Gulfport Light	0.134	0.441	0.624	9.281	0.632	0.632
Merrill Shell	0.123	0.411	0.655	5.819	0.614	0.614

Table 1.6- Water surface elevation and salinity validation statistics for January 1st to December 31st, 2019.

* Based on entire simulation period: January 1st to December 31st, 2019.

** Missing data removed. Based on February 1st to December 31st, 2019.

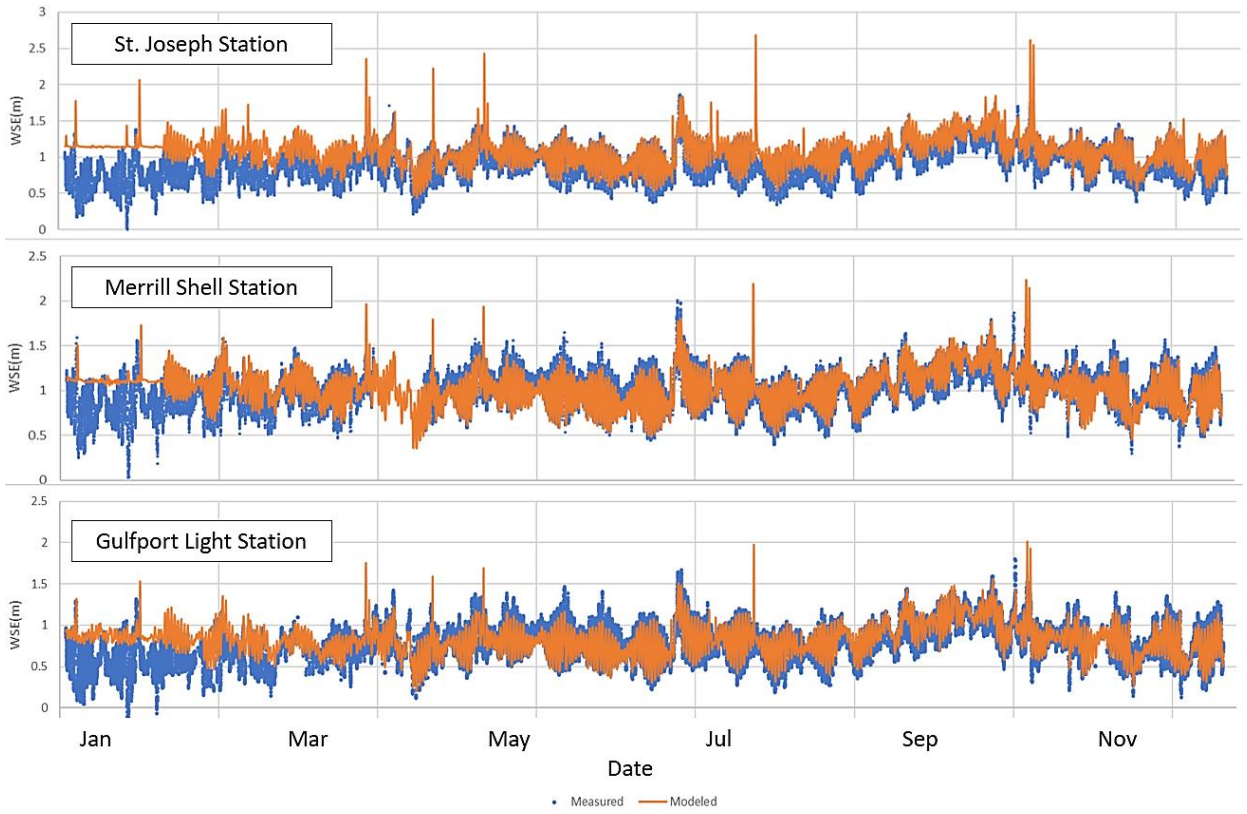

Figure 1.4- Water surface elevation validation time series for three USGS stations (A: St.Joseph, B: Gulfport light, C: Merrill Shell) from January 1st to December 31st, 2019.

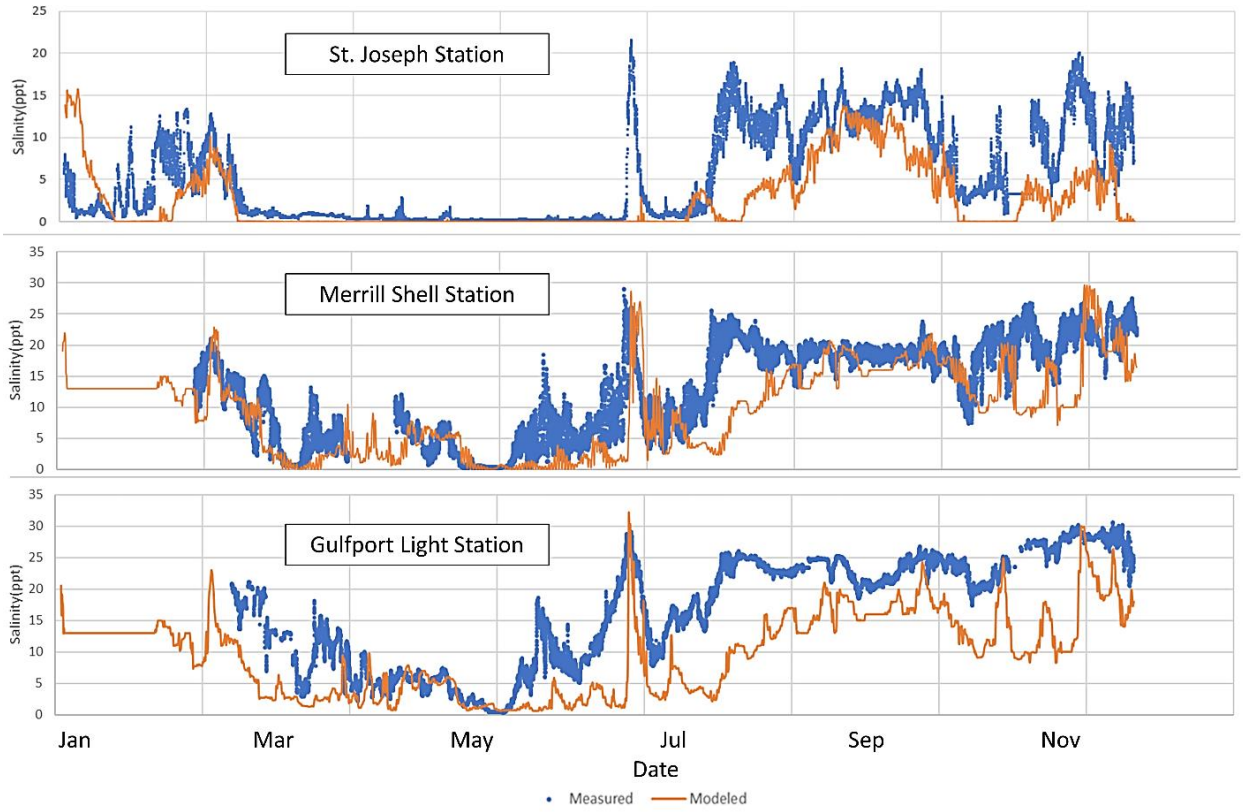

Figure 1.5- Salinity validation time series for three stations (A: St. Joseph, B: Gulfport light, C: Merrill Shell) from January 1st to December 31st, 2019.

1.4.3 Lagrangian Particle Tracking

Lagrangian particles move with the fluid velocity field; therefore, the drifters' simulation is coupled to a fluid flow model. Governing equations for fluid flow used in the EFDC+ modeling software are the Navier-Stokes and advection-diffusion equations for the salinity, temperature, mass transport, etc. (DSI LLC., 2023). The advection-diffusion equation for mass transport in a three-dimensional curvilinear orthogonal coordinate system is given in Equation 1.1 and the differential equations for the lagrangian movement of drifters in x, y, z coordinates are shown in Equations 1.2-1.4:

$$\frac{\partial C}{\partial t} + \frac{\partial (uC)}{\partial x} + \frac{\partial (vC)}{\partial y} + \frac{\partial (wC)}{\partial z} = \frac{\partial}{\partial x}\left(A_H \frac{\partial C}{\partial x}\right) + \frac{\partial}{\partial y}\left(A_H \frac{\partial C}{\partial y}\right) + \frac{\partial}{\partial z}\left(A_b \frac{\partial C}{\partial z}\right) \quad \text{Eq. 1.1}$$

$$dx = \left(u + \frac{\partial A_H}{\partial x}\right) dt + (2p - 1)\sqrt{2A_H dt} \quad \text{Eq. 1.2}$$

$$dy = \left(v + \frac{\partial A_H}{\partial y}\right) dt + (2p - 1)\sqrt{2A_H dt} \quad \text{Eq. 1.3}$$

$$dz = \left(w + \frac{\partial A_b}{\partial z}\right) dt + (2p - 1)\sqrt{2A_b dt} \quad \text{Eq. 1.4}$$

Where (u, v, w) are the lagrangian velocity vectors in (x, y, z) directions, A_H and A_b are the horizontal and vertical diffusion coefficients which specify the amount of substance that diffuses across a unit area in one second under the influence of a gradient, and C is the concentration. The time step is shown by dt, and p is a random number from a random variable generator.

The numerical solutions in equations 1.2 to 1.4 are divided into two parts; the first term on the righthand side is related to the advective transport, and the second term calculates the random movements. Each of these terms can be separately modified, and the random movement term can be used or not.

If the particles are on the water's surface (such as is assumed for the dolphins), wind drag can play a role in moving those particles. The effect of wind drag was considered in addition to the advection-diffusion movements in EFDC+ by turning on the wind drag calculations in the module using the drag parameters from Kim et al. 2014. Another important set-up that made the simulation more realistic was considering no wall slippage. This means that the velocity of the particles becomes zero when they hit a close boundary; thus, they become beached particles.

1.4.4 Forward Tracking

The research utilizes forward tracking methodology due to the absence of a backtracking module in the EFDC+ software. Consequently, instead of directly backtracking the stranded dolphins, the approach involves tracking forward particles across the entire model domain. By tracing these particles, the study aims to identify those that ultimately reach the vicinity of the stranded dolphin. This methodological choice allows for the investigation of potential pathways and sources leading to the observed dolphin strandings despite the software's limitation in backtracking capabilities.

A Lagrangian particle tracking (LPT) module simulating the floating dolphin carcasses was configured for tracking forward numerous particles representing dead dolphins in different time windows. 19 carcasses were investigated, one at a time. For each carcass, five days before the death of each individual dolphin, 63,084 particles (approximately one particle in each grid cell) were placed uniformly throughout the model's spatial domain at the water surface, with each particle being 300 m away from its adjacent particles in the x and y directions. Each particle group was tracked forward for five days prior to each stranding date because a freshly dead dolphin (decomposition code 2) is estimated to be dead for a maximum of five days.

Because there is uncertainty in the prediction of the initial location of death, a target zone of 50.26 km^2, which is equal to a four km radius circle, was created around the location of each stranded dolphin. Particles that passed within the 4 km radius of the dolphin's stranding location between two and five days prior to the date of stranding were flagged and considered to be potential dolphin carcasses. The two to five days range is based on the uncertainty in the time of death for the dolphins (Table 2.2). Figure 1.6 illustrates particle trajectories for a segment of the model over

four consecutive days. The initial location of each flagged particle was mapped. The mapping process was done by assigning a number to each of the particles from 1 to 63,084. After identifying the flagged particles, their numbers were recorded, and their initial place at the LPT module's start date was specified. The process was repeated for each of the 19 stranded dolphins.

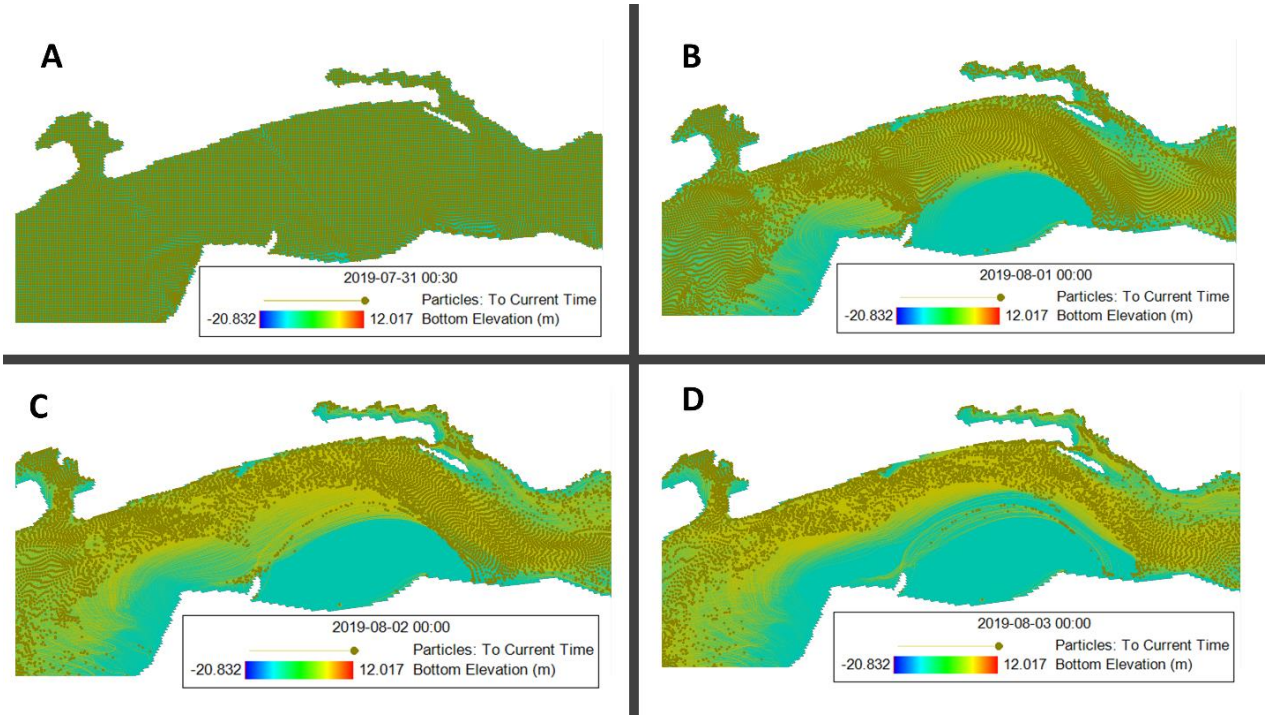

Figure 1.6- Particle trajectories in 4 consecutive days in the area between Bay St. Louis and Biloxi using the LPT module of a hydrodynamic model of Mississippi Sound; the dots are the particles, and the yellow lines are the trajectories. A shows time 0, B shows the location of the particles on day 1, C shows the location of the particles on day 2, and D shows the location of the particles on day 3.

1.4.5 Kernel Density Analysis

The results from the LPT gave numerous data points for the potential location of death for each stranded dolphin. To analyze these results, Kernel Density estimation analysis (KDE) in ArcGIS Pro was used (Esri, 2022). These results provide a heat map showing the likelihood of location of death for each dolphin. KDE uses a probability density function to fit a smoothly curved

surface over each point. The density surface shows the concentrated areas of point features. This surface value is highest at the point location and decreases as the distance from the point increases, and it becomes zero at the specified search radius for the analysis. The search radius used for this study was one km based on the general distance between the point data. Figure 1.7 gives an example of how KDE transforms raw point data into a heatmap that shows probability.

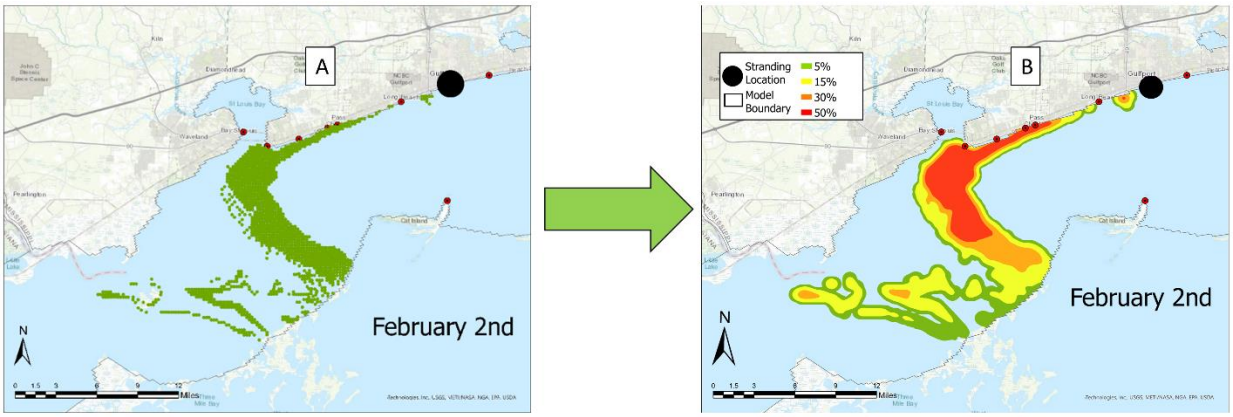

Figure 1.7- An example of converting points to a heat map using KDE. A) The modeled locations of death for the dolphin found near Gulfport on February 2nd are shown with green points and the black circle is the stranding location. B) The result of KDE.

1.4.6 Salinity Analysis

Salinity analyses were conducted to demonstrate the salinity range at the probable locations of death for the dolphins during the estimated time of death period. Initially, the average salinity of the cells estimated to have the highest likelihood of being the origin of death for each dolphin during the estimated time of death was calculated. Then based on the absolute average differences between the salinities predicted by the hydrodynamic model and the real salinities at three USGS stations, an uncertainty band was created. This was done to account for any over or under-predictions made by the model. The results were compared to the dangerous salinity range for dolphins.

Furthermore, the impact of the BC Spillway openings in 2019 on the low salinities at the dolphins' locations of death was investigated. This was done by creating salinity boxplots based on the salinities extracted from the hydrodynamic model for each dolphin at three different time periods: 1) during the BC Spillway opening days in 2019, 2) during the non-opening days in 2019, and 3) during the likely time of death period for each of the 19 dolphins. These analyses allowed us to gain insight into the potential effects of the BC Spillway openings on the salinity levels in the MSS and the impact on the mortality of the dolphins.

1.5 Results and Discussion

There have been several papers published that use Lagrangian particle tracking to simulate the drift of marine mammals (ex. Díaz-Gamboa et al., 2022; Harlan, 2014; Headlam et al., 2020; Junior et al., 2019; Nero et al., 2013; Peltier et al., 2012; Santos et al., 2018; Wirasaet et al., 2015). There have also been a few papers that investigate the impact of salinity on dolphin health (Hornsby et al., 2017; Deming et al., 2020; Takeshita et al., 2021). This is the first study of its kind to use Lagrangian particle tracking to understand the relevance of anthropogenic impacts of salinity to changes in marine mammals. This novel study presents a new method for understanding how anthropogenic changes in salinity can affect marine species.

Prior to using drifters to discover the original place of death for each dolphin and scrutinizing the salinity of that exact place and time, some general analyses have been performed to check if there is any potential relationship between measured salinity, BC Spillway opening, and dolphins' death. Gulfport Light station is chosen for the measured salinity due to its location in the middle of the model domain and the absence of significant data gaps. Two graphs are

prepared for this purpose, Figure 1.8 shows daily salinity data of Gulfport Light station, MSS from 2011 to 2020 extracted from USGS shown a Cumulative summation of dead dolphins found in the MSS from 2011 to 2020, and the BC spillway opening dates, the results indicate that there is a drop in salinity and a jump in the number of deaths during the BC opening dates. Figure 1.9 compares the salinity levels of Gulfport Light station, MSS from 2011 to 2020 extracted from USGS during dolphin mortally dates to examine if dolphins usually die when salinity in the MSS is generally lower than average. The results indicate that more than 50% of the deaths happened when salinity was lower than the average of 20 ppt.

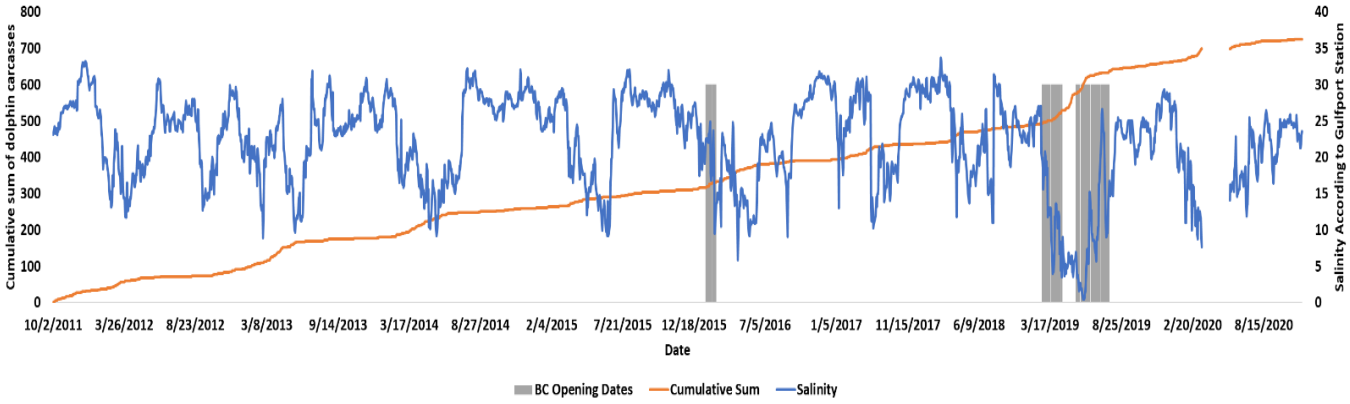

Figure 1.8- Daily salinity data of Gulfport Light station, MS from 2011 to 2020 extracted from USGS shown in blue, Cumulative summation of dead dolphins found in the Mississippi Sound from 2011-2020 in orange. And gray parts show the Bonnet Carre spillway opening dates.

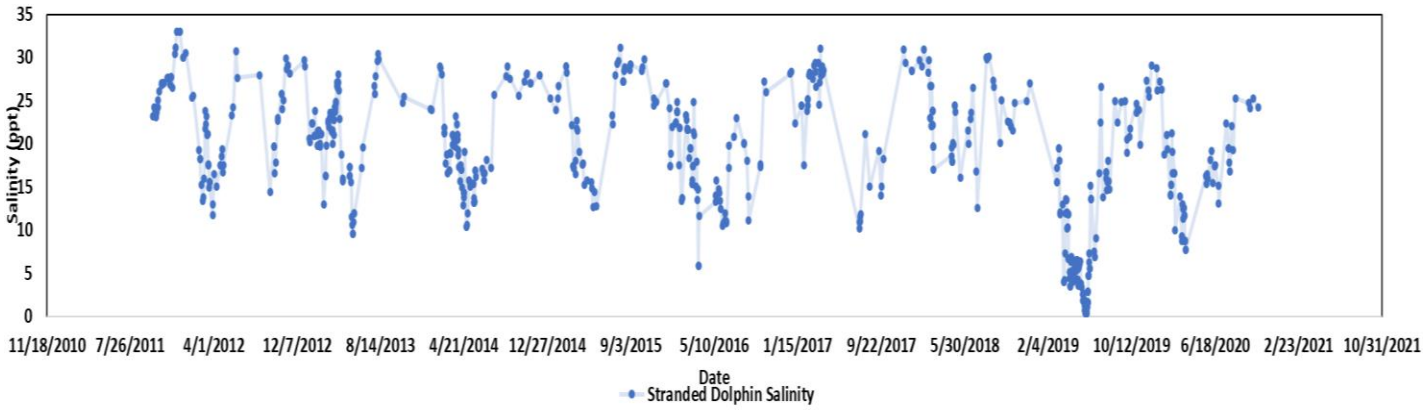

Figure 1.9- Comparing salinity levels of Gulfport Light station, MS from 2011 to 2020 extracted from USGS during dolphin mortally dates.

The particle tracking results, which are in the form of 19 heat maps (Figure 1.10) represent the probable origin of death for each individual dolphin. In each of the heat maps, red areas show the most probable origin of death, with 50% of the particles originating from the red regions. As the color changes from red to green, the probability of the origin of death decreases, and the green areas are the least probable origins with a probability of origin of 5%. According to Figure *1.10*, the distance that each dolphin's body traveled after death until it was beached ranges between 4 and 80 km. The average distance is 38.5 km.

The results show that the primary place of death for 14 of the 19 dolphins (12 stranded on the beaches of Mississippi and two stranded on barrier islands) was west of their stranding location. The two dolphins stranded around Dauphin Island on August 30th and November 3rd died in the Mobile Bay area north of the location they were found. The three remaining dolphins that were found on the barrier islands originally died in close proximity to their stranding location. These results should not be used to infer the direction of dolphin drift in other years. BC Spillway

openings divert an enormous amount of water and likely impact currents and resulting carcass drift.

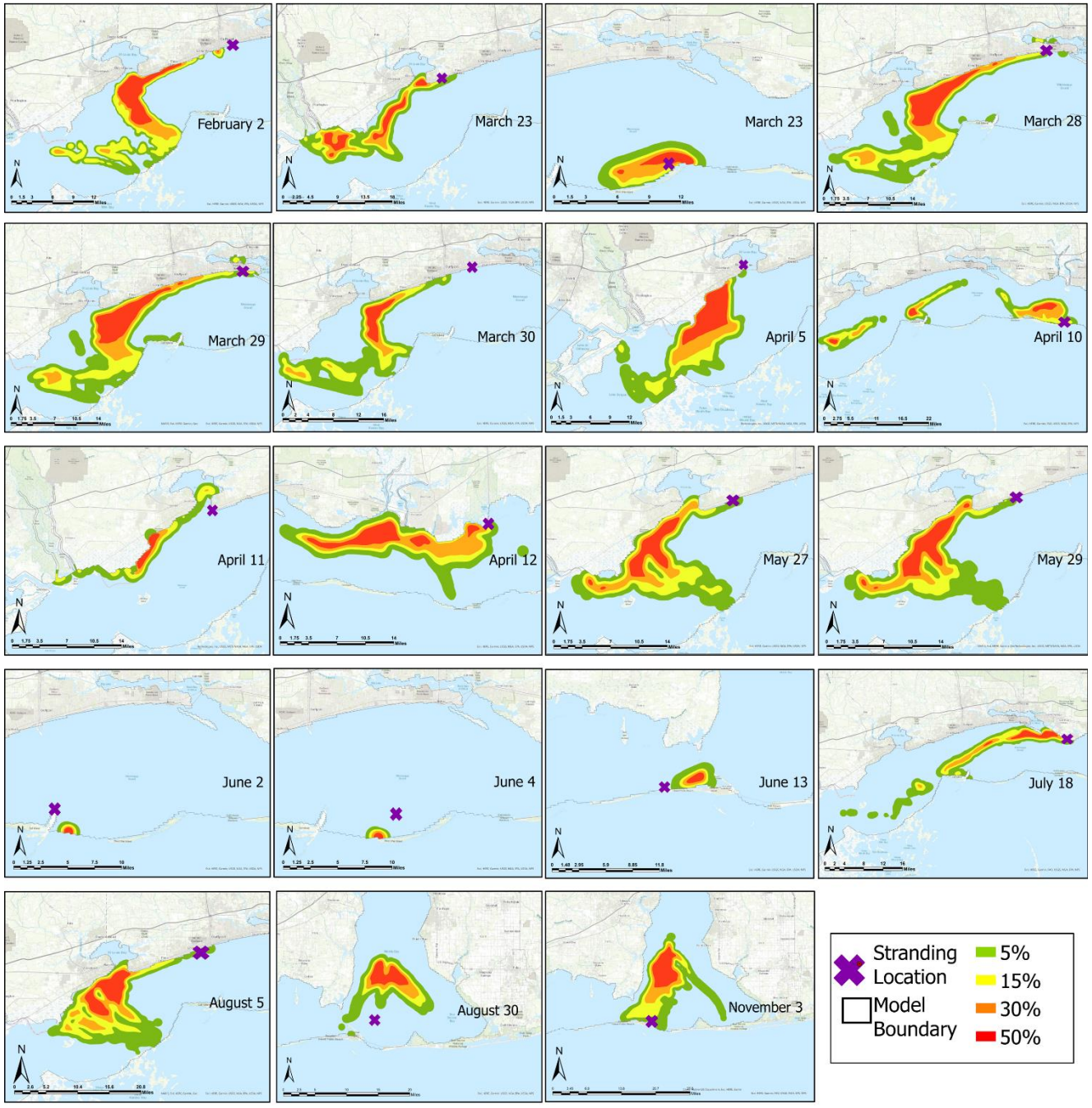

Figure 1.10- Hotspot maps indicating the likely initial locations of death for freshly dead dolphins from February to November 2019. Red areas are where the probability of the origin is the highest (50%) and green shows where the probability is the least (5%).

Next, the average salinity of the most probable location of death for each dolphin (red cells in Figure 1.10) was obtained from the hydrodynamic model of the MSS during the five-day tracking period for each of the stranded animals. Figure 1.11 shows a time series of the simulated average salinity for each individual carcass. The critical salinity for the dolphins to live for short periods of time is five and for longer periods is ten (Deming et al., 2020; Takeshita et al., 2021). As the plots show, in all the cases, the average salinity of the most probable origin in the tracking period is less than four. The only exceptions are the dolphins found stranded on February 2nd near the Gulfport, which died before the BC Spillway openings in 2019 and the dolphin found stranded on July 18th. Although there are numerous other factors that should be analyzed to come to a conclusion, these results reinforce that the low salinity in the Mississippi Sound is a potential reason for the unusually high number of dolphin deaths between February and November 2019.

Due to salinity over or under prediction by the hydrodynamic model, an uncertainty band was created around each of the average plot lines in Figure 1.11 based on the absolute average salinity difference between the measured and modeled salinities using the data from Merrill Shell, St. Joseph, and Gulfport Light USGS stations. This method was used in order to account for the maximum uncertainty between the simulated and measured salinity. Even by considering the model's uncertainty, the salinity is still lower than 10 in 16 cases out of the 19 examined. Also, two out of the three exceptions (Feb. 2nd and Aug. 30th) did not occur during the BC Spillway opening times. Also, the considerable uncertainty of these two dates (Feb. 2nd and Aug. 30th) is due to missing salinity data in the Near Grand Pass open boundary.

One of the reasons for the decrease in the MSS salinity is the BC Spillway opening. According to the US Army Corps of Engineers, there were two openings in 2019. This event which released flood waters in both the spring and summer, had severe consequences. It led to the closure

of 25 Gulf Coast beaches due to a toxic algal bloom, a significant number of dolphin deaths, and the complete loss of shellfisheries in many areas of the MSS (Gledhill et al., 2020; Hendon et al., 2020). The average flow from the BC during 2019 was 3830 m^3/s in the first opening and 3370 m^3/s in the second opening.

Another potential reason for low salinities in the region may be local riverine flows. The nearest large freshwater sources in the area are the Pearl River, and Pascagoula River. Average annual high flows varied between 1194 m^3/s and 1583 m^3/s in the Pearl River and between 1132.67 and 3539.6 m^3/s in the Pascagoula River in the years 2018 and 2019. The flows from the Pearl River, Pascagoula River, Mobile River and BC Spillway from March 2018 to April 2020 are compared and the flow from BC Spillway openings was more than two times the Pearl River and Pascagoula River flows in 2019 during the BC Spillway openings (Figure 1.12).

Armstrong et al., (2021) simulated the 2019 spillway openings (BCS) and compared them to a simulation with only riverine forcing. This allowed us to analyze the impact of spillway diversion and riverine forcing on oceanic variables separately. They found that the 2019 BCS led to an average of 17 cumulative days and 23 consecutive days of bottom salinity below 2 in the Mississippi Sound (MSS). Additionally, central and western MSS experienced over 40 consecutive days of low salinity bottom water. Oyster reef locations near Bay St. Louis and Biloxi Bay, encountered 40 to 60 days of low salinity bottom water during the spring BCS opening and an additional 50 to 100 days during the summer opening.

Boxplots in Figure 1.13 compares the distribution of salinity values associated with the most probable origin of death for each individual dolphin in three different scenarios, 1) during the BC Spillway opening days in 2019, 2) During the non-opening days in 2019, 3) and during the likely time of death period for each of the 19 dolphins. The results indicate that for all the dolphin

data, the average salinity of their original location of death is very low and similar to the average salinity of the BC Spillway opening dates.

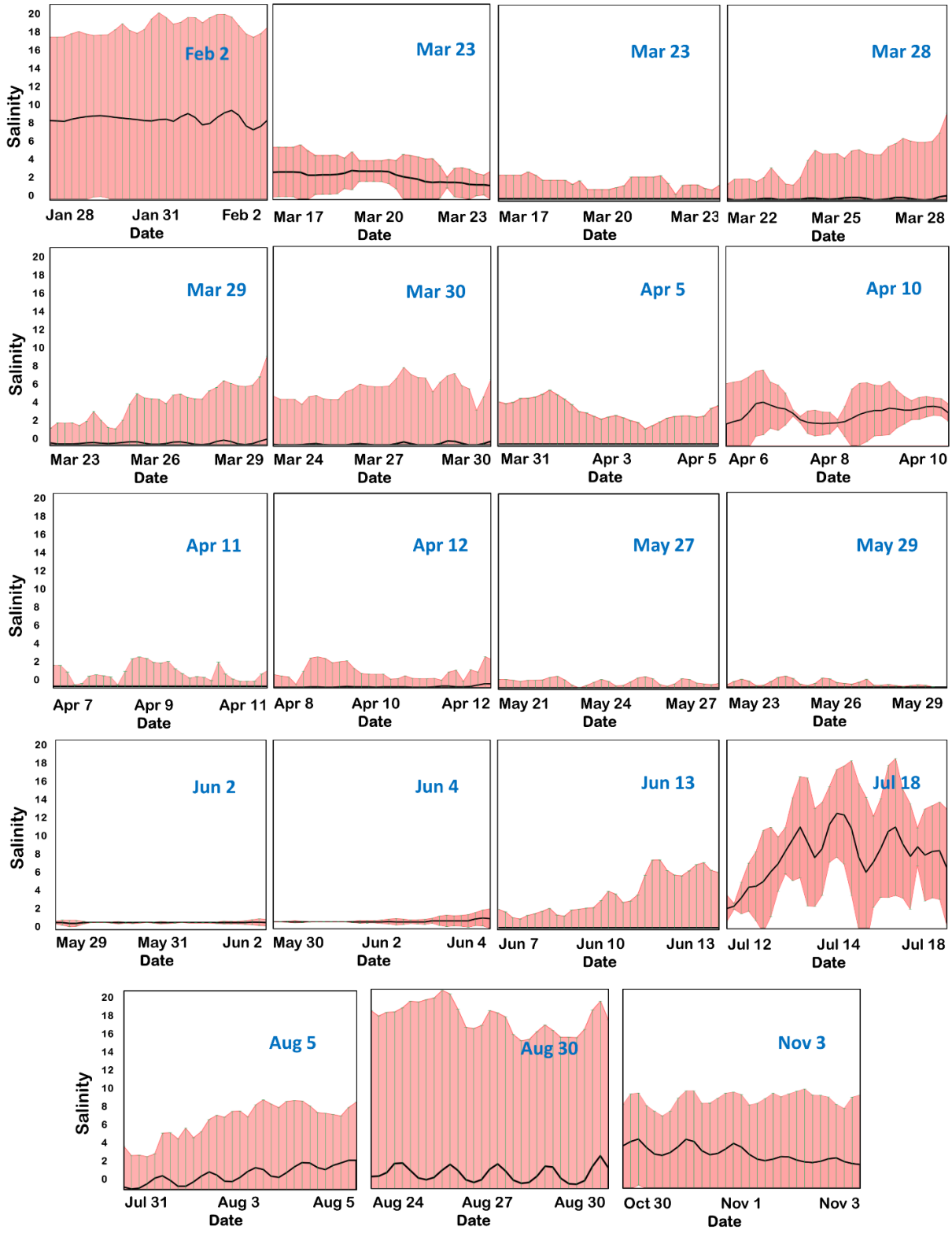

Figure 1.11- Average salinity of the most likely locations of death (red areas in the previous figure heat maps) for each stranded dolphin data along with the uncertainty bounds created around the average salinity of the most likely locations of death to account for the model's over and under predictions.

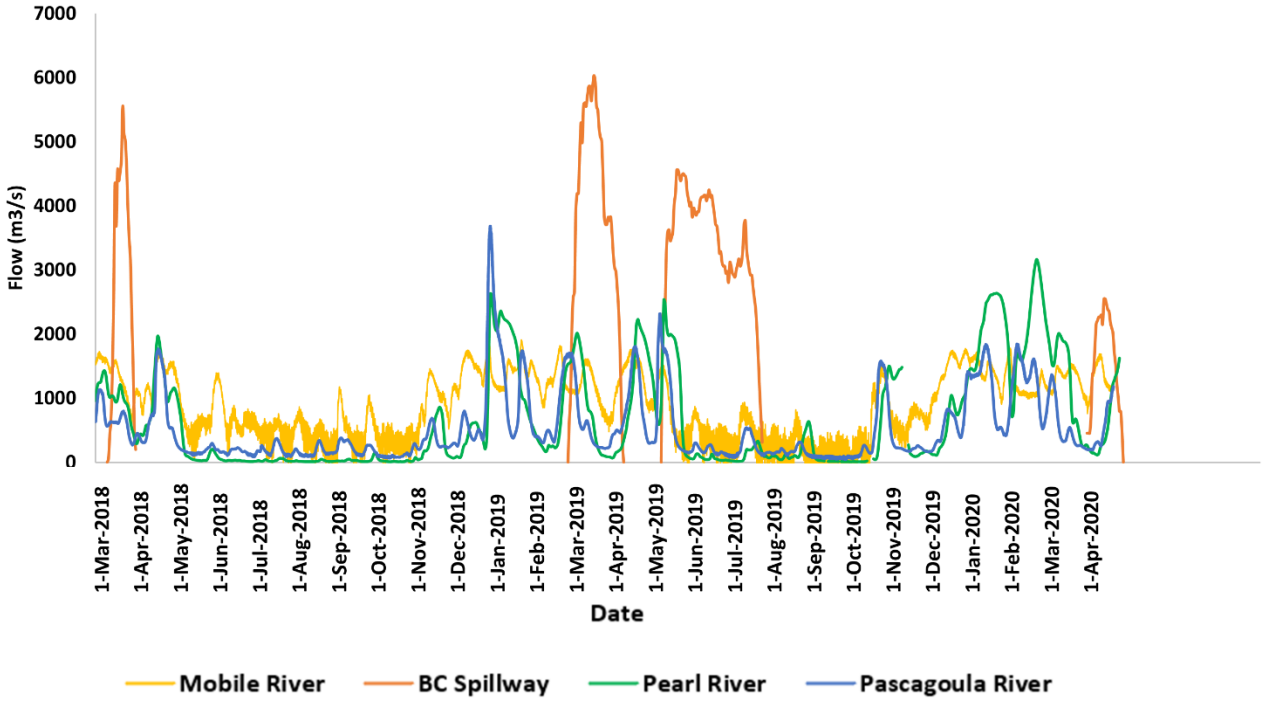

Figure 1.12- Flows from the Pearl River (Pearl River at Pearl station), Pascagoula River (Pascagoula River at Graham Ferry), Mobile River (Mobile River at River Mile 31) and BC Spillway from March 2018 to April 2020

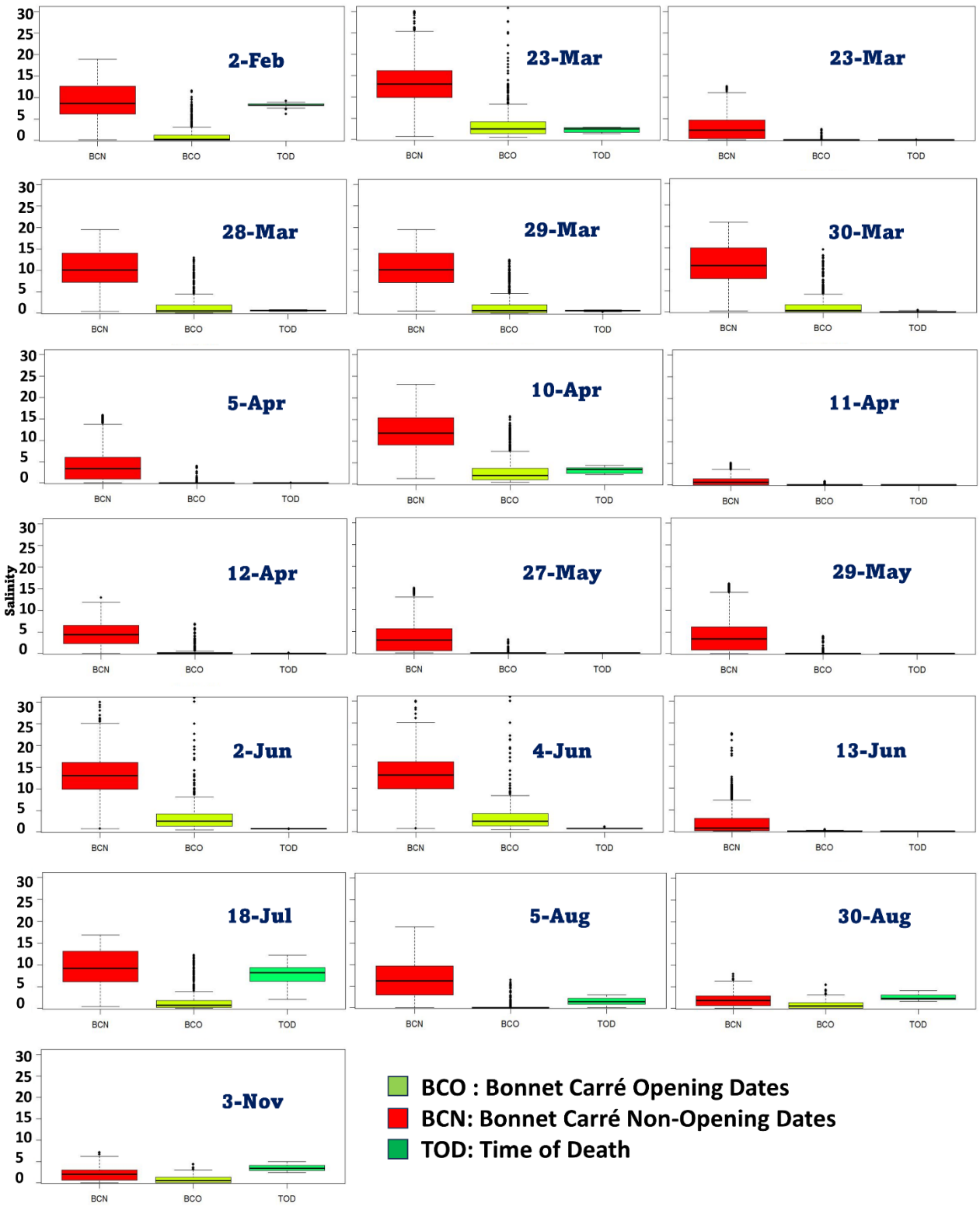

Figure 1.13- Boxplots comparing the salinity of the predicted initial locations of death for each individual dolphin at the Bonnet Carré opening dates, the time of death, and the non-opening dates.

1.6 Conclusion

A drifter simulation representing floating dead dolphins was performed using Lagrangian particle tracking in a hydrodynamic model of the MS Sound. The results simulate the initial location of 19 freshly dead dolphins stranded on the beaches of MS in 2019. A Kernel density estimation analysis was performed, which shows the likelihood of each dolphin's location at its time of death. In most cases, the dolphins died south and west of the stranding location and the average distance traversed by the particles was 38.5 km. Secondly, the average salinity of the probable time of death at the most probable location of death was calculated using the salinity data from the hydrodynamic model. The average salinity for 17 of the 19 dolphins was lower than five and considering the models under-predictions the average salinity for 16 of the 19 dolphins was lower than ten, which respectively is estimated to be the critical dangerous salinity for dolphins in short and prolonged periods of time (Deming et al., 2020; Takeshita et al., 2021). Finally, an examination was conducted to assess the impact of the BC spillway opening on the salinity levels at the initial locations of death. The findings reveal a greater alignment between the mean salinity levels at these locations and the salinity levels observed on days when the spillway was opened, as opposed to non-opening days. These results suggest a relationship between dolphin mortality and BC spillway openings in 2019.

Chapter 2

2. Sensitivity Analysis and Calibration of Lagrangian Particle Tracking in a Hydrodynamic Model of the Mississippi Sound Using GPS-Tagged Drifters

2.1 Abstract

A hydrodynamic model of the Mississippi Sound incorporating a Lagrangian Particle Tracking (LPT) module is used. The current research utilizes six GPS-tagged drifter data collected on April 2017 by researchers in NOAA, to conduct a sensitivity analysis on the LPT model and further calibration. This analysis delves into the influence of specific parameters, notably the wind drag and model dimensionality. Alterations to these parameters resulted in observable changes in the trajectories of tracked particles. The results of the sensitivity experiments were compared using the Skill score (SS) proposed by Liu and Weisberg (2011). Adding wind drag to the LPT was found to be a pivotal alteration, substantially augmenting the model's predictive capabilities by increasing the SS value from 0.4 to 0.7. In particular, an examination of the impact of varying wind drag coefficients implemented in the EFDC+ software, revealed that coefficient A has a larger impact on the models predictions compared to coefficient B. Finally, the results suggested that the transition from a two-dimensional (2D) to a three-dimensional (3D) model improves the model slightly, increasing the SS value by 0.02, but doesn't have a notable influence on the model's accuracy. The study's results have valuable implications for coastal management, disaster response, and environmental monitoring including the cetacean stranding events.

Keywords—Hydrodynamic model, Lagrangian particle tracking, Drifter data, Sensitivity analysis, EFDC+, Mississippi Sound, 2D vs. 3D model, Wind drag, Calibration.

2.2 Introduction

Lagrangian particle tracking (LPT) is a widely used technique in hydrodynamic modeling for tracing the origins and destinations of drifting objects or water masses (Mariano et al. 2002). In the realm of oceanography, this methodology finds application in assessing the risk of toxic algae blooms (Havens et al. 2010), investigating larval transport and connectivity for fishery management (Nicolle et al. 2013; Robins et al. 2013; Bidegain et al. 2013) and oil spill responses (Broström et al. 2011; Yang et al. 2013; Anguiano-García et al. 2019; Liu et al. 2013; Ribotti et al. 2018; De Dominicis et al. 2013). Additionally, Lagrangian transport simulations play a crucial role in tracking plastic debris, contributing to an enhanced understanding of its dispersion within the ocean (Iskandar et al. 2022; Iskandar et al. 2021; Duhec et al. 2015; Kako et al. 2014; Lebreton and Andrady 2019; Liubartseva et al. 2018; Maximenko et al. 2012; Seo and Park 2020). Lagrangian Drift models are extensively utilized to simulate stranding events for various large, floating aquatic species, including sea turtles (Nero et al. 2013; Santos et al. 2018); Portuguese man-of-war (Headlam et al. 2020; Ferrer et al. 2015; Ferrer and Pastor 2017); and stranded cetacean carcasses such as pygmy sperm whales (Harlan 2014), fin whales (Díaz-Gamboa et al. 2022), humpback and bryde whales (Junior et al. 2019), harbor porpoises (Peltier et al. 2012; Haelters et al. 2006), cuvier's beaked whales (Carlucci et al. 2020), short-beaked common dolphins (Gilbert et al. 2021; Peltier et al. 2012), and bottlenose dolphins (Wirasaet et al. 2015; Shahidzadehasadi et al. 2023).

In Lagrangian particle tracking studies, measured data is obtained from oceanographic instruments, known as drifters, which are small, floating buoys or devices designed to passively drift along with ocean currents. These drifters are often equipped with GPS or satellite tracking systems, enabling researchers to monitor their movement as well as collect additional data,

including surface currents, sea temperature, and wave characteristics. Drifter data plays a pivotal role in understanding ocean circulation patterns, examining marine ecosystems, and tracking the dispersion of pollutants or floating objects.

Accurate calibration of LPT models is essential to ensure reliable predictions of particle trajectories and dispersion behavior. The calibration process involves refining the model parameters to match observed particle behavior and optimize the accuracy of simulated particle paths within the fluid flow. Calibration ensures that the simulated trajectories closely match real-world particle movement, enhancing the model's reliability for various scientific and engineering applications. Sensitivity analysis (SA) is another vital tool in modeling, focusing on identifying key parameters influencing model performance. SA plays a crucial role in model parameterization, calibration, optimization, and uncertainty quantification. It evaluates how changes in input parameters impact model outcomes, helping prioritize calibration efforts for the most influential parameters (Song et al. 2015).

SA, calibration. and validation of LPT models has been carried out in numerous studies using drifter data (Abascal et al. 2009; Callies et al. 2017; De Dominicis et al. 2013; Liu and Weisberg 2011; Ribotti et al. 2018; van der Mheen et al. 2020; Ferrer et al. 2015; Nero et al. 2013; Huntley et al. 2011). Various software tools were employed for LPT and hydrodynamic modeling in these studies. Abascal et al. (2009) used PICHI (Castanedo et al., 2006), while De Dominicis et al. (2013), as well as Ribotti et al. (2018) employed MEDSLIK-II. Callies et al. (2017) used the PELETS-2D module (U. Callies, 2016) alongside two independent models, BSHcmod and TRIM. Liu and Weisberg (2011) employed HYCOM, van der Mheen et al. (2020) used OceanParcels-v2 (Lange and Sebille, 2017; Delandmeter and Van Sebille, 2019), Huntley, Lipphardt, and Kirwan (2011) used the US Navy's EAS16 model which is adapted from the operational NCOM (Navy

Coastal Ocean Model) (P. Martin 2000), and Ferrer et al. (2015) made use of the Regional Ocean Modeling System (ROMS) (Debreu et al. 2012) in conjunction with the Sediment, Oil spill, and Fish Tracking model (SOFT).

The cited publications cover a range of geographical areas. Abascal et al. (2009) and Ferrer et al. (2015) focused their investigations on the Bay of Biscay extended from Cape Ortegal, northwestern Spain to the French coast. De Dominicis et al. (2013) conducted their study in the Mediterranean Sea. Callies et al. (2017) examined the German Bight in the North Sea, while Liu and Weisberg (2011) centered their research on the Gulf of Mexico. Ribotti et al. (2018) conducted their analysis in the Italian Sea, specifically the Sicily Channel and the Adriatic Sea areas. Huntley et al. (2011) study domain was the East China Sea. Finally, van der Mheen et al. (2020) explored the Rottnest Shelf in Western Australia.

Among the aforementioned publications, only Abascal et al. (2009); Ferrer et al. (2015); and Nero et al. (2013) calibrated their LPT models, and only De Dominicis et al. (2013); and Huntley, Lipphardt, and Kirwan (2011) performed a SA. The remaining studies primarily focused on model validation through the use of drifter data. Abascal et al. (2009) used an automated method to calibrate wave coefficient (CH), current coefficient (CC), and α and β, which represent the wind drag coefficient (CD). The parameters that L. Ferrer et al. (2015) clibrated include CROMS and CWRF, which are the current coefficient and wind drag coefficient, respectively. Finally, Nero et al. (2013) calibrated their model by changing the leeway drift coefficient (K), which refers to the movement of sea turtles on the surface of the water due to the influence of wind and currents. De Dominicis et al. (2013) specifically conducted a SA on their model, examining its responsiveness to various factors such as horizontal current resolution, time frequency, depth of currents, local wind correction, and Stokes velocity. Huntley, Lipphardt, and Kirwan (2011) conducted SA on

the removal of the near-surface tidal velocities, changes in launch location, and changes in launch time.

To our knowledge, there exists a notable research gap related to the simultaneous application of SA and model calibration within the context of LPT models, particularly in the context of calibrating dolphin carcass movement using drifter data. Furthermore, there is a lack of studies examining model sensitivity to dimensionality and the distinctions between 2D and 3D configurations. This research aims to bridge these knowledge gaps through a SA and calibration of a hydrodynamic Largangian particle tracking model that simulates bottlenose dolphin carcass movement using the EFDC+ model software within the Mississippi Sound and Mobile Bay, northern Gulf of Mexico.

In this study, two types of GPS-tagged drifter data were provided by Cook et al. (2021), including turtle carcasses and wooden effigies designed to reproduce turtle carcass drift. Data from these drifters were utilized to: (1) conduct a SA on a LPT module to the wind drag existence, dimensionality (including 2D vs. 3D model), and wind drag coefficients A and B within an existing hydrodynamic model previously simulated by Shahidzadehasadi et al. (2023); and (2) calibrate the model using the results from the SA. This study contributes valuable insights into the applicability and reliability of LPT techniques in understanding ocean dynamics and ecological processes, with implications for various environmental and marine management applications.

2.3 Study Area and Data

2.3.1 Study Area

The study area consists of the Mississippi Sound (MSS) and Mobile Bay. The MSS is a large, shallow, and semi-open sound located in the north-central Gulf of Mexico. The MSS has a surface area of 2,129 km2, an average depth of 2.98 m at mean low water and a salinity range of 0-35. From east to west, the MSS extends from Cedar Point, AL, to Half Moon Island, LA, and is bordered to the north by Mississippi and Alabama and to the south by Bay Boudreau, LA, and five barrier islands: Dauphin, Petit Bois, Horn, Ship, and Cat. It connects with the Gulf through passes between a series of five barrier islands. Mobile Bay is a shallow estuary in the northern Gulf of Mexico, extending 48 km long and ranging from 14–34 km wide. The relatively shallow uniform bathymetry averages 3 m, except for the shipping channel, which is 12 m deep. Mobile Bay is connected to the MSS through the Pass Aux Herons outlet in the southwest. The MSS and Mobile Bay are ecologically and economically important areas (Scircle et al. 2020), hosting a diverse range of habitats and species, including oyster reefs (MacKenzie Jr 1997) and several species of fish and marine mammals (Mullin et al. 2004).

2.3.2 Data

In a previous investigation conducted by the National Oceanic and Atmospheric Administration (NOAA), GPS-tagged sea turtle carcasses and effigy drifters were deployed in the coastal and offshore waters of the northern Gulf of Mexico during May 2017 (Cook et al. 2021). While Cook's original study represented turtle drift, I use the same data to represent dolphin drift due to similar the size and buoyancy of the carcasses. The drifters deployed by NOAA were not entirely contained within our model domain. Therefore, a subset (n = 6) of the larger NOAA data

was chosen that either remained within the domain throughout the observation period or entered the domain at some point during their trajectory (Table 2.1 and Figure 2.1). Moreover, preference was given to those drifters with relatively straightforward and uncomplicated trajectories.

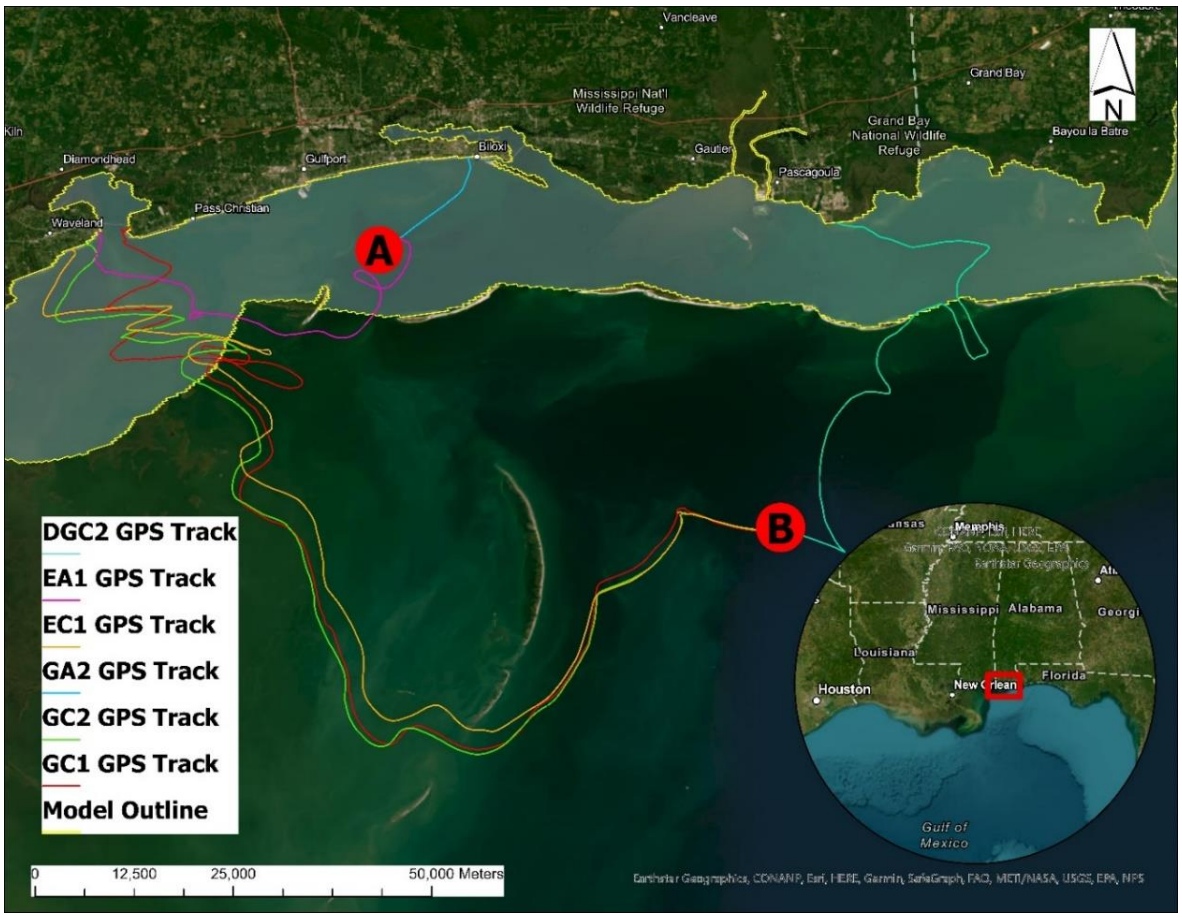

Figure 2.1- GPS-tagged sea turtle carcasses and effigy drifters data in the nGOM in 2017 collected by (Cook et al. 2021). A and B are the locations where the drifters were released from.

Drifter	ID	Release Station	Drifter release time/date	Stranding time/date
Turtle-Green	GC1	B	4/12/2017 11:19	4/22/2017 8:27
Turtle-Green	GC2	B	4/12/2017 11:19	4/20/2017 12:08
Effigy	EC1	B	4/12/2017 11:19	4/20/2017 9:36
Effigy	EA1	A	4/12/2017 9:18	4/16/2017 2:23
Turtle-Green	DGC2	B	4/25/2017 9:35	4/29/2017 10:20
Turtle-Green	GA2	A	4/25/2017 13:13	4/26/2017 8:10

Table 2.1 - Turtle and effigy data provided by (Cook et al. 2021).

2.4 Methods

2.4.1 Hydrodynamic Model

An existing 2D hydrodynamic and water quality model of the MSS simulated in Environmental Fluid Dynamic Code Plus (EFDC+) version 11.2 was used for this study (Shahidzadehasadi et al., 2023; Armandei, Linhoss, and Camacho 2021). The EFDC+ software is a modeling tool engineered for simulating aquatic systems across one, two, and three dimensions. (DSI LLC., 2023; EFDC+ Source Code, 2022). The hydrodynamic model employed in this study was initially developed by Armandei, Linhoss, and Camacho (2021). Over time, the model's grid was expanded to encompass Lake Pontchartrain and Mobile Bay. Subsequently, Shahidzadehasadi et al. (2023) integrated an LPT module into the model to track the origins of mortalities for stranded dolphins along the shores of Mississippi and Alabama. In this study, the grid from Shahidzadehasadi et al. (2023) was modified to exclude the Isle Aux Herbes and Gaillard Island in the east and the Grand Island in the west of the model domain. Currently, the model is composed of a computational curvilinear grid consisting of 70,674 cells (245 rows and 962 columns), which covers an area of 5,678.8 km^2 extending from Lake Pontchartrain (LA) in the east to Mobile Bay (AL) in the west.

The unit system is metric, the projection or horizontal datum is WGS 1984, and the vertical datum is NAVD88.

Several modifications have been implemented regarding the model's open boundary conditions. Firstly, the number of water level time series data was expanded from two to three, with the addition of water level data from the Dauphin Island station (Dauphin Island Sea Lab 2023). These revised boundary conditions are depicted in Figure 2.2. Secondly, adjustments were made to eliminate the offset between the measured water level data from East Ship, Near Grand Pass, and Dauphin, ensuring uniformity and consistency in the data. Table 2.2 presents the amount subtracted from each water level data time series and average water level data after the removal of the vertical offset.

Open Boundary	**Amount added (m)**	**Average Water Level (m)**
Near Grand Pass	- 0.5857	0.3085
East Ship	0	0.3088
Dauphin	- 1.7926	0.3085

Table 2.2- Open boundary conditions used in the hydrodynamic model.

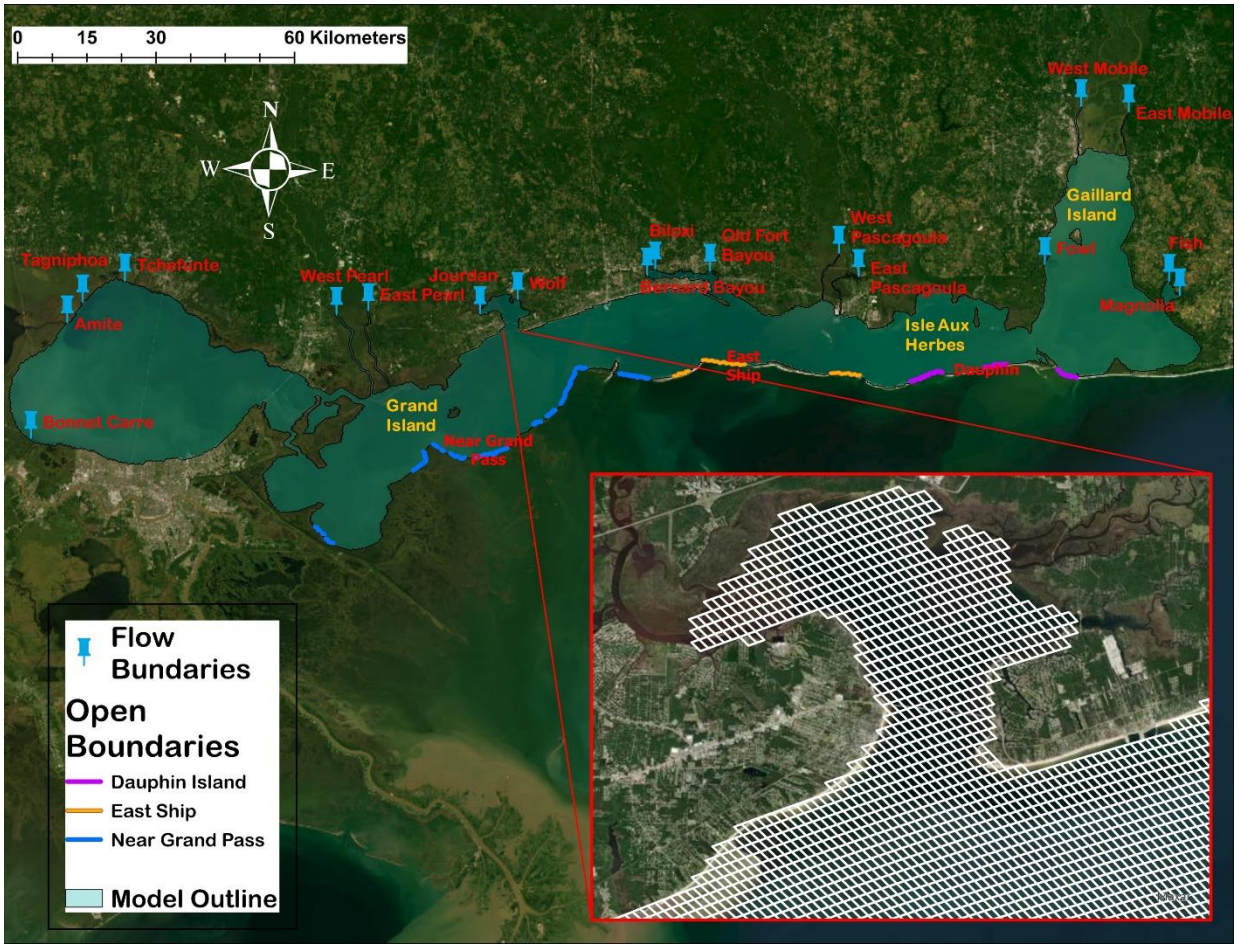

Figure 2.2- New model boundary conditions set-up.

The hydrodynamic model utilized in Shahidzadehasadi et al. (2023) integrated data from five distinct wind stations, as depicted in Figure 2.3. Table 2.3 shows the average wind velocity and direction recorded at each of these stations. Notably, in this investigation, equal weighting was assigned to all wind stations, signifying that the data from each station held equal significance within the model's computations. A visual representation of this equitable weighting scheme for each station can be found in Figure 2.4.

Station Name	Average velocity (m/s)	Average Direction
Slidell airport	2.228	192.04
Bay St. Louis Stennis International Airport	4.061	198.24
Gulfport Biloxi airport	2.964	205.03
Biloxi Keesler AFB	3.384	185.73
Pascagoula Lott international airport	1.992	193.09

Table 2.3- Average wind velocity and direction of the wind stations used in the model

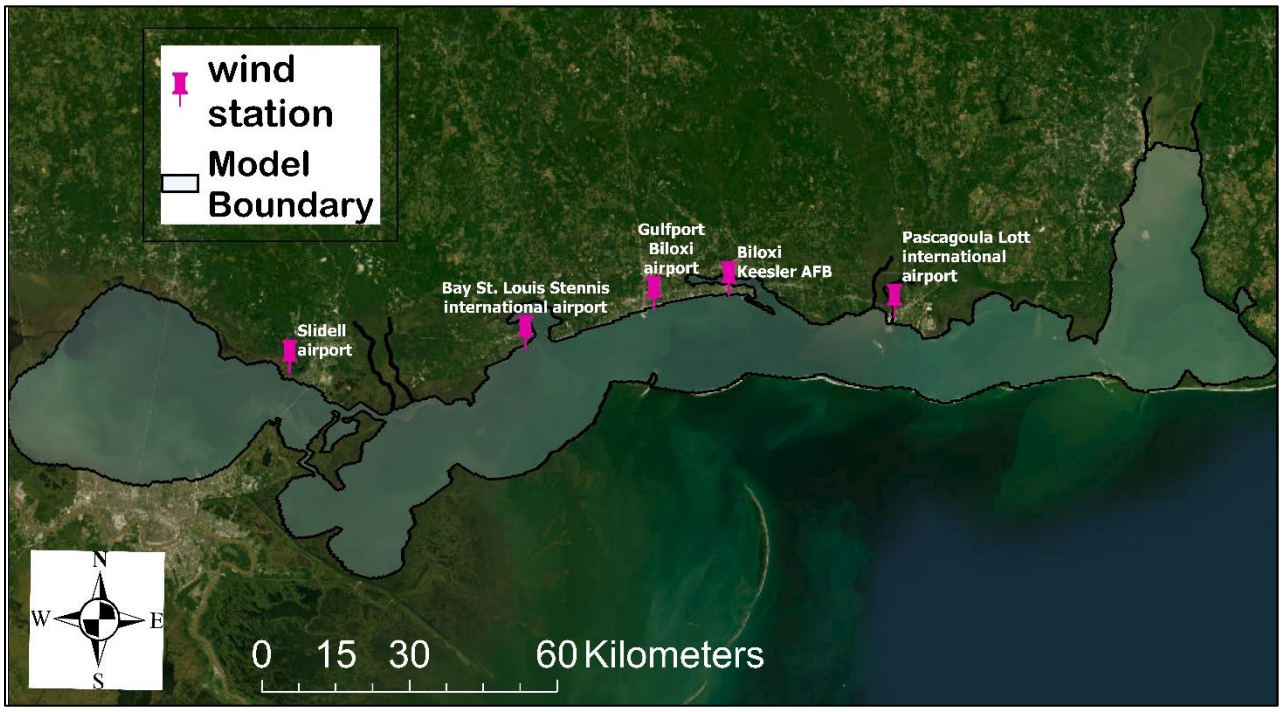

Figure 2.3- Location of the wind stations used in the hydrodynamic model.

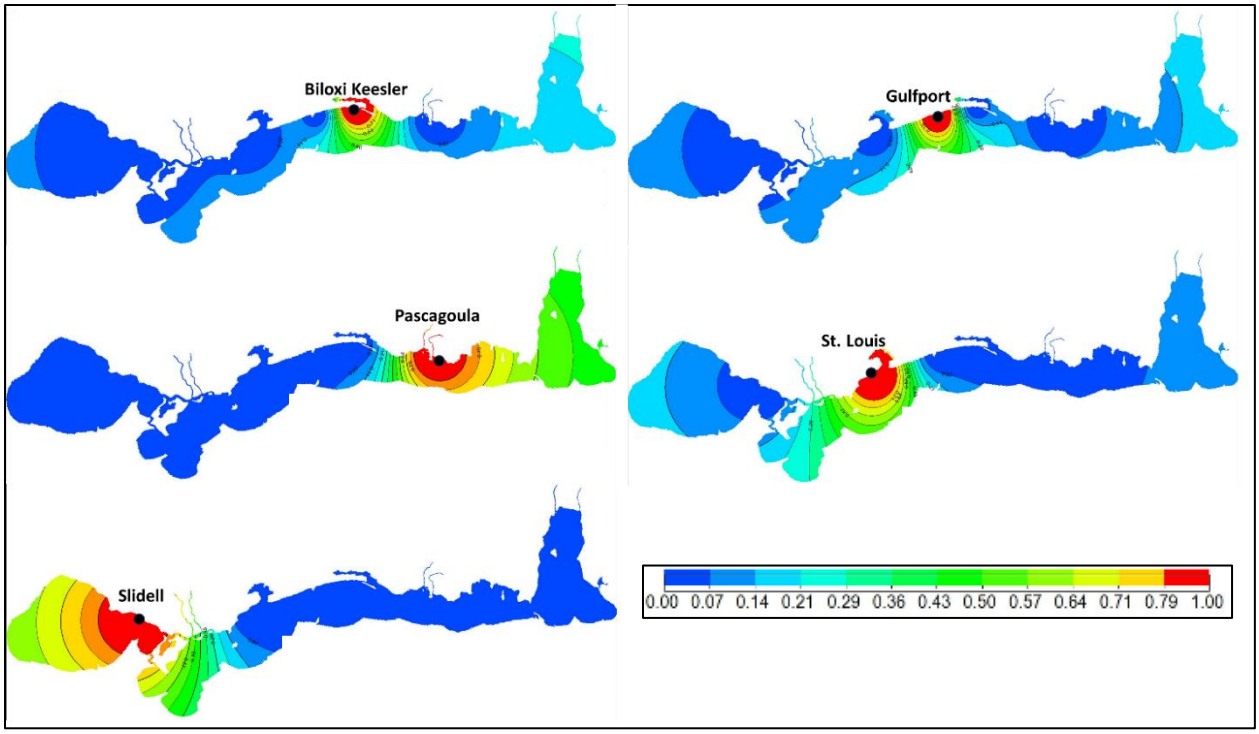

Figure 2.4- Wind weighting (%) of the five wind stations used in the hydrodynamic model.

2.4.2 Lagrangian Particle Tracking

The LPT is a powerful tool used to simulate the movement of particles or tracers in a fluid flow field. Lagrangian particles move along with the fluid velocity field, which means that the simulation of drifters is linked to a fluid flow model. The governing equations for fluid flow in the EFDC+ modeling software are the Navier-Stokes and advection-diffusion equations for salinity, temperature, dye, toxic substances and suspended sediment transport. (DSI LLC. 2023). The advection-diffusion equation for mass transport in a three-dimensional curvilinear orthogonal coordinate system is expressed in Equation 2.1, while Equations 2.2-2.4 illustrate the differential equations for the Lagrangian movement of drifters in the x, y, and z coordinates.

$$\frac{\partial C}{\partial t} + \frac{\partial (uC)}{\partial x} + \frac{\partial (vC)}{\partial y} + \frac{\partial (wC)}{\partial z} = \frac{\partial}{\partial x}\left(A_H \frac{\partial C}{\partial x}\right) + \frac{\partial}{\partial y}\left(A_H \frac{\partial C}{\partial y}\right) + \frac{\partial}{\partial z}\left(A_b \frac{\partial C}{\partial z}\right) \quad \text{Eq. 2.1}$$

$$dx = \left(u + \frac{\partial A_H}{\partial x}\right) dt + (2p - 1)\sqrt{2A_H dt} \quad \text{Eq. 2.2}$$

$$dy = \left(v + \frac{\partial A_H}{\partial y}\right) dt + (2p - 1)\sqrt{2A_H dt} \quad \text{Eq. 2.3}$$

$$dz = \left(w + \frac{\partial A_b}{\partial z}\right) dt + (2p - 1)\sqrt{2A_b dt} \quad \text{Eq. 2.4}$$

The variables (u, v, w) in this equation correspond to the Lagrangian velocity vectors along the (x, y, z) axes. A_H and A_b are the coefficients of horizontal and vertical diffusion, respectively. C denotes the concentration, dt represents the time step, and p is a random number produced from a random variable. Equations 2.2 to 2.4 contain numerical solutions that are comprised of two parts. The first term on the right-hand side accounts for advective transport, while the second term calculates random movements. Each of these terms can be modified independently, and the random movement term can be utilized or not.

Wind drag indicates how much resistance the air exerts on the water's surface when wind blows over it and has a significant impact on how wind affects the flow of water. Wind drag directly influences the strength and direction of surface currents, which in turn affects the movement of water within the MSS. When particles are situated on the water's surface, such as drifters, wind drag can also influence their movement. To account for this effect, the EFDC+ module uses wind drag calculations according to the drag parameters from Kim et al. (2014) in addition to the advection-diffusion movements.

$$V_{\text{particle}} = V_{\text{current}} + (CD \times V_{\text{wind}}) \quad \text{Eq. 2.5}$$

Where the wind speed used is at the height of 10 m, and CD is the wind drag coefficient in EFDC+, equation 5.

$$CD_x = A \times V_{windx} + B \quad \text{Eq. 2.6}$$

$$CD_y = A \times V_{windy} + B \quad \text{Eq. 2.7}$$

In equations 2.6 and 2.7, coefficient A has units expressed in s/m, while coefficient B has no unit of measurement. CD is also dimensionless, and the velocity terms are all given in m/s. If A is equal to zero, a constant drag coefficient is employed. The CD values can range from 0.0 to 0.1 but generally fall between 0.02 to 0.03.

Another crucial factor that contributed to a more realistic simulation was the inclusion of no wall slippage. This means that once particles hit a nearby boundary, their velocity becomes zero, causing them to become beached particles.

2.4.3 Seeding Particles

In this research, an examination is conducted on six particles, each representing one of the six drifters. The initial positions of the drifters in their respective cells determine the starting locations for each particle group. Among the six sets of drifters, five have initial release points outside the model domain. To address this, the initial seeding point for each particle group was selected after the drifters entered the model domain. To avoid boundary effects, the drifters were not simulated until they were well within the spatial domain (Figure 2.5). These particles were released on the same date that the drifters were released within the respective cells. Subsequently, their trajectories were tracked forward in time until they either reached the shoreline or exited the model domain. This methodology enabled us to precisely simulate particle trajectories and draw comparisons with the observed paths of the drifters. It should be noted that although each grid cell

covers an approximate area of 69,000 m^2, all the particles within the same group traverse a very similar path, and there is no need to seed them at the exact point where the drifters are released.

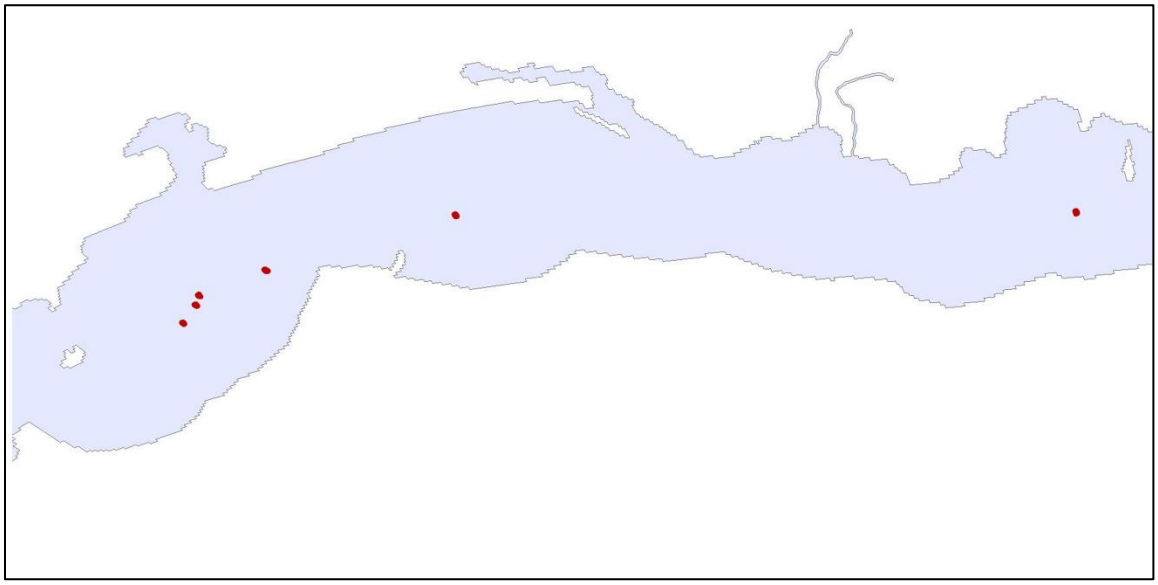

Figure 2.5- six particle groups' initial locations are shown.

2.4.4 Sensitivity Analysis

The sensitivity of model dimensionality, existence of wind, and wind drag parameters A and B were assessed. The SA was conducted by altering each parameter one at a time.

The first parameter investigated in the SA was the number of vertical layers. In hydrodynamic simulations, water columns are often divided into multiple layers or vertical cells. In this research, the model was initially set up with a 2D configuration, having only one vertical layer. The model was converted to 3D, and the layer count was increased to three and then to five

in order to understand the influence that altering the number of layers has on the model results (Table 2.4).

	Scenario 1	Scenario 2	Scenario 3
Number of layers	1	3	5
Wind Coeff A	0.005	0.005	0.005
Wind Coeff B	0.015	0.015	0.015

Table 2.4- Designing of three scenarios changing vertical layering.

In the second experiment, the impact of the existence of wind on the predictive accuracy of the model was examined. A comparative analysis of the model's results was conducted under two different scenarios: one where wind drag was enabled and the other where it was disabled. By analyzing the differences between the two sets of results, insights into the extent to which wind affects the model's ability to make accurate predictions were gained.

In the third and fourth experiments, the sensitivity of the model to variations in coefficients A and B was investigated, respectively. I adjusted A and B by +/- 80% from their default values, as originally determined by Kim et al. (2014) (Tables 2.5 and 2.6). The default value for A is 0.005 and the default value for B is 0.015.

	Scenario 1	Scenario 2	Scenario 3
Number of layers	3	3	3
Wind Coeff A	0.005	0.009	0.001
Wind Coeff B	0.015	0.015	0.015

Table 2.5- Designing of three scenarios changing coefficients A.

	Scenario 1	Scenario 2	Scenario 3
Number of layers	3	3	3
Wind Coeff A	0.005	0.005	0.005
Wind Coeff B	0.015	0.027	0.003

Table 2.6- Designing of three scenarios changing coefficients B.

2.4.5 Calibration

Once the most important parameters were identified in the SA, I moved on to model calibration. It is important to note that the calibration process was manually executed and not automated. Calibration began by adjusting the most influential parameter within their permissible ranges calculated in the previous section (A between 0.001 to 0.009, and B between 0.003 to 0.027) and progressively moving to those with lesser impact. After each adjustment, statistical metrics were computed, ultimately leading to the final calibrated model.

The comparison between observed and simulated drifter trajectories in both SA and calibration was evaluated by two statistics. The first statistic is absolute error (AE), calculated from the separation distance between the observed and the simulated trajectories as a function of the simulation time (Eq. 2.8):

$$AE\ (t_i) = d_i(x_s(t_i), x_o(t_i)) \quad \text{Eq. 2.8}$$

Where d_i is the distance between the simulated (x_s) and the observed (x_o) drifter positions at time step t_i. This metric is useful for quantifying the evolving separation distance between the measured data and the model as the simulation time progresses.

The second statistic used is the skill score (SS) proposed by Liu and Weisberg (2011). It is a non-dimensional score that normalizes the cumulative separation distances by the lengths of the observed trajectories. In order to calculate SS, first, the s index should be calculated (Eq. 2.9).

$$s = \frac{\sum_{i=1}^{N} d_i}{\sum_{i=1}^{N} l_{oi}} \quad \text{Eq. 2.9}$$

Where l_{oi} is the length of the observed trajectory at the corresponding time, t_i and N is total number of time steps. This statistic tends to reduce the evaluation errors that may arise using the Lagrangian separation distance. Then, s is used to define a model SS (Eq. 2.10):

$$SS = \begin{cases} 1 - \frac{s}{n}, & s \leq n \\ 0, & s > n \end{cases} \quad \text{Eq. 2.10}$$

Where n is a dimensionless positive number that defines threshold of no skill (SS = 0). In this study, n = 1 is used based on Liu and Weisberg's (2011) suggestion that the cumulative separation distance should not exceed the accumulated length of the drifter's trajectory. The higher the SS value, the better the performance, with an SS = 1 implying a perfect fit between observed and simulated data and an SS = 0 indicating the model simulations have no skill. This statistic is used in several studies comparing measured and simulated particle trajectories (Röhrs et al. 2012; Lars Robert Hole, Cecilie Wettre, and Röhrs 2012; L. Ferrer et al. 2015).

2.5 Result and Discussion

2.5.1 Sensitivity Analysis

The sensitivity results are presented in three formats. The first format shows maps of the measured and simulated trajectories. The second format is the SS statistic, which provides a single

quantitative evaluation of the results. Lastly, the Absolute Error at a given time AE (t_i) is shown using plots of separation distance against the simulation time for each drifter.

In the first experiment the impact of the number of vertical layers in the hydrodynamic model was investigated. A 2D representation was employed in the initial model (1 layer), while in two subsequent scenarios, three and five layers were introduced (Table 2.4). In this experiment, wind was turned on and the A and B coefficients were set to the default values, 0.005, and 0.015 respectively. Due to the relatively smooth bathymetric variation in the model domain, the vertical coordinate was discretized using a sigma layer approach. As shown in Figure 2.6, a marginal difference in most of the cases was revealed when transitioning from the 2D model to the 3D model, as the particles' paths shifted westward in the 3D model compared to the 2D model, and the SS value increased slightly. However, the change of the number of layers from three to five did not significantly affect the results. Overall, the model displayed limited sensitivity to the number of vertical layers, as shown by the calculated SS values for the three experiments (Table 2.7). This demonstrates that the 2D model serves as a suitable representation of the study area, especially for running over longer periods of time where computational cost becomes an issue.

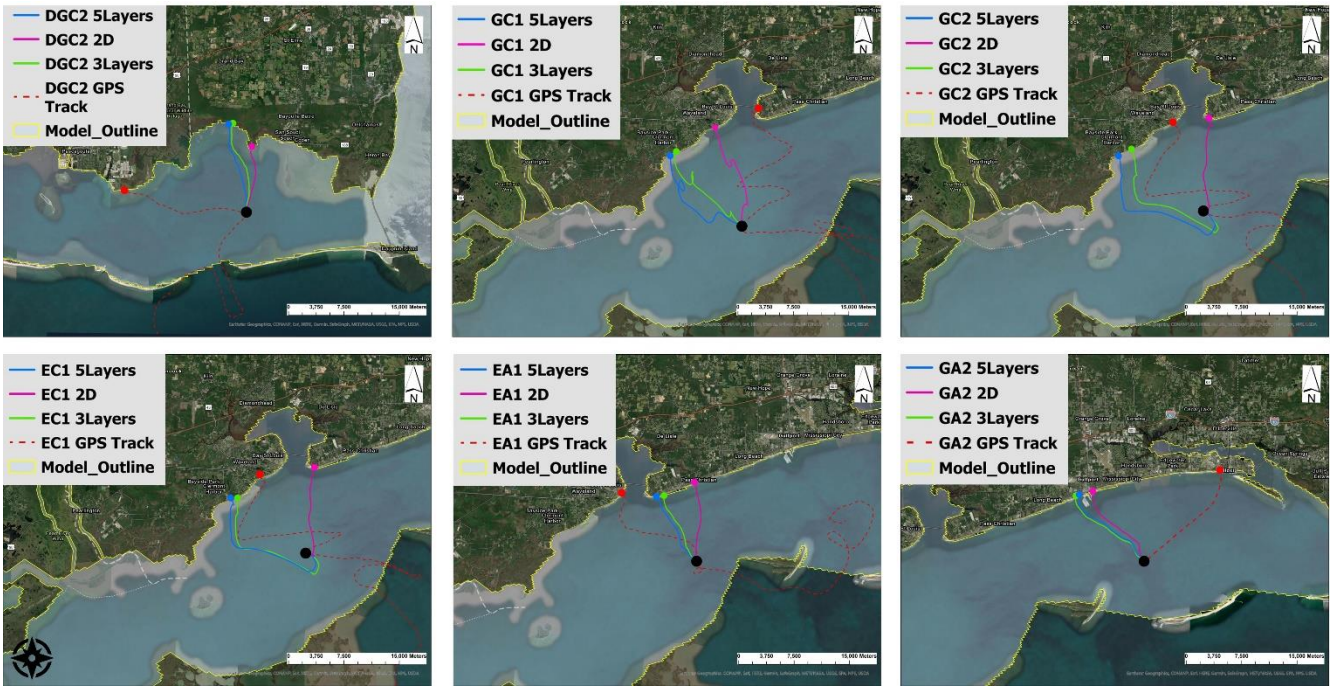

Figure 2.6- The result of changing the vertical layering. The pink line shows the 2D case, the green line shows the three vertical layers case, the blue line shows the five vertical layers case, and the dashed red line shows the drifter track line.

Particle Group	ec1	gc1	gc2	dgc2	ea1	ga2	Average
SS (2D; 1 layer)	0.79	0.83	0.83	0.66	0.77	0	0.64
SS (3D; 3 layers)	0.87	0.67	0.86	0.71	0.87	0	0.66
SS (3D; 5 layers)	0.88	0.63	0.83	0.72	0.88	0	0.66

Table 2.7- SS calculated for the 2D, 3D with three layers, and 3D with five layers models.

In the second experiment the existence of wind drag was examined. The model used in this experiment was 3D with three vertical layers, coefficient A was set to 0.005, and coefficient B was set to 0.015. Figure 2.7 and Table 2.8 depict the trajectories and statistics comparing the model with and without wind. When wind was turned off, model results were notably poorer. In contrast, when wind drag was turned on, trajectory prediction accuracy was significantly enhanced.

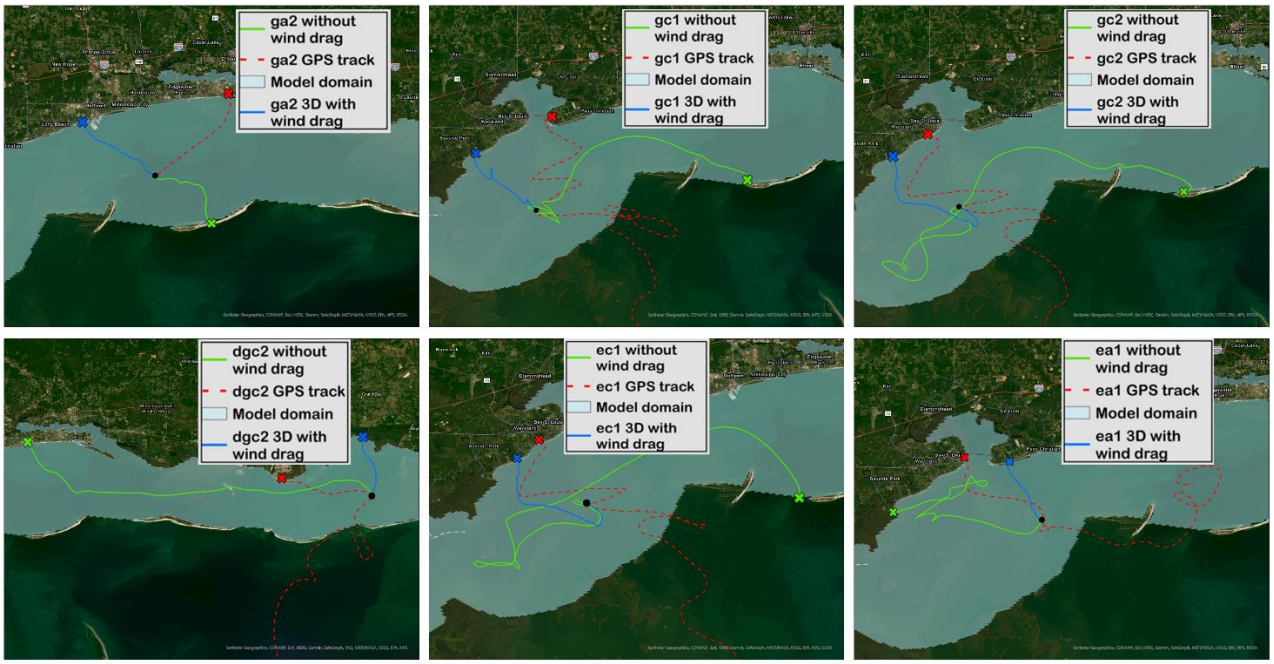

Figure 2.7- Wind drag effect on the accuracy of predicting particle trajectory. The green line shows the case excluding wind drag, the blue line shows the case including the wind drag, and the dashed red line shows the drifter track line.

Particle Group	ec1	gc1	gc2	dgc2	ea1	ga2	Average
SS (wind)	0.87	0.67	0.86	0.71	0.87	0	0.66
SS (no wind)	0.62	0.39	0.62	0.09	0.78	0	0.42

Table 2.8- SS calculated for the model incorporating wind drag, and the model which doesn't incorporate wind drag. The last column shows the average of all the six cases.

In the third experiment coefficient A was adjusted (Figure 2.8). In this experiment, wind was turned on, the model was set to 3D with three vertical layers, and the B coefficient was set to the default value 0.015. Increasing the A coefficient led to an eastward shift in particle movement, bringing their paths closer to those measured for gc1, gc2, ec1, and ga2. Conversely, reducing the A coefficient resulted in a westward movement of particles, more closely aligning the paths of dgc2 and ea1 with their measured trajectories. As such, a higher A coefficient aided in matching observed paths in four cases, while a lower A coefficient aided in matching observed paths in only

two cases. Statistical analysis supported these results and demonstrated that decreasing the A parameter to 0.001 resulted in a -0.04 change in the average SS value across the six cases. Increasing A to 0.009, resulted in no change in the average SS value across the six cases (Table 2.9).

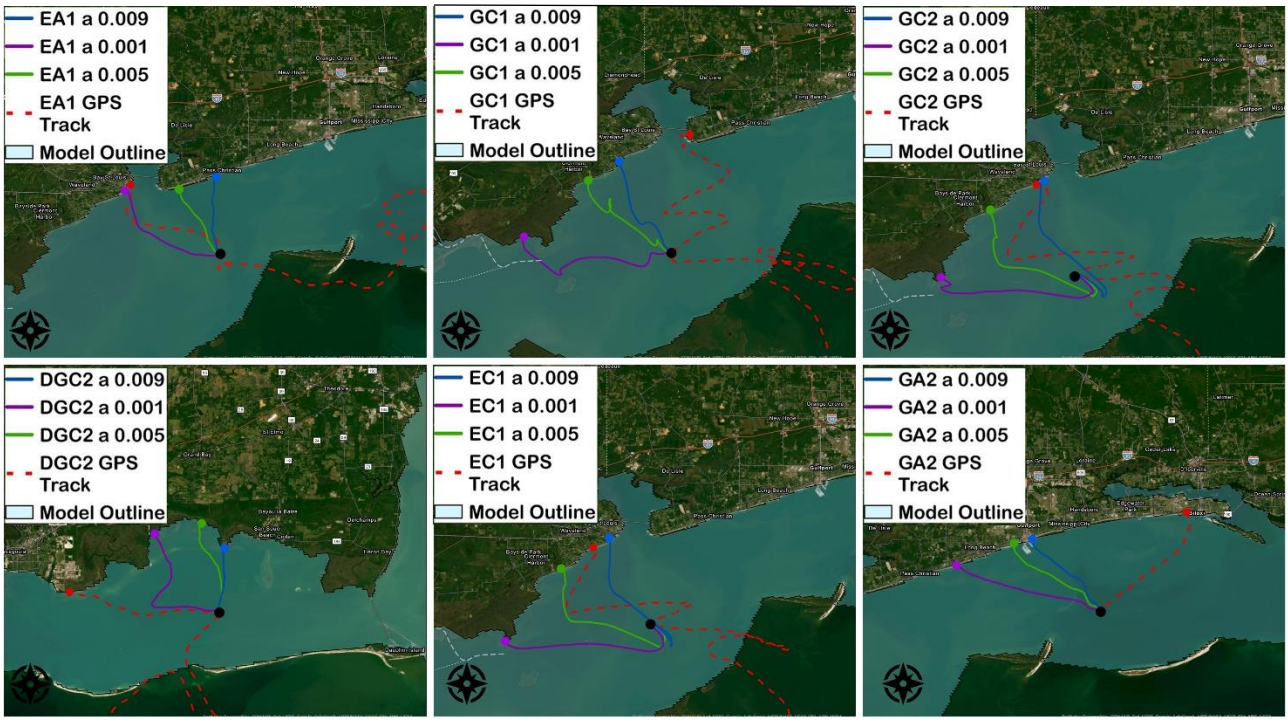

Figure 2.8- The result from changing coefficient A. The green line shows the case a = 0.005, the blue line shows the case a = 0.009, the purple line shows the case a = 0.001, and the dashed red line shows the drifter track line.

Particle Group	ec1	gc1	gc2	dgc2	ea1	ga2	Average
SS (A = 0.001)	0.74	0.45	0.74	0.87	0.92	0	0.62
SS (A = 0.005)	0.87	0.67	0.86	0.71	0.87	0	0.66
SS (A = 0.009)	0.85	0.72	0.88	0.66	0.87	0	0.66

Table 2.9- SS calculated for a=0.001, a=0.005, and a=0.009 models. The last column shows the average of all the 6 cases.

In the fourth experiment coefficient B was adjusted. In this experiment, wind was turned on, the model was set to 3D with three vertical layers, and the A coefficient was set to the default value 0.005. Both Figure 2.9 and Table 2.10 reveal minor adjustments in trajectories when the B parameter was modified. Figure 9 shows that changing the B coefficient did not consistently steer the particles in a particular direction. Increasing B resulted in an eastward movement for gc1 and ga2 and a westward shift in all other cases. While increasing or decreasing B did change the travel time and trajectory length, the overall impact on the location of stranding was limited. Statistical analysis demonstrated that increasing the B parameter to 0.027 resulted in no change in the average SS value across the six cases. Decreasing B to 0.003, resulted in -0.03 change in the average SS value across the six cases (Table 2.10). In summary, the model demonstrated less sensitivity to changes in coefficient B compared to coefficient A.

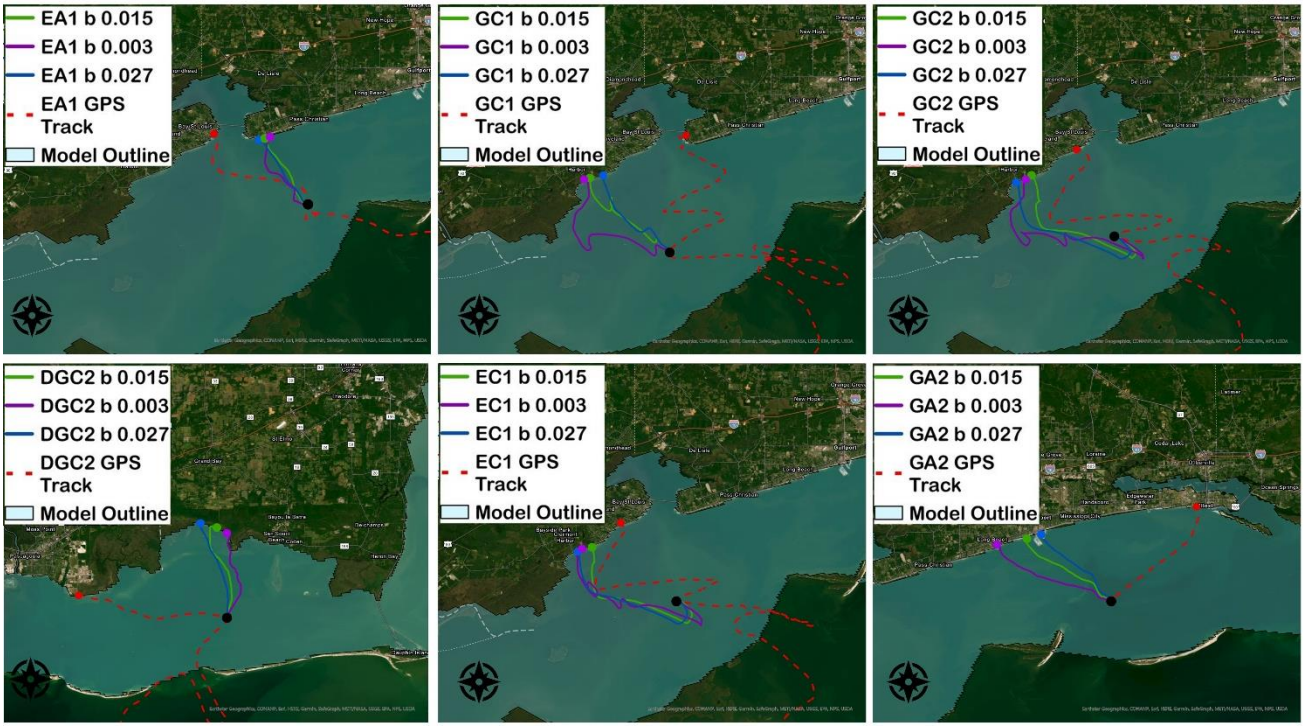

Figure 2.9- The result from changing coefficient B. The green line shows the case b = 0.015, the blue line shows the case b = 0.027, the purple line shows the case b = 0.003, and the dashed red line shows the drifter track line.

Particle Group	ec1	gc1	gc2	dgc2	ea1	ga2	Average
SS (B = 0.003)	0.81	0.58	0.82	0.70	0.87	0	0.63
SS (B = 0.015)	0.87	0.67	0.86	0.71	0.87	0	0.66
SS (B = 0.027)	0.86	0.67	0.83	0.70	0.87	0	0.66

Table 2.10- SS calculated for the b=0.003, b=0.015, and b=0.027 models. The last column shows the average of all the 6 cases.

To summarize the four experiments, the separation distances between the GPS-tagged drifter trajectories and the simulated trajectories were plotted against the simulation time for each drifter in each experiment (Figure 2.10). The most influential factor overall is turning wind on.

The main reason behind employing three distinct methods to analyze SA is that one method alone may not adequately represent model behavior. This is evidenced in the ga2 case, where the absolute errors show that none of the experiments were able to improve the simulated path of ga2 with any degree of satisfaction (Figure 2.10). However, the mapped trajectory (Figure 2.7) shows that the scenario without wind predicted ga2 moving southward toward the Gulf of Mexico, whereas the scenario with wind showed ga2 moving northward toward the shore.

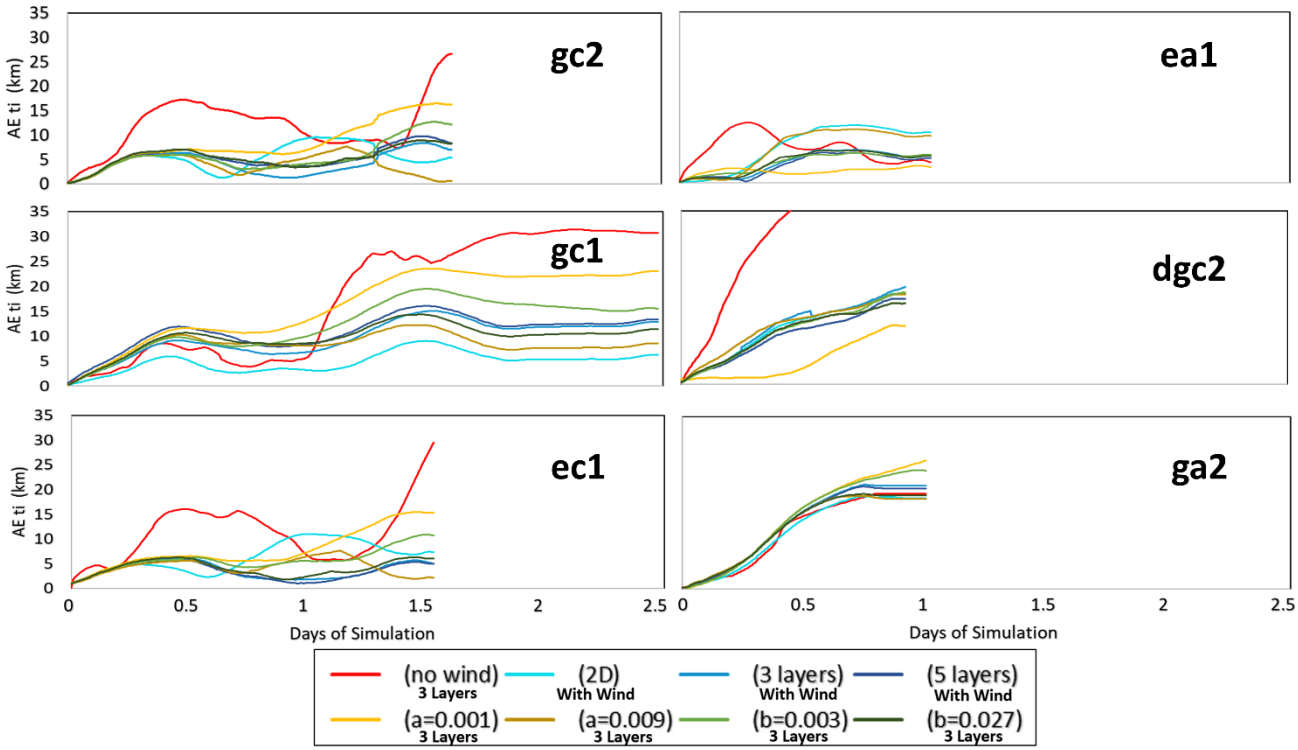

Figure 2.10- Absolute Error in Drifter Trajectory Prediction Against Days of Simulation: Comparison of Eight Experiment Scenarios for Each Drifter.

2.5.2 Calibration

Based on the findings from the SA, during calibration the model was initially set to 3D with wind turned on. The A and B wind drag coefficients were then hand tuned to improve the

match between modeled and measured data. The A and B values that resulted in the best representation of the actual trajectories were 0.006 and 0.018, respectively. The trajectory graphics (Figure 2.11) show that the calibrated values of A and B performed better than the default values in 4 out of 6 cases, including ec1, gc1, gc2, and ga2.

Once the A and B parameters were adjusted, model dimensionality was calibrated. It should be noted that the 2D model is not sensitive to changing the A and B coefficients. Consequently, when calibrating the 2D model, the only adjustment required is activating the wind component and there is no need to adjust the A and B wind coefficients. Figure 2.12 provides a representation of this calibration. Figure 2.12A shows that the 3D calibrated model outperformed the non-calibrated model in cases of ec1, gc1, gc2, and ga2. Furthermore, Figure 2.12B indicates that the calibrated model exhibited superior performance in scenarios involving ec1, gc2, and ea1 when compared to the 2D model.

The calculated SS values from this analysis are cataloged in Table 2.11. Upon reviewing these SS values, notable trends emerged. The calibration of the 3D model enhanced trajectory predictions for the ec1, gc1, and gc2 cases, whereas it adversely affected predictions for the dgc2 and ea1 scenarios when compared to the non-calibrated 3D model. Furthermore, comparing the calibrated 3D model with the 2D model, I observed improvements in trajectory predictions for ec1, gc2, and ea1 scenarios. However, the prediction for gc1 worsened, and the dgc1 case remained unaffected. Unfortunately, the trajectory predictions for the ga2 case were unsatisfactory in all three scenarios. Averaging the SS value for all six cases revealed that the calibrated 3D model performed virtually the same as the non-calibrated model and the average SS increased by 0.03 when comparing the 2D and 3D calibrated models.

Finally, the separation distance between the modeled and measured trajectories was calculated for all the drifters at the 24-hour mark from the simulation start time, considering the 3D calibrated, 3D non-calibrated, and 2D calibrated models. As shown in Table 2.12, the average value of this parameter for the six drifters indicated a significant improvement of 2.76 km compared to the 2D calibrated model and a 0.42 km enhancement compared to the 3D non-calibrated model in the case of the calibrated model.

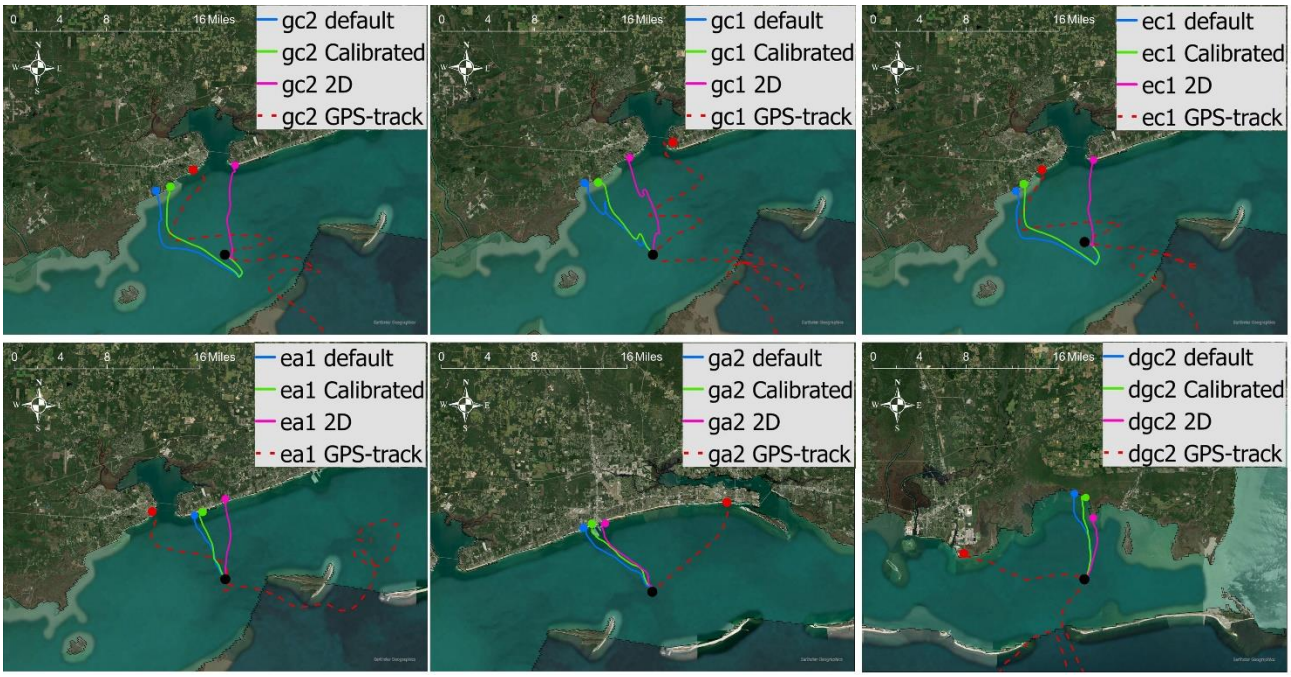

Figure 2.11- Calibration results in comparison with the model with wind turned on and default A and B values. The green line shows the calibrated 3D case, the blue line shows the default, the pink line shows the 2D calibrated model, and the dashed red line shows the drifter track line.

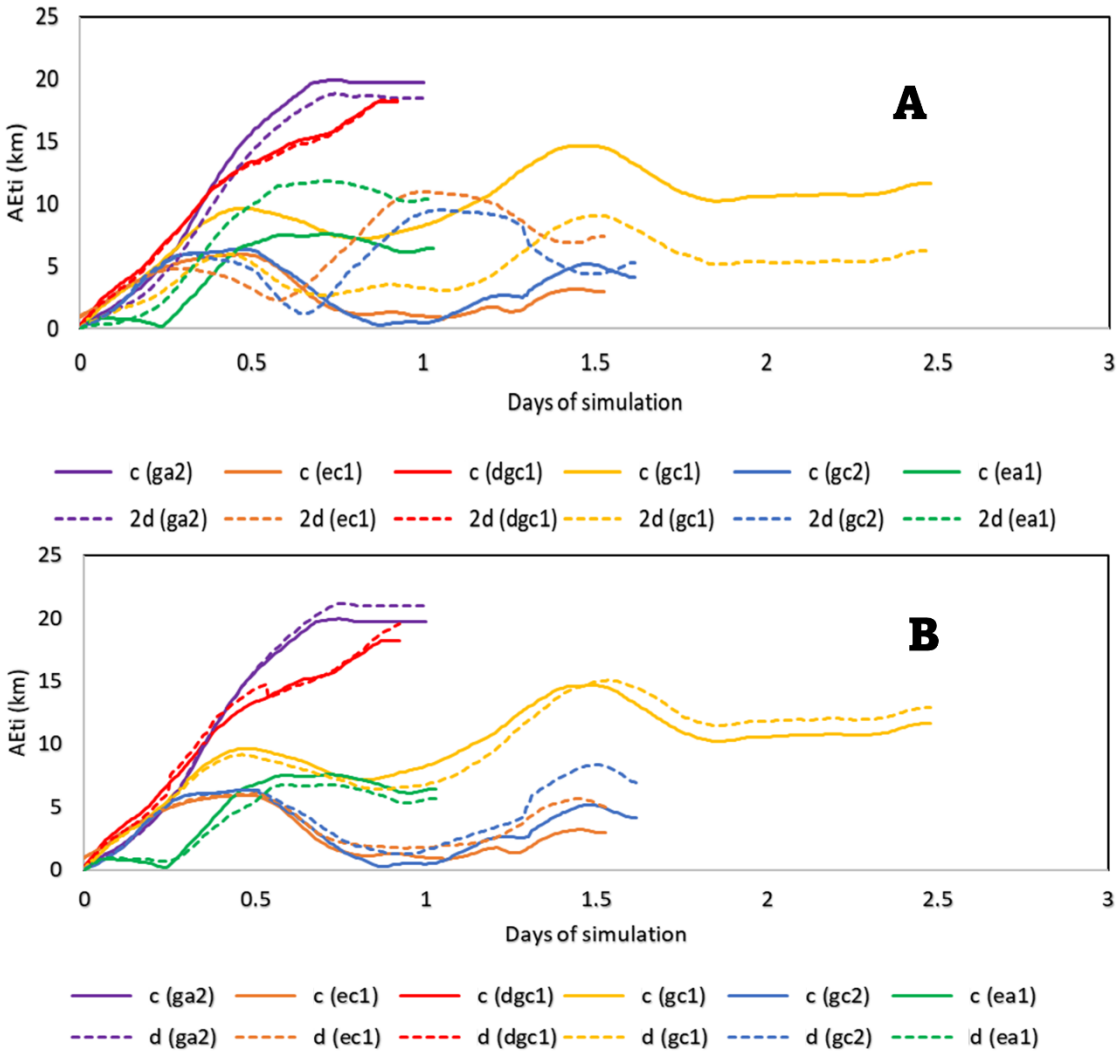

Figure 2.12- Comparing the absolute error (distance) between the measured data and modeled results during the simulation time. c represents the distance between the modeled and measured in calibrated version, 2d represents the distance between the modeled and measured in the 2D version, and d represents the between the modeled and measured in the 3D non-calibrated version. In these plots, the solid lines depict the separation distances for the 3D calibrated model, while the dashed lines in Figure 12A represent the separation for the 2D model, and in Figure 12B, they indicate the separation for the 3D non-calibrated model.

Particle Group	ec1	gc1	gc2	dgc2	ea1	ga2	Average
SS (2D calibrated)	0.79	0.83	0.83	0.66	0.77	0	0.64
SS (3D default)	0.87	0.67	0.86	0.71	0.87	0	0.66
SS (3D calibrated)	0.90	0.68	0.90	0.68	0.86	0	0.67

Table 2.11- SS calculated for the 2D model, 3D non-calibrated and 3D calibrated. The last column shows the average of all the 6 cases.

Particle Group	ec1	gc1	gc2	dgc2	ea1	ga2	Average
AE $_{24h}$ (2D) (km)	10.95	3.21	9.25	18.26	10.33	18.44	11.74
AE $_{24h}$ (3D default) (km)	1.76	6.78	1.56	19.58	5.59	20.96	9.40
AE $_{24h}$ (3D calibrated) (km)	0.97	8.22	0.46	18.22	6.34	19.71	8.98

Table 2.12- Separation distance after 24 hours passed simulation (AE $_{24h}$) calculated for the 2D model, 3D non-calibrated and 3D calibrated. The last column shows the average of all the 6 cases.

The calibrated model's performance was compared to similar studies that evaluated LPT predictive skill. It's important to note that not all studies employed the same statistical metrics as used in this analysis; therefore, I focus only on those studies that utilized the 24-hour separation distance or SS value for comparison. Liu and Weisberg (2011) reported an average SS value of 0.41 after one day of simulation in the Gulf of Mexico shelf. Ferrer et al. (2015) conducted an extensive analysis of calibrated models, reporting SS values ranging between 0.22 and 0.94 for different drifters released at different times. In comparison, the average SS value obtained in this study was 0.67, showcasing strong performance. Another study by Huntley et al. (2011) indicated that, on average, model trajectories diverged from observations by roughly 15 km after the first day. In our study, the average 24-hour separation distance for the six cases was 8.98 km.

2.6 Conclusion

In conclusion, this publication initially highlights the sensitivity of LPT in a hydrodynamic model to wind, dimensionality, and wind drag coefficients A and B. Then calibrate the LPT model using these parameters. The results can be summarized as below:

1- Incorporating wind into the LPT model greatly improves its predictive capacity, as evidenced by the average Skill Score (SS) increasing from 0.42 to 0.66.

2- The wind drag coefficient A exerts a larger impact on model predictions compared to coefficient B (average SS changes 0.01 more changing A compared to B).

3- Transition from 2D to 3D model offers marginal improvement (average SS increased by 0.03), which could be because of the MSS's smooth bathymetry. Importantly, this transition provides a valuable advantage to modelers as 2D models offer computational efficiency compared to 3D models.

4- Calibrating the LPT model across an extensive area of 5,678.8 km^2 presents challenges, as enhancing the model's accuracy in one region may lead to a deterioration in performance in another.

5- The calibrated A and B values in this study are 0.006 and 0.018, respectively, which are very close to the values used in Kim et al.'s study (2014) investigating the effects of the wind drift factor under strong tidal conditions in the western coastal area of Korea on the movement of oil slicks caused by the Hebei Spirit oil spill accident in 2007. As a result, I can conclude that these values are transferable to study areas, over time, and to different floating objects.

6- Utilizing a combination of visual graphics and statistical analyses proves valuable in understanding the impact of varying parameters.

3. Funding

Funding for this project was generously provided by the Mississippi Department of Marine Resources (Gulf of Mexico Energy Security Act project number 3000027046). This research project was also supported by the intramural research program of the U.S. Department of Agriculture, National Institute of Food and Agriculture (Hatch Accession Number 7004342). Special thanks to MMHSRP for providing us with the dolphin's stranding and GPS-tagged drifter data, respectively.

4. References

Armandei, M., Linhoss, A. C., & Camacho, R. A. (2021). Hydrodynamic modeling of the Western Mississippi Sound using a linked model system. Regional Studies in Marine Science, 44, 101685. https://doi.org/10.1016/j.rsma.2021.101685

Armstrong, B. N., Cambazoglu, M. K., & Wiggert, J. D. (2021). Modeling the impact of the 2019 Bonnet Carré Spillway opening and local river flooding on the Mississippi Sound. Oceans Conference Record (IEEE), 2021-Septe. https://doi.org/10.23919/OCEANS44145.2021.9705854

Boehning, G. D., Brunnick, B. J., Harzen, S., & Hirons, A. C. (2023). Site Fidelity of Coastal Bottlenose Dolphins (Tursiops truncatus) off Southeast Florida, USA. Aquatic Mammals, 49(3), 256–264. https://doi.org/10.1578/AM.49.3.2023.256

Booth, C., & Thomas, L. (2021). An Expert Elicitation of the Effects of Low Salinity Water Exposure on Bottlenose Dolphins. Oceans, 2(1), 179–192. https://doi.org/10.3390/oceans2010011

Carlucci, R., Cipriano, G., Santacesaria, F. C., Ricci, P., Maglietta, R., Petrella, A., Mazzariol, S., de Padova, D., Mossa, M., Bellomo, S., & Fanizza, C. (2020). Exploring data from an individual stranding of a Cuvier's beaked whale in the Gulf of Taranto (Northern Ionian Sea, Central-eastern Mediterranean Sea). Journal of Experimental Marine Biology and Ecology, 533. https://doi.org/10.1016/j.jembe.2020.151473

Cook, M., Reneker, J. L., Nero, R. W., Stacy, B. A., Hanisko, D. S., & Wang, Z. (2021). Use of Drift Studies to Understand Seasonal Variability in Sea Turtle Stranding Patterns in Mississippi. Frontiers in Marine Science, 8. https://doi.org/10.3389/fmars.2021.659536

Deming, A. C., Wingers, N. L., Moore, D. P., Rotstein, D., Wells, R. S., Ewing, R., Hodanbosi, M. R., & Carmichael, R. H. (2020). Health Impacts and Recovery From Prolonged Freshwater Exposure in a Common Bottlenose Dolphin (Tursiops 75runcates). Frontiers in Veterinary Science, 7. https://doi.org/10.3389/fvets.2020.00235

Díaz-Gamboa, R. E., Tamayo-Millán, C., Poot-López, G., González-Salas, C., Villegas-Hernández, H., & Guillén-Hernández, S. (2022). First Stranding Record of Fin Whale (Balaenoptera physalus) in the Mexican Waters of the Gulf of Mexico. Aquatic Mammals, 48(1), 92–96. https://doi.org/10.1578/AM.48.1.2022.92

Duignan, P. J., Stephens, N. S., & Robb, K. (2020). Fresh water skin disease in dolphins: a case definition based on pathology and environmental factors in Australia. Scientific Reports, 10(1), 21979. https://doi.org/10.1038/s41598-020-78858-2

DSI LLC. (2023). EFDC+ Theory, Version 11. Published by DSI LLC, Edmonds WA. Available at https://www.eemodelingsystem.com/wp-content/Download/Documentation/EFDC_Theory_Document_Ver_11.pdf

EFDC+ Source code. (2022, May). https://github.com/dsi-llc/EFDCPlus

Esri, A. P. 3. . (2022). Kernel Density (Spatial Analyst). Retrieved July 1, 2022, from https://pro.arcgis.com/en/pro-app/latest/tool-reference/spatial-analyst/kernel-density.htm

Ferrer, L., N. Zaldua-Mendizabal, A. Del Campo, J. Franco, J. Mader, U. Cotano, I. Fraile, A. Rubio, Ad Uriarte, and A. Caballero. 2015. “Operational Protocol for the Sighting and Tracking of Portuguese Man-of-War in the Southeastern Bay of Biscay: Observations and Modeling.” *Continental Shelf Research* 95: 39–53. https://doi.org/10.1016/j.csr.2014.12.011.

Ferrer, Luis, and Ane Pastor. 2017. “The Portuguese Man-of-War: Gone with the Wind.” *Regional Studies in Marine Science* 14: 53–62. https://doi.org/10.1016/j.rsma.2017.05.004.

Gilbert, L, E Rouby, E Tew-Kaï, J Spitz, H Peltier, V Quilfen, and M Authier. 2021. “Spatiotemporal Models Highlight Influence of Oceanographic Conditions on Common Dolphin Bycatch Risk in the Bay of Biscay.” *Marine Ecology Progress Series* 679 (November): 195–212. https://doi.org/10.3354/meps13894.

Gledhill, J. H., Barnett, A. F., Slattery, M., Willett, K. L., Easson, G. L., Otts, S. S., & Gochfeld, D. J. (2020). Mass Mortality of the Eastern Oyster Crassostrea virginica in the Western Mississippi Sound following Unprecedented Mississippi River Flooding in 2019. Journal of Shellfish Research, 39(2), 235–244. https://doi.org/10.2983/035.039.0205

Haelters, J., Jauniaux, T., Kerckhof, F., Ozer, J., & Scory, S. (2006). Using models to investigate a harbour porpoise bycatch problem in the southern North Sea – eastern Channel in spring 2005. ICES CM 2006/L:03. In Gulledelle (Vol. 3).

Harlan, A. J. (2014). Utlizing a lagrangian drift model to investigate pygmy sperm whale (Kogia breviceps, De Blainville 1838) stranding along the south Atlantic bight. The graduate school of the college of Charleston.

Havens, Heather, Mark E. Luther, Steven D. Meyers, and Cynthia A. Heil. 2010. “Lagrangian Particle Tracking of a Toxic Dinoflagellate Bloom within the Tampa Bay Estuary.” *Marine Pollution Bulletin* 60 (12): 2233–41. https://doi.org/10.1016/j.marpolbul.2010.08.013.

Hayes, Sean A. (Sean Arthur) (ed.), et al., & Corporate Authors(s) : United States, N. M. F. S. F. S. C. (U. S.). (2018). US Atlantic and Gulf of Mexico Marine Mammal Stock Assessments – 2017: (Second Edition). In Series : NOAA technical memorandum NMFS-NE ; 245.

https://doi.org/https://doi.org/10.25923/e764-9g81

Headlam, J. L., Lyons, K., Kenny, J., Lenihan, E. S., Quigley, D. T. G., Helps, W., Dugon, M. M., & Doyle, T. K. (2020). Insights on the origin and drift trajectories of Portuguese man of war (Physalia physalis) over the Celtic Sea shelf area. Estuarine, Coastal and Shelf Science, 246. https://doi.org/10.1016/j.ecss.2020.107033

Hendon, J. R., Wiggert, J. D., Hendon, J., & Armstrong, B. N. (2020). Monitoring 2019 Bonnet Carré Spillway Impacts – Final Report Mid-Breton Sediment Diversion (MBrSD) Assessment – Final Report Project Personnel. https://doi.org/10.18785/sose.002

Hornsby, F. E., McDonald, T. L., Balmer, B. C., Speakman, T. R., Mullin, K. D., Rosel, P. E., Wells, R. S., Telander, A. C., Marcy, P. W., Klaphake, K. C., & Schwacke, L. H. (2017). Using salinity to identify common bottlenose dolphin habitat in Barataria Bay, Louisiana, USA. Endangered Species Research, 33(1), 181–192. https://doi.org/10.3354/esr00807

Hubard, C. W., Maze-Foley, K., Mullin, K. D., & Schroeder, W. W. (2005). Seasonal Abundance and Site Fidelity of Bottlenose Dolphins (<I>Tursiops truncatus</I>) in Mississippi Sound. Aquatic Mammals, 30(2), 299–310. https://doi.org/10.1578/am.30.2.2004.299

Huntley, Helga S., B. L. Lipphardt, and A. D. Kirwan. 2011. “Lagrangian Predictability Assessed in the East China Sea.” *Ocean Modelling* 36 (1–2): 163–78. https://doi.org/10.1016/j.ocemod.2010.11.001.

Iskandar, Mochamad Riza, Muhammad Reza Cordova, and Young Gyu Park. 2022. “Pathways and Destinations of Floating Marine Plastic Debris from 10 Major Rivers in Java and Bali, Indonesia: A Lagrangian Particle Tracking Perspective.” *Marine Pollution Bulletin* 185 (PA): 114331. https://doi.org/10.1016/j.marpolbul.2022.114331.

Iskandar, Mochamad Riza, Dewi Surinati, Muhammad Reza Cordova, and Kian Siong. 2021. “Pathways of Floating Marine Debris in Jakarta Bay, Indonesia.” *Marine Pollution Bulletin* 169 (August): 112511. https://doi.org/10.1016/j.marpolbul.2021.112511.

Junior, J., Kalas, F., Rodrigues, P., Juliano, M., Neto, H., Jeveaux, J., & Neto, A. (2019). Application of MOHID platform to simulate the drift of cetaceans stranded in coastal regions. A case study in the Paulista coastline. Revista Cereus, 11(3). https://doi.org/10.18605/2175-7275/cereus.v11n3p178-189

Kako, Shin’ichiro, Atsuhiko Isobe, Tomoya Kataoka, and Hirofumi Hinata. 2014. “A Decadal Prediction of the Quantity of Plastic Marine Debris Littered on Beaches of the East Asian Marginal Seas.” *Marine Pollution Bulletin* 81 (1): 174–84. https://doi.org/10.1016/j.marpolbul.2014.01.057.

Kim, T. H., Yang, C. S., Oh, J. H., & Ouchi, K. (2014). Analysis of the contribution of wind drift factor to oil slick movement under strong tidal condition: Hebei Spirit oil spill case. PloS ONE, 9(1). https://doi.org/10.1371/journal.pone.0087393

Lars Robert Hole, Igor Ivichev, Lev Karlin Cecilie Wettre, and Johannes Röhrs. 2012. “Comparison of Operational Oil Spill Trajectory Forecasts with Surface Drifter Trajectories in the Barents Sea.” *Journal of Geology & Geosciences* 01 (01). https://doi.org/10.4172/2329-6755.1000105.

Lebreton, Laurent, and Anthony Andrady. 2019. “Future Scenarios of Global Plastic Waste Generation and Disposal.” *Palgrave Communications* 5 (1): 6. https://doi.org/10.1057/s41599-018-0212-7.

Liu, Yonggang, and Robert H. Weisberg. 2011. “Evaluation of Trajectory Modeling in Different Dynamic Regions Using Normalized Cumulative Lagrangian Separation.” *Journal of Geophysical Research: Oceans* 116 (9): 1–13. https://doi.org/10.1029/2010JC006837.

Liu, Yonggang, Robert H. Weisberg, Chuanmin Hu, and Lianyuan Zheng. 2013. “Trajectory Forecast as a

Rapid Response to the Deepwater Horizon Oil Spill." *Monitoring and Modeling the Deepwater Horizon Oil Spill: A Record Breaking Enterprise*, 153–65. https://doi.org/10.1029/2011GM001121.

Liubartseva, S., G. Coppini, R. Lecci, and E. Clementi. 2018. "Tracking Plastics in the Mediterranean: 2D Lagrangian Model." *Marine Pollution Bulletin* 129 (1): 151–62. https://doi.org/10.1016/j.marpolbul.2018.02.019.

MacKenzie Jr, C. L. 1997. "Development of an Aquacultural Program for Rehabilitation of Damaged Oyster Reefs in Mississippi."

Mantovanelli, A., M. L. Heron, A. Prytz, C. R. Steinberg, and D. Wisdom. 2011. "Validation of Radar-Based Lagrangian Trajectories against Surface-Drogued Drifters in the Coral Sea, Australia." *OCEANS'11 - MTS/IEEE Kona, Program Book*, 22–25. https://doi.org/10.23919/oceans.2011.6107233.

Mariano, Arthur J., Annalisa Griffa, Tamay M. Özgökmen, and Enrico Zambianchi. 2002. "Lagrangian Analysis and Predictability of Coastal and Ocean Dynamics 2000." *Journal of Atmospheric and Oceanic Technology* 19 (7): 1114–26. https://doi.org/10.1175/1520-0426(2002)019<1114:LAAPOC>2.0.CO;2.

Martin, Nadia, Veronica W. Varela, F. James Dwyer, Peter Tuttle, R. Glenn Ford, and Janet Casey. 2019. "Evaluation of the Fate of Carcasses and Dummies Deployed in the Nearshore and Offshore Waters of the Northern Gulf of Mexico." *Environmental Monitoring and Assessment* 191 (2019). https://doi.org/10.1007/s10661-019-7923-0.

Martin, PJ. 2000. "Description of the Navy Coastal Ocean Model Version 1.0." *Ocean Dynamics and Prediction Branch, Oceanography Division, Naval Research Laboratory*, 1–45. http://oai.dtic.mil/oai/oai?verb=getRecord&metadataPrefix=html&identifier=ADA387444.

Maximenko, Nikolai, Jan Hafner, and Peter Niiler. 2012. "Pathways of Marine Debris Derived from Trajectories of Lagrangian Drifters." *Marine Pollution Bulletin* 65 (1–3): 51–62. https://doi.org/10.1016/j.marpolbul.2011.04.016.

McClain, A. M., Daniels, R., Gomez, F. M., Ridgway, S. H., Takeshita, R., Jensen, E. D., & Smith, C. R. (2020). Physiological Effects of Low Salinity Exposure on Bottlenose Dolphins (Tursiops 77runcates). Journal of Zoological and Botanical Gardens, 1(1), 61–75. https://doi.org/10.3390/jzbg1010005

McBride-Kebert, S., & Toms, C. N. (2021). Common Bottlenose Dolphin, Tursiops truncatus, Behavioral Response to a Record-Breaking Flood Event in Pensacola Bay, Florida. Journal of Zoological and Botanical Gardens, 2(3), 351–369. https://doi.org/10.3390/jzbg2030025

Mheen, Mirjam van der, Charitha Pattiaratchi, Simone Cosoli, and Moritz Wandres. 2020. "Depth-Dependent Correction for Wind-Driven Drift Current in Particle Tracking Applications." *Frontiers in Marine Science* 7 (May): 1–10. https://doi.org/10.3389/fmars.2020.00305.

Mullin, Keith D., Wayne Hoggard, and Larry J. Hansen. 2004. "Abundance and Seasonal Occurrence of Cetaceans in Outer Continental Shelf and Slope Waters of the North-Central and Northwestern Gulf of Mexico." *Gulf of Mexico Science* 22 (1). https://doi.org/10.18785/goms.2201.06.

Nero, R. W., Cook, M., Coleman, A. T., Solangi, M., & Hardy, R. (2013). Using an ocean model to predict likely drift tracks of sea turtle carcasses in the north central Gulf of Mexico. Endangered Species Research, 21(3), 191–203. https://doi.org/10.3354/esr00516

Nicolle, Amandine, Franck Dumas, Aurélie Foveau, Eric Foucher, and Eric Thiébaut. 2013. "Modelling Larval Dispersal of the King Scallop (Pecten Maximus) in the English Channel: Examples from the

Bay of Saint-Brieuc and the Bay of Seine." *Ocean Dynamics* 63 (6): 661–78. https://doi.org/10.1007/s10236-013-0617-1.

NOAA Data access viewer. 2023 "NOAA Data Acess Viewer." Retrieved (https://coast.noaa.gov/dataviewer/#/lidar/search/).

NOAA. (2023). National Stranding Database Public Access. Retrieved April 5, 2023, from https://www.fisheries.noaa.gov/national/marine-life-distress/national-stranding-database-public-access

NOAA National Centers for Environmental Information. Local climatological data. Retrieved February 6, 2022, from https://www.ncei.noaa.gov/maps/lcd/

NOAA Fisheries Marine Life Distress. (2022). 2019 Bottlenose Dolphin Unusual Mortality Event Along the Northern Gulf of Mexico. Retrieved June 19, 2022, from https://www.fisheries.noaa.gov/national/marine-life-distress/2019-bottlenose-dolphin-unusual-mortality-event-along-northern-gulf

NOAA Fisheries Marin Mammal Protection. Marine Mammal Unusual Mortality Events. Retrieved April 5, 2023, from fisheries.noaa.gov/national/marine-mammal-protection/marine-mammal-unusual-mortality-events

Parra, S. M., Sanial, V., Boyette, A. D., Cambazoglu, M. K., Soto, I. M., Greer, A. T., Chiaverano, L. M., Hoover, A., & Dinniman, M. S. (2020). Bonnet carré spillway freshwater transport and corresponding biochemical properties in the mississippi bight. Continental Shelf Research, 199, 104114. https://doi.org/10.1016/j.csr.2020.104114

Passeri, D. L., Hagen, S. C., Bilskie, M. v., & Medeiros, S. C. (2015). On the significance of incorporating shoreline changes for evaluating coastal hydrodynamics under sea level rise scenarios. Natural Hazards, 75(2), 1599–1617. https://doi.org/10.1007/s11069-014-1386-y

Peltier, H., Authier, M., Dabin, W., Dars, C., Demaret, F., Doremus, G., Canneyt, O. van, Laran, S., Mendez-Fernandez, P., Spitz, J., Daniel, P., & Ridoux, V. (2020). Can modelling the drift of bycaught dolphin stranded carcasses help identify involved fisheries? An exploratory study. Global Ecology and Conservation, 21, e00843. https://doi.org/10.1016/j.gecco.2019.e00843

Peltier, H., Dabin, W., Daniel, P., van Canneyt, O., Dorémus, G., Huon, M., & Ridoux, V. (2012). The significance of stranding data as indicators of cetacean populations at sea: Modelling the drift of cetacean carcasses. Ecological Indicators, 18, 278–290. https://doi.org/10.1016/j.ecolind.2011.11.014

Pitchford, J. L., Pulis, E. E., Evans, K., Shelley, J. K., Serafin, B. J. S., & Solangi, M. (2016). Seasonal Density Estimates of Tursiops 78runcates (Bottlenose Dolphin) in the Mississippi Sound from 2011 to 2013. Southeastern Naturalist, 15(2), 188–206. https://doi.org/10.1656/058.015.0201

Quinlan, B. M. and W. (1999). From spawning grounds to the estuary: Using linked individual-based and hydrodynamic models to interpret patterns and processes in the oceanic phase of Atlantic menhaden Brevoortia tyrannus life history. Fisheries Oceanography.

Quirós, Y. B. De, Hartwick, M., Rotstein, D. S., Garner, M. M., Bogomolni, A., Greer, W., Niemeyer, M. E., Early, G., Wenzel, F., & Moore, M. (2018). Quiroz et al 2018. 127, 83–95.

Ribotti, Alberto, Fabio Antognarelli, Andrea Cucco, Marcello Francesco Falcieri, Leopoldo Fazioli, Christian Ferrarin, Antonio Olita, et al. 2018. "An Operational Marine Oil Spill Forecasting Tool for the Management of Emergencies in the Italian Seas." *Journal of Marine Science and Engineering* 7 (1). https://doi.org/10.3390/jmse7010001.

Robins, Peter E., Simon P. Neill, Luis Giménez, Stuart R. Jenkins, and Shelagh K. Malham. 2013. "Physical and Biological Controls on Larval Dispersal and Connectivity in a Highly Energetic Shelf Sea." *Limnology and Oceanography* 58 (2): 505–24. https://doi.org/10.4319/lo.2013.58.2.0505.

Röhrs, Johannes, Kai Håkon Christensen, Lars Robert Hole, Göran Broström, Magnus Drivdal, and Svein Sundby. 2012. "Observation-Based Evaluation of Surface Wave Effects on Currents and Trajectory Forecasts." *Ocean Dynamics* 62 (10–12): 1519–33. https://doi.org/10.1007/s10236-012-0576-y.

Santos, Bianca S., Marjorie A.M. Friedrichs, Sarah A. Rose, Susan G. Barco, and David M. Kaplan. 2018. "Likely Locations of Sea Turtle Stranding Mortality Using Experimentally-Calibrated, Time and Space-Specific Drift Models." *Biological Conservation* 226 (October): 127–43. https://doi.org/10.1016/j.biocon.2018.06.029.

Scircle, Austin, James V. Cizdziel, Louis Tisinger, Tarun Anumol, and Darren Robey. 2020. "Occurrence of Microplastic Pollution at Oyster Reefs and Other Coastal Sites in the Mississippi Sound, USA: Impacts of Freshwater Inflows from Flooding." *Toxics* 8 (2): 35. https://doi.org/10.3390/toxics8020035.

Seo, Seongbong, and Young-Gyu Park. 2020. "Destination of Floating Plastic Debris Released from Ten Major Rivers around the Korean Peninsula." *Environment International* 138 (May): 105655. https://doi.org/10.1016/j.envint.2020.105655.

Song, Xiaomeng, Jianyun Zhang, Chesheng Zhan, Yunqing Xuan, Ming Ye, and Chonggang Xu. 2015. "Global Sensitivity Analysis in Hydrological Modeling: Review of Concepts, Methods, Theoretical Framework, and Applications." *Journal of Hydrology* 523 (225): 739–57. https://doi.org/10.1016/j.jhydrol.2015.02.013.

Takeshita, R., Balmer, B. C., Messina, F., Zolman, E. S., Thomas, L., Wells, R. S., Smith, C. R., Rowles, T. K., & Schwacke, L. H. (2021). High site-fidelity in common bottlenose dolphins despite low salinity exposure and associated indicators of compromised health. PLOS ONE, 16(9), e0258031. https://doi.org/10.1371/journal.pone.0258031

Toms, C. N., Stone, T., & Och, T. (2021). Skin lesion and mortality rate estimates for common bottlenose dolphin (Tursiops 79runcates) in the Florida Panhandle following a historic flood. PloS ONE, 16(10 October). https://doi.org/10.1371/journal.pone.0257526

US Army Corps of Engineers. (2016). Historic Operations Of The Bonnet Carre' Spillway. Retrieved November 1, 2022, from https://www.mvn.usace.army.mil/Missions/Mississippi-River-Flood-Control/Bonnet-Carre-Spillway-Overview/Historic-Operation-of-Bonnet-Carre/

US Army Corps of Engineers. (2020). USACE, 2019. Spillway Operation Information. Retrieved November 1, 2022, from https://www.mvn.usace.army.mil/Missions/Mississippi-River-Flood-Control/Bonnet-Carre-Spillway-Overview/Spillway-Operation-Information/

U.S. Geological Survey. (2023). Map of real-time streamflow compared to historical streamflow for the day of the year (United States). Retrieved April 5, 2023, from https://waterwatch.usgs.gov/?id=ww_current

Wirasaet, D. W., Meixner, J. D., & Esterink, J. J. W. (2015). DWH NRDA Marine Mammal Technical Working Group Report: Assessing the Likelihood of Dolphin Carcass Strandings in the Northern Gulf of Mexico.

Woodcock, A. H., & McBride, A. F. (1961). Wave-riding dolphins. In Science (Vol. 133, Issue 3447, pp. 204–205). https://doi.org/10.1126/science.133.3447.204

Yang, Yi, Zhi Li Chen, Ying Li, Xiao Xiao, Qi Dan, Ting Hong Yang, and Zhen Jie Ren. 2013.

"Numerical Simulation of Oil Spill in the Gulf of Mexico Based on the GNOME and ADIOS." *Applied Mechanics and Materials* 295–298 (February): 1535–42. https://doi.org/10.4028/www.scientific.net/AMM.295-298.1535.

5. Appendices

Appendix 1

This supplemental document intends to ease the replication of results and help other researchers conduct similar studies using the methodology of this work.

1. Set up the Lagrangian Particle Tracking module in EFDC+.

- Activate the Lagrangian Particle Tracking (LPT) module by RMC on the Modules and then check the Lagrangian Particle Tracking box and click OK (Figure 5.1).
- In the "LPT Main Options", the "Compute Drifters" box should be checked (Figure 5.2).
- The start and end date of the particle tracking and the frequency in which we need the output should be specified.
- For the vertical placement of the particles, the "Particle Depths are FIXED at the Initial Seeding Depths" option is selected since the dolphins are assumed to be floating during the simulation period.
- In the wind drift effect, "Separate Drag Coeff. For Each Wind Component" is selected, and coefficients A = 0.006 and B = 0.018 are the calibrated values.
- Don't turn on the random walk.
- For the initial vertical position of the particles, select "Depth is specified".
- The Start and End Date of the LPT should also be specified.

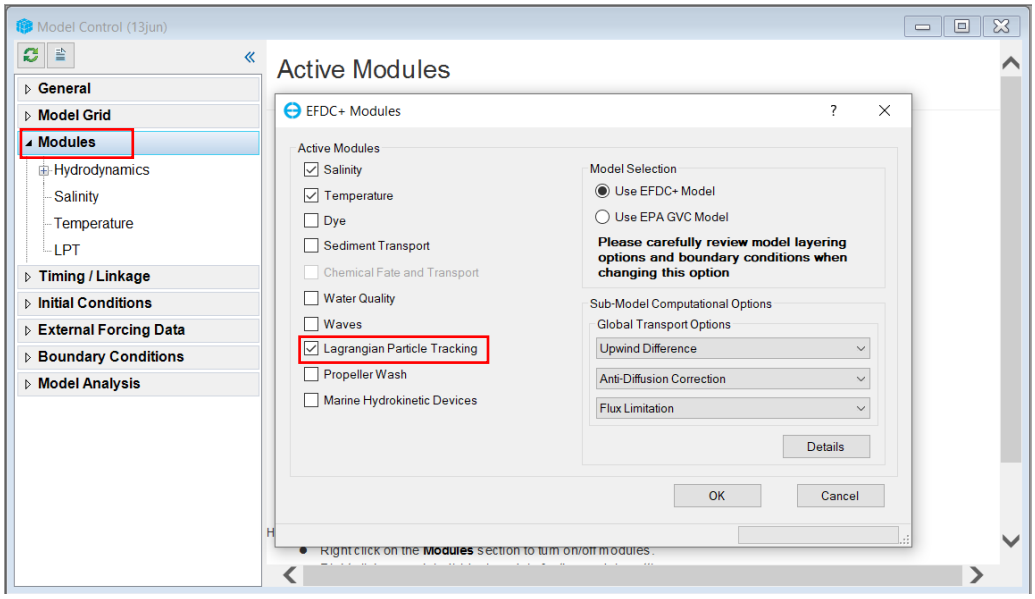

Figure 5.1- EFDC+ modules menu.

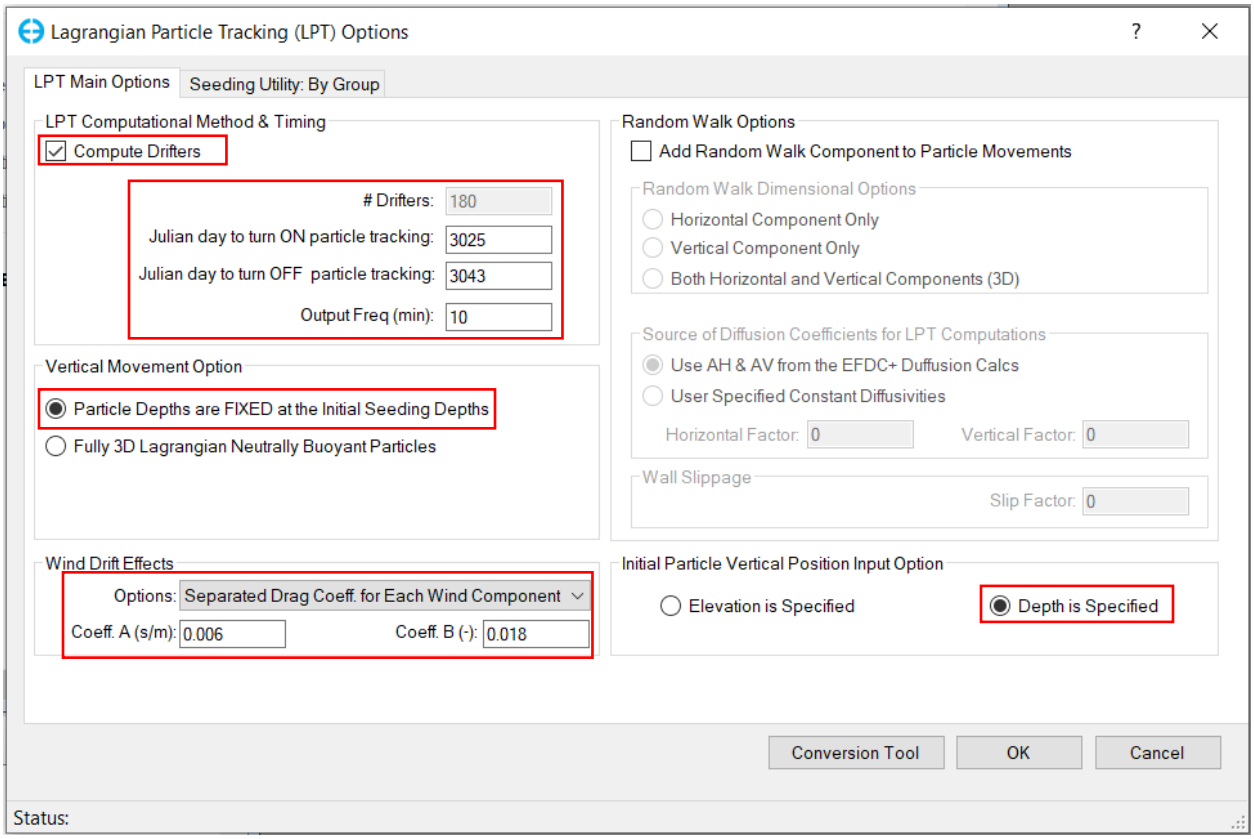

Figure 5.2- LPT main options menu.

2. Seed one particle in each grid cell uniformly (Figure 5.3).

- In the Seeding Utility: By Group" menu, set the horizontal placement to uniform spacing, then click on "Set to Model Extents".
- Then, set Delta X to 250 m, and Delta Y to 300 m, which are the approximate grid dimensions.
- In the "Number of Particles to Seed in Next Create", put a number larger than the number of grid cells (70964). Here I put the number 90000. Remember that it doesn't matter what number you put in this box as long as it is larger than the number of grid cells because it is going to seed the particles uniformly according to the model extents and the specified Delta X and Delta Y.
- In the "Vertical (Depth) Options", check "Fixed Depth" and put 0 in the "Fixed Depth (m)" box. This way, the particles are seeded on the surface of the water (Figure 5.4).
- The Start and End Date of the LPT should also be specified here again.

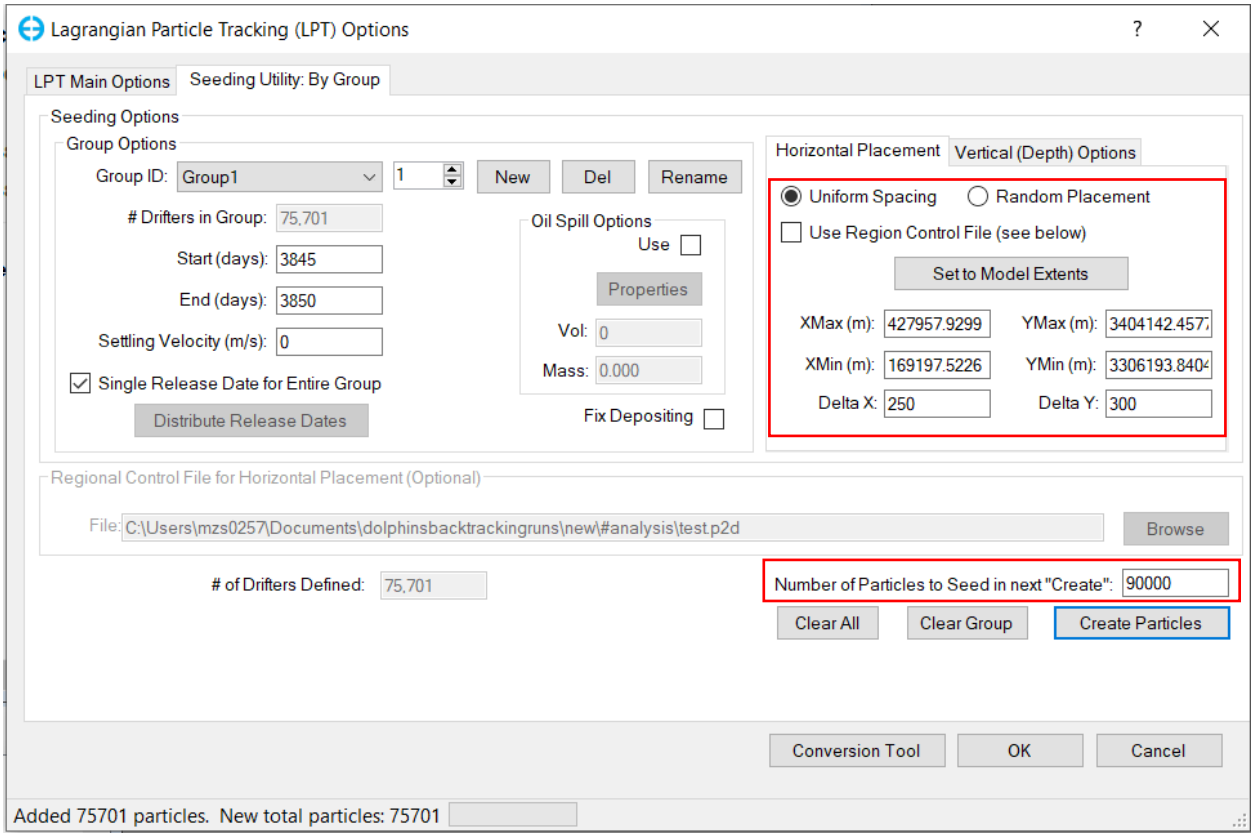

Figure 5.3- LPT seeding utility by group menu.

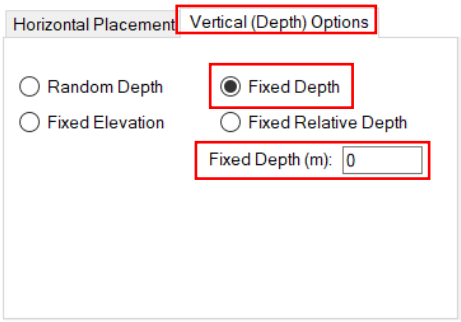

Figure 5.4- LPT seeding utility by group, vertical (depth) options sub-menu.

3. Run the model with at least 4 months of warm-up, starting 4 months prior to the stranding date and ending at the stranding date.

4. start the LPT 5 days prior to each dolphin stranding event and end it on the stranding date for dolphins with code 2 and for other codes, use Table 5.1 for reference:

DECOMPOSITION CODE	TIME PASSED SINCE DEATH
CODE 1: ALIVE ANIMAL	< 2 days
CODE 2: FRESH DEAD	2 to 5 days
CODE 3: MODERATE	5 to 15 days
CODE 4: ADVANCED	15 to 30 days
CODE 5: SKELETON/ MUMMIFIED	> 30 days

Table 5.1- Time passed since death for different decomposition codes.

5. Turn on the LPT in 2DH view and use extract particle, then extract the particles in 5, 4, 3, and 2 days prior to the stranding and the initial seeding location as .txt files (Figure 5.5).

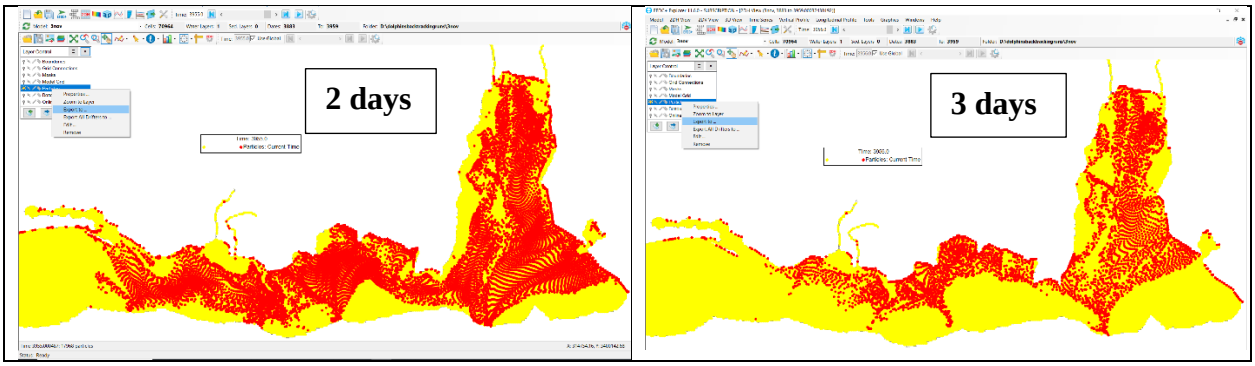

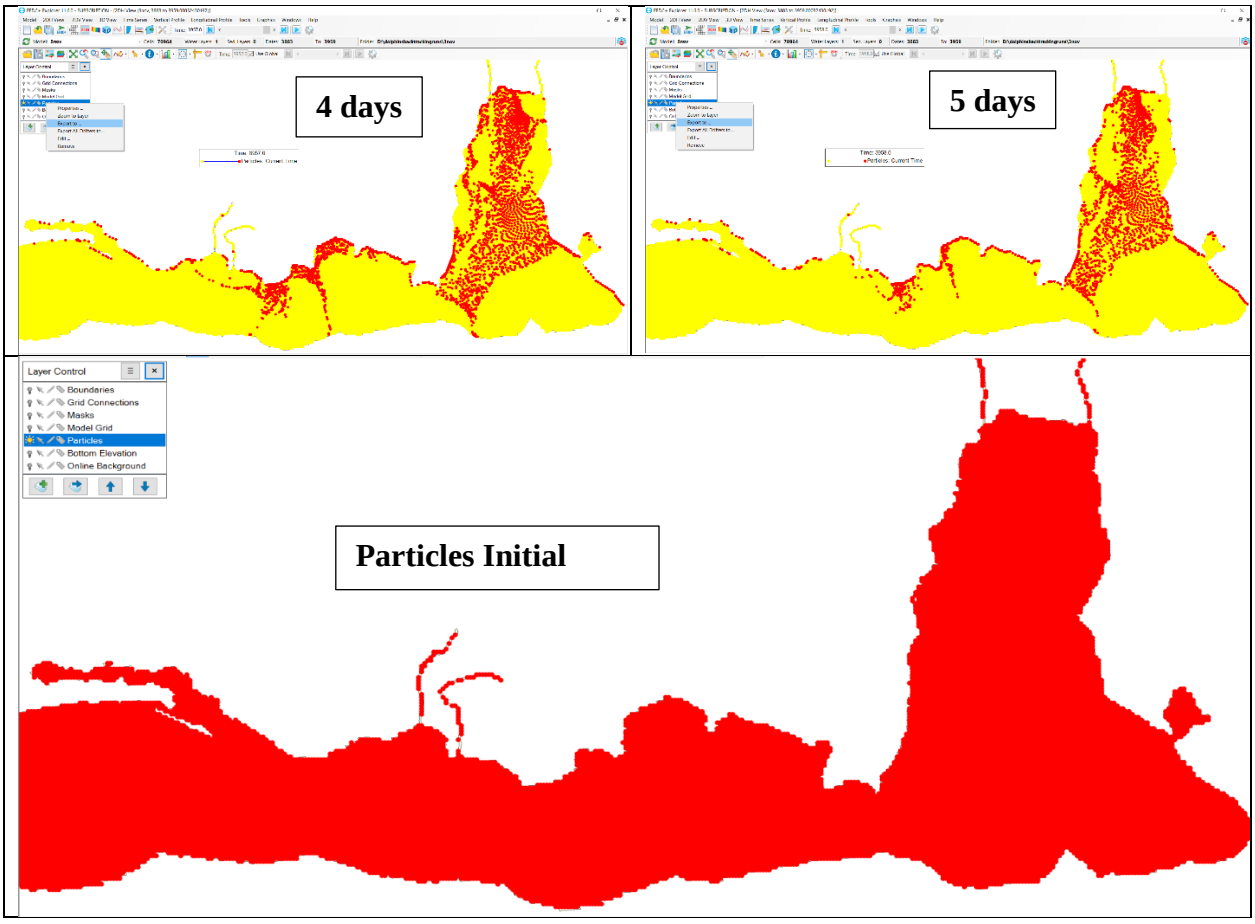

Figure 5.5- Exporting particles location in 5, 4, 3, and 2 days prior to the stranding and the initial seeding location

6. Export the Grid Outlines from the EFDC+ software (Figure 5.6).

- RMC on the “Model Grid” in the “Layer control”, in 2DH view.
- Click “Export Grid Outlines”.
- Select the format as .shp file.

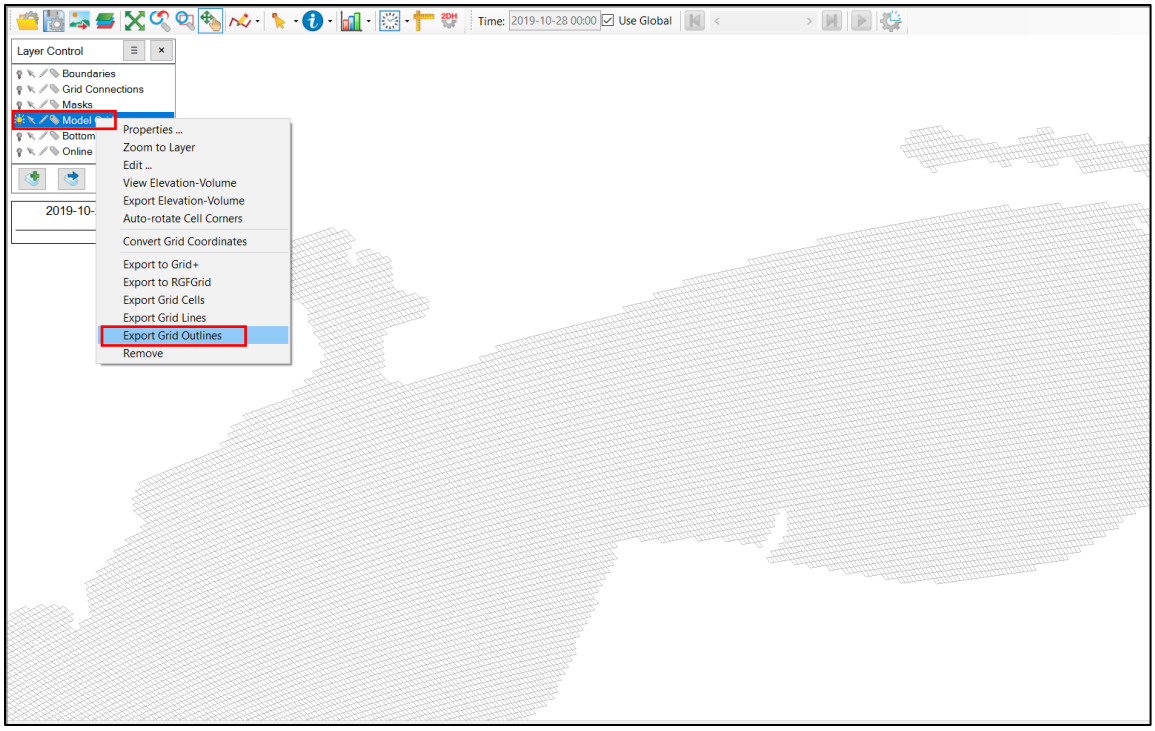

Figure 5.6- Exporting grid outline.

7. Add those 5 .txt files into the ArcGIS pro along with the .shp file showing the dolphin stranding locations and the .shp showing the model outlines (Figure 5.7).

- Clean up the .txt files by feeling the empty cells (time steps) with -99 and save them as .csv files.
- Add the .csv files into the ArcGIS pro window.
- RMC on each of them and click “Display XY Data”.
- Select the XLA, and YLA for the X and Y fields, respectively, and choose the “UTM Zone 16” for the coordinate system. Then click OK.
- Add the model_outline.shp file into the ArcGIS pro window.
- Add the dolphin stranding locations file into the ArcGIS pro window.

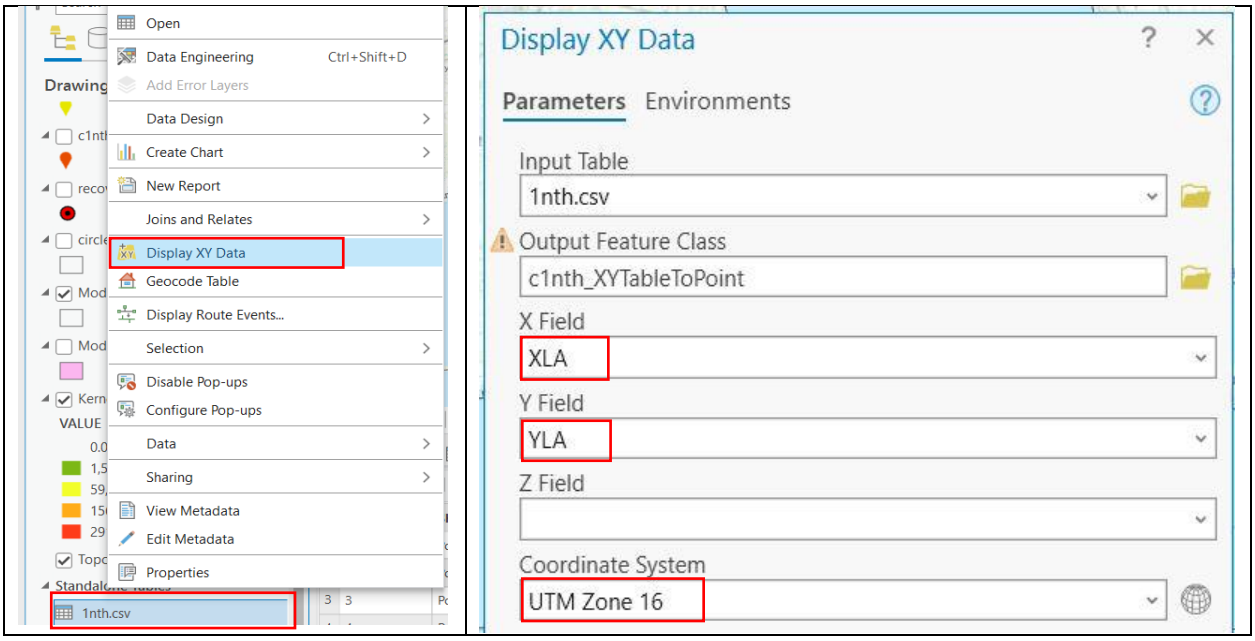

Figure 5.7- Create XY data points from the particles text files in ArcGIS pro.

8. Create a circle feature with a radius of 4km and the center of the stranded dolphin following these steps (Figure 5.8).

- Open the catalog pane, RMC on the current database, navigate to New, and then click Feature Class.
- In “Feature Class Type”, choose “Polygon” and name it Circle.
- Enable Edit, then click “Create”, then click on the recently created feature named “Circle”, then among the suggested polygon shapes, choose a circle.
- Click on the stranding location and draw a circle, then RMC and choose “Radius”.
- Finally, enter the radius (4 km) and save edits.
- Don’t forget to disable edits.

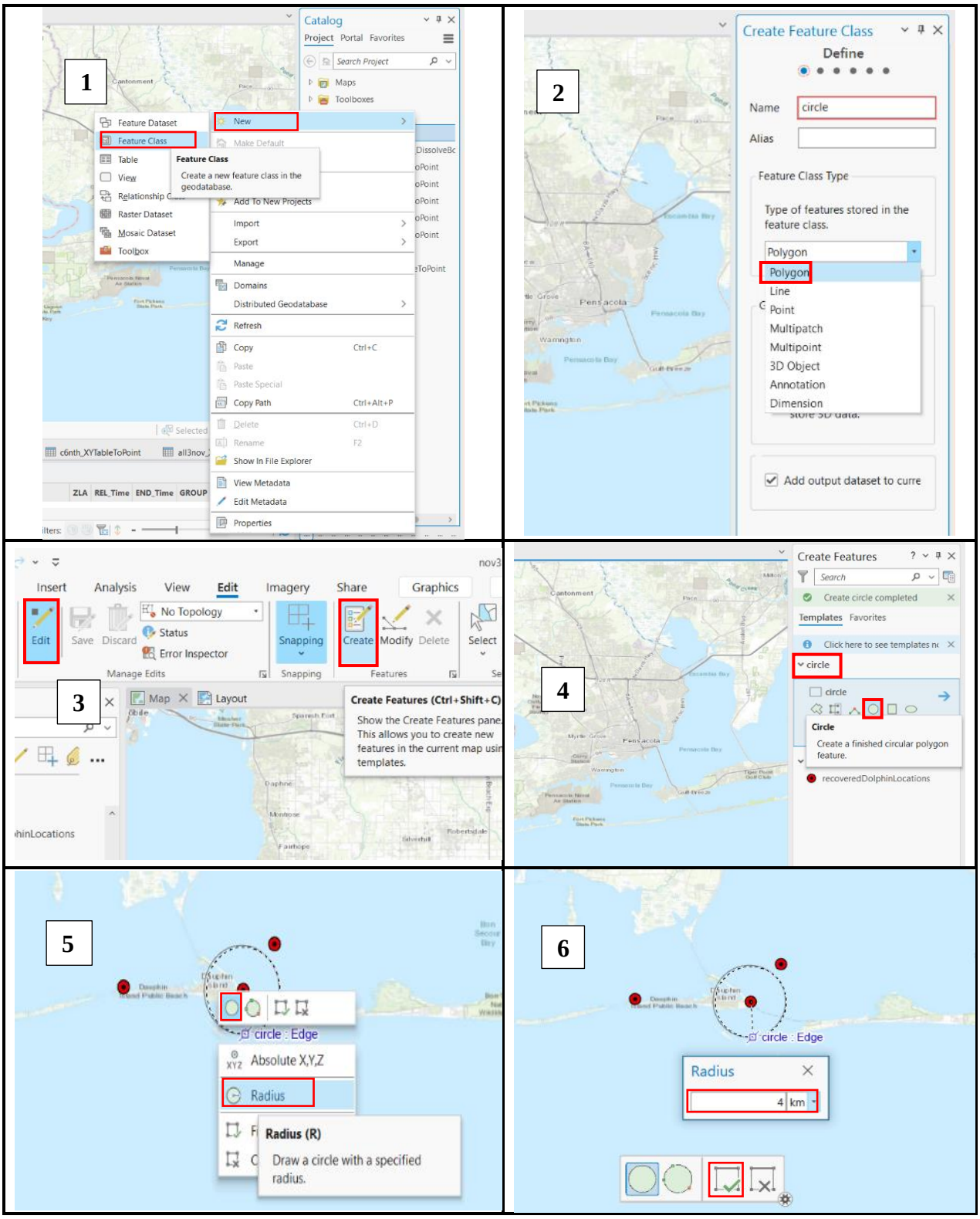

Figure 5.8- Creatin 4 km radius circle around the stranding location.

9. After the circle is created, a “join” is performed between the .shp file of the initial location of particles and the .shp files of 5 days, 4 days, 3 days, and 2 days prior to stranding using the object ID to join the attribute table of each of the 5 days, 4 days, 3 days, and 2 days prior to stranding files to their initial seeding location (Figure 5.9).

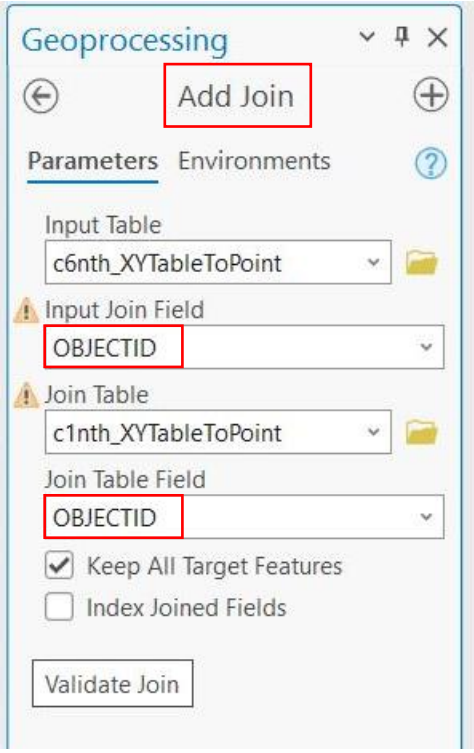

Figure 5.9- Performing a join.

10. Then select all the particles in the 5 days, 4 days, 3 days, and 2 days prior to stranding files that fall within the 4 km radius circle (Figure 5.10).

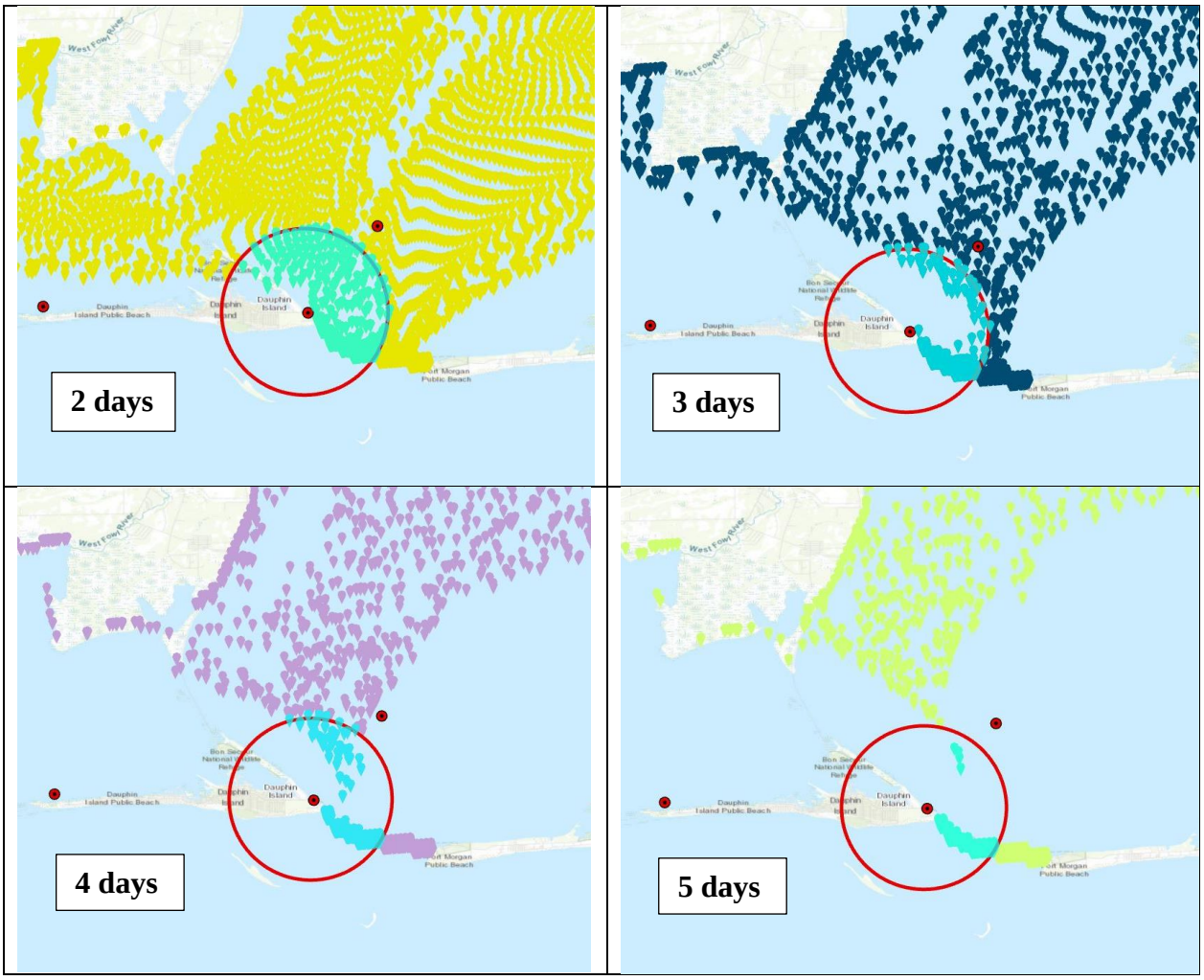
2 days
3 days
4 days
5 days

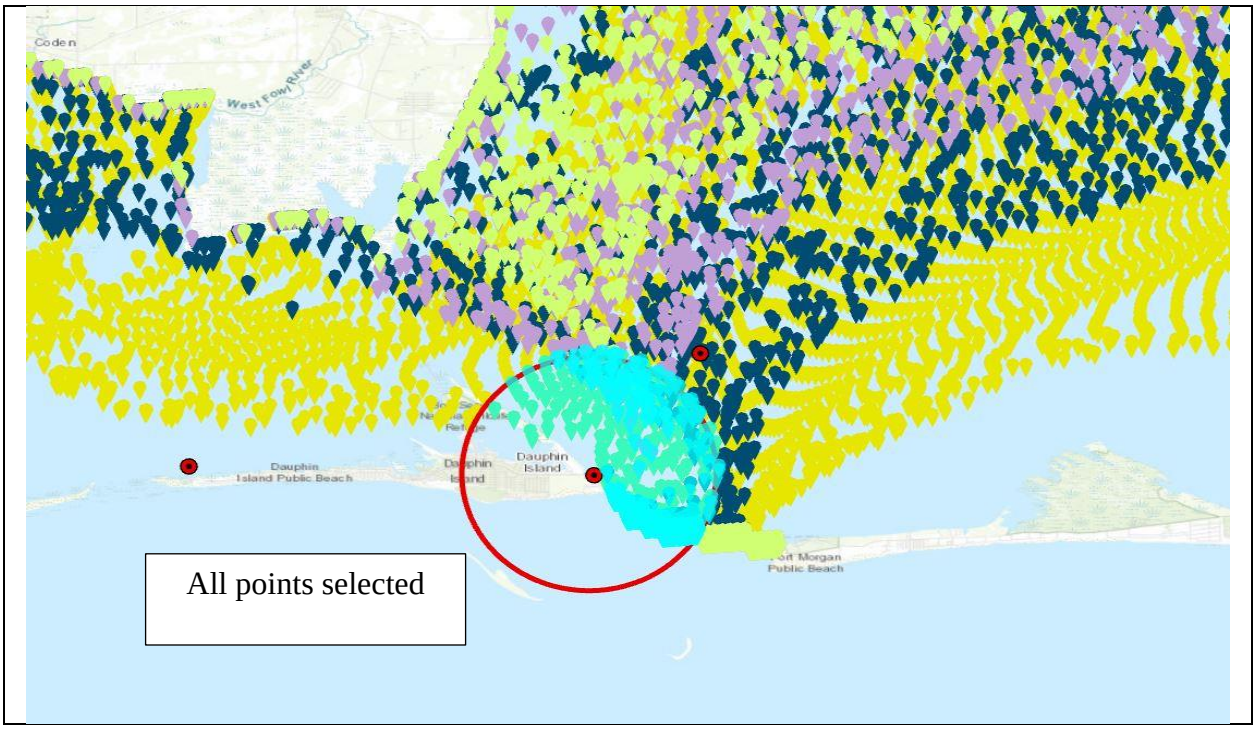

Figure 5.10- Selecting the particles entering the created circle.

11. Then, the attribute tables of the selected points in each of the 5 days, 4 days, 3 days, and 2 days prior to stranding files are copied into an Excel file. Since these files were joined to the file of initial locations of the particles, the second X, and Y columns specify the initial seeding location of the selected particles (Figure 5.11).

- The Excel file should be cleaned in a way that there is no repeating particles.
- Save the final Excel as a .csv file.

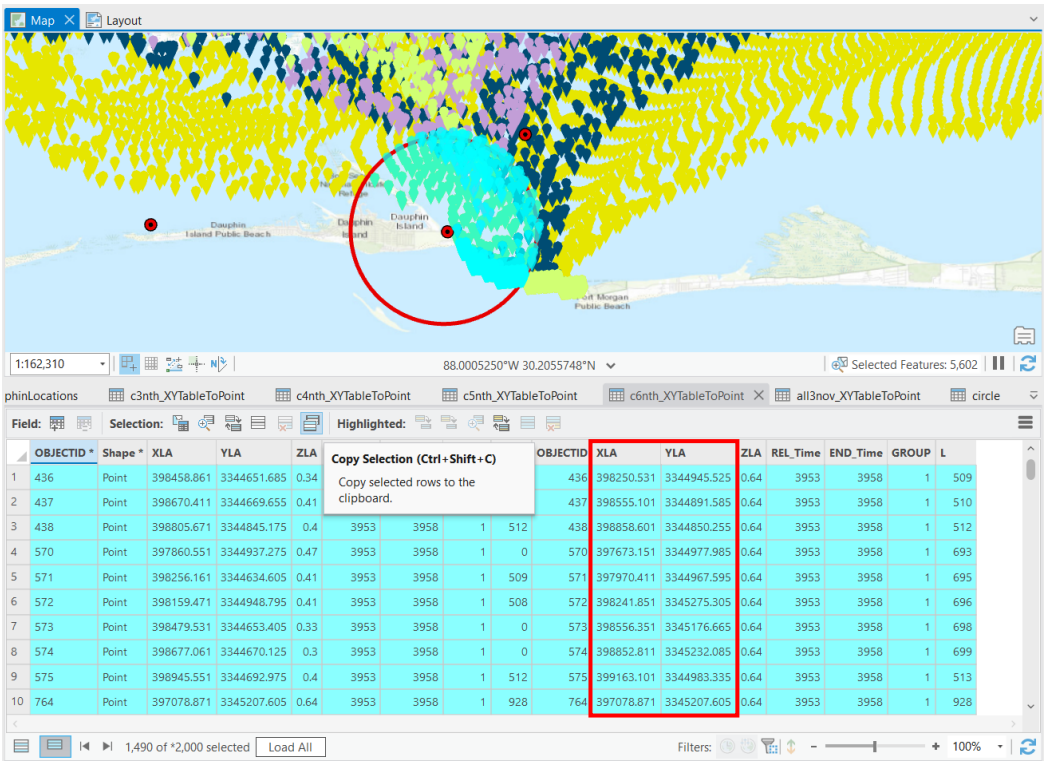

	OBJECTID *	Shape *	XLA	YLA	ZLA					OBJECTID	XLA	YLA	ZLA	REL_Time	END_Time	GROUP	L
1	436	Point	398458.861	3344651.685	0.34					436	398250.531	3344945.525	0.64	3953	3958	1	509
2	437	Point	398670.411	3344669.655	0.41					437	398555.101	3344891.585	0.64	3953	3958	1	510
3	438	Point	398805.671	3344845.175	0.4	3953	3958	1	512	438	398858.601	3344850.255	0.64	3953	3958	1	512
4	570	Point	397860.551	3344937.275	0.47	3953	3958	1	0	570	397673.151	3344977.985	0.64	3953	3958	1	693
5	571	Point	398256.161	3344634.605	0.41	3953	3958	1	509	571	397970.411	3344967.595	0.64	3953	3958	1	695
6	572	Point	398159.471	3344948.795	0.41	3953	3958	1	508	572	398241.851	3345275.305	0.64	3953	3958	1	696
7	573	Point	398479.531	3344653.405	0.33	3953	3958	1	0	573	398556.351	3345176.665	0.64	3953	3958	1	698
8	574	Point	398677.061	3344670.125	0.3	3953	3958	1	0	574	398852.811	3345232.085	0.64	3953	3958	1	699
9	575	Point	398945.551	3344692.975	0.4	3953	3958	1	512	575	399163.101	3344983.335	0.64	3953	3958	1	513
10	764	Point	397078.871	3345207.605	0.64	3953	3958	1	928	764	397078.871	3345207.605	0.64	3953	3958	1	928

Figure 5.11- Copying the attribute tables of selected points.

12. Then, the .csv file containing the initial location of the selected particles is added to the ArcGIS pro environment (Figure 5.12).

- The .csv file in this step should be transformed into a point feature data exactly similar to step 7.

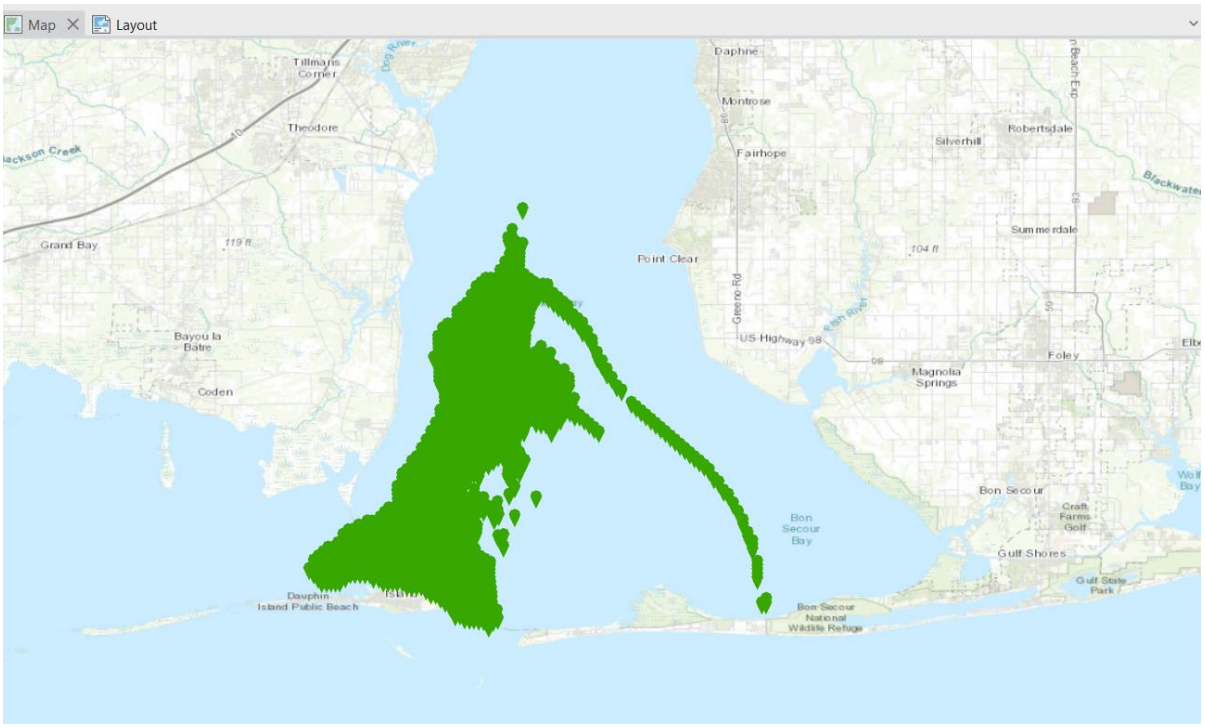

Figure 5.12- Adding the file containing initial location of the selected particles into ArcGIS pro.

13. Finally, a Kernel Density Analysis is performed to show the locations where the density of particles is the highest (Figure 5.13).

- For the input, choose the dataset of the initial location of selected points, created in Excel in the previous steps.
- For the population Field, Select None.
- Configure the output cell size to 30, and set the search radius to 1500 meters, with the unit area expressed in square kilometers. This choice of cell size ensures that the results remain smooth and free from pixelation artifacts. Furthermore, the selected search radius aligns with the margin of error considered for identifying particles in close proximity to the stranding location, which is approximately 4 kilometers. Notably, the default value generated by ArcGIS Pro, approximately 1500 meters, falls within the same order of magnitude (4 km) and is, therefore a logically consistent choice for use as the search radius across all cases. This approach maintains consistency in our analyses.
- Add the model boundaries as an input barrier feature for the results to be created only inside the model domain.

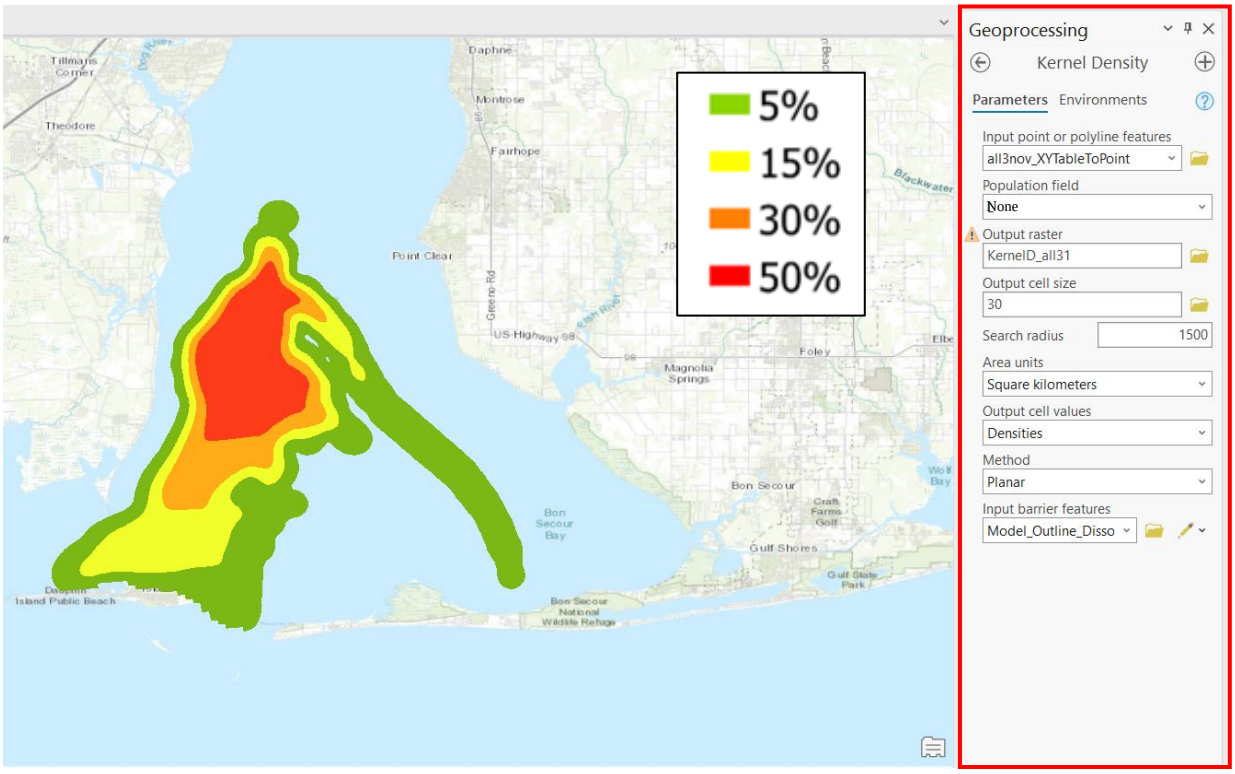

Figure 5.13- Kernel Density Analysis setup.

14. In the symbology of the Kernel Density layer, set the number of intervals to 5, then set the number of points in the first interval to zero and justify the 4 other intervals in a way that each color contains a certain percentage of points.

- Red = 50%, Orange = 30%, Yellow = 15%, Green = 5% of the total points.